CoT Distillation LLMs enable cost effective Artificial Intelligence for On-Premises Services

Why I chose this subject

I am interested in creating an actual proposal to some co-workers on this subject. The idea of presenting a cost-effective tool that skirts some of the legal challenges vendor provided AI as a service have seems quite attractive. Additionally, I would develop a greater understanding of LLMs and how they might be beneficial to my industry.

Synopsis

Given the recent industry rocking discoveries in DeepSeek V3 and other distillation LLMs and costs associated with AI as a service, On-Premises AI services begin to gain traction as an attractive solution for small to medium setups. Beginning with other off-the-shelf tools such as vLLMs, the idea of On-Premises AI services has materialized into experimental projects investigating the viability of internal AI tooling. This paper will explore how CoT Distillation can produce models with greater portability, cost efficiency, and capability compared to alternative open-source models such as vLLMs.

Related Journals

- DeepSeek-V3 Technical Report
- Learning to Maximize Mutual Information for Chain-of-Thought Distillation
- On-Premise Artificial Intelligence as a Service for Small and Medium Size Setups

Citations

Choi, W., Kim, W. K., Yoo, M., & Woo, H. (2024). Embodied cot distillation from llm to off-the-shelf agents. https://arxiv.org/abs/2412.11499

DeepSeek-AI, Liu, A., Feng, B., Xue, B., Wang, B., Wu, B., Lu, C., Zhao, C., Deng, C., Zhang, C., Ruan, C., Dai, D., Guo, D., Yang, D., Chen, D., Ji, D., Li, E., Lin, F., Dai, F., . . . Pan, Z. (2024). Deepseek-v3 technical report. https://arxiv.org/abs/2412.19437

Fortuna, C., Muši´c, D., Cerar, G., ˇCampa, A., Kapsalis, P., & Mohorˇciˇc, M. (2022). On-premise artificial intelligence as a service for small and medium size setups. https://arxiv.org/abs/2210.06956

Source BibTeX Code

```
@misc{choi2024embodiedcotdistillationllm,
      title={Embodied CoT Distillation From LLM To Off-the-shelf Agents},
      author={Wonje Choi and Woo Kyung Kim and Minjong Yoo and Honguk Woo},
      year={2024},
      eprint={2412.11499},
      archivePrefix={arXiv},
      primaryClass={cs.AI},
      url={https://arxiv.org/abs/2412.11499},
}

@misc{deepseekai2024deepseekv3technicalreport,
      title={DeepSeek-V3 Technical Report},
      author={DeepSeek-AI and Aixin Liu and Bei Feng and Bing Xue and Bingxuan Wang and Bochao
Wu and Chengda Lu and Chenggang Zhao and Chengqi Deng and Chenyu Zhang and Chong Ruan and
Damai Dai and Daya Guo and Dejian Yang and Deli Chen and Dongjie Ji and Erhang Li and Fangyun
Lin and Fucong Dai and Fuli Luo and Guangbo Hao and Guanting Chen and Guowei Li and H. Zhang
and Han Bao and Hanwei Xu and Haocheng Wang and Haowei Zhang and Honghui Ding and Huajian Xin
and Huazuo Gao and Hui Li and Hui Qu and J. L. Cai and Jian Liang and Jianzhong Guo and Jiaqi
Ni and Jiashi Li and Jiawei Wang and Jin Chen and Jingchang Chen and Jingyang Yuan and Junjie
Qiu and Junlong Li and Junxiao Song and Kai Dong and Kai Hu and Kaige Gao and Kang Guan and
Kexin Huang and Kuai Yu and Lean Wang and Lecong Zhang and Lei Xu and Leyi Xia and Liang Zhao
and Litong Wang and Liyue Zhang and Meng Li and Miaojun Wang and Mingchuan Zhang and Minghua
Zhang and Minghui Tang and Mingming Li and Ning Tian and Panpan Huang and Peiyi Wang and Peng
Zhang and Qiancheng Wang and Qihao Zhu and Qinyu Chen and Qiushi Du and R. J. Chen and R. L.
Jin and Ruiqi Ge and Ruisong Zhang and Ruizhe Pan and Runji Wang and Runxin Xu and Ruoyu Zhang
and Ruyi Chen and S. S. Li and Shanghao Lu and Shangyan Zhou and Shanhuang Chen and Shaoqing
Wu and Shengfeng Ye and Shengfeng Ye and Shirong Ma and Shiyu Wang and Shuang Zhou and
Shuiping Yu and Shunfeng Zhou and Shuting Pan and T. Wang and Tao Yun and Tian Pei and Tianyu
Sun and W. L. Xiao and Wangding Zeng and Wanjia Zhao and Wei An and Wen Liu and Wenfeng Liang
and Wenjun Gao and Wenqin Yu and Wentao Zhang and X. Q. Li and Xiangyue Jin and Xianzu Wang
and Xiao Bi and Xiaodong Liu and Xiaohan Wang and Xiaojin Shen and Xiaokang Chen and Xiaokang
Zhang and Xiaosha Chen and Xiaotao Nie and Xiaowen Sun and Xiaoxiang Wang and Xin Cheng and
Xin Liu and Xin Xie and Xingchao Liu and Xingkai Yu and Xinnan Song and Xinxia Shan and Xinyi
Zhou and Xinyu Yang and Xinyuan Li and Xuecheng Su and Xuheng Lin and Y. K. Li and Y. Q. Wang
and Y. X. Wei and Y. X. Zhu and Yang Zhang and Yanhong Xu and Yanhong Xu and Yanping Huang and
Yao Li and Yao Zhao and Yaofeng Sun and Yaohui Li and Yaohui Wang and Yi Yu and Yi Zheng and
Yichao Zhang and Yifan Shi and Yiliang Xiong and Ying He and Ying Tang and Yishi Piao and
Yisong Wang and Yixuan Tan and Yiyang Ma and Yiyuan Liu and Yongqiang Guo and Yu Wu and Yuan
Ou and Yuchen Zhu and Yuduan Wang and Yue Gong and Yuheng Zou and Yujia He and Yukun Zha and
Yunfan Xiong and Yunxian Ma and Yuting Yan and Yuxiang Luo and Yuxiang You and Yuxuan Liu and
Yuyang Zhou and Z. F. Wu and Z. Z. Ren and Zehui Ren and Zhangli Sha and Zhe Fu and Zhean Xu
and Zhen Huang and Zhen Zhang and Zhenda Xie and Zhengyan Zhang and Zhewen Hao and Zhibin Gou
and Zhicheng Ma and Zhigang Yan and Zhihong Shao and Zhipeng Xu and Zhiyu Wu and Zhongyu Zhang
and Zhuoshu Li and Zihui Gu and Zijia Zhu and Zijun Liu and Zilin Li and Ziwei Xie and Ziyang
Song and Ziyi Gao and Zizheng Pan},
      year={2024},
      eprint={2412.19437},
      archivePrefix={arXiv},
      primaryClass={cs.CL},
      url={https://arxiv.org/abs/2412.19437},
}

@misc{fortuna2022onpremiseartificialintelligenceservice,
      title={On-Premise Artificial Intelligence as a Service for Small and Medium Size
Setups},
      author={Carolina Fortuna and Din Mu≈°iƒá and Gregor Cerar and Andrej ƒåampa and
Panagiotis Kapsalis and Mihael Mohorƒçiƒç},
      year={2022},
      eprint={2210.06956},
      archivePrefix={arXiv},
      primaryClass={cs.SE},
      url={https://arxiv.org/abs/2210.06956},
}
```

DeepSeek-V3 Technical Report

DeepSeek-AI

research@deepseek.com

Abstract

We present DeepSeek-V3, a strong Mixture-of-Experts (MoE) language model with 671B total parameters with 37B activated for each token. To achieve efficient inference and cost-effective training, DeepSeek-V3 adopts Multi-head Latent Attention (MLA) and DeepSeekMoE architectures, which were thoroughly validated in DeepSeek-V2. Furthermore, DeepSeek-V3 pioneers an auxiliary-loss-free strategy for load balancing and sets a multi-token prediction training objective for stronger performance. We pre-train DeepSeek-V3 on 14.8 trillion diverse and high-quality tokens, followed by Supervised Fine-Tuning and Reinforcement Learning stages to fully harness its capabilities. Comprehensive evaluations reveal that DeepSeek-V3 outperforms other open-source models and achieves performance comparable to leading closed-source models. Despite its excellent performance, DeepSeek-V3 requires only 2.788M H800 GPU hours for its full training. In addition, its training process is remarkably stable. Throughout the entire training process, we did not experience any irrecoverable loss spikes or perform any rollbacks. The model checkpoints are available at `https://github.com/deepseek-ai/DeepSeek-V3`.

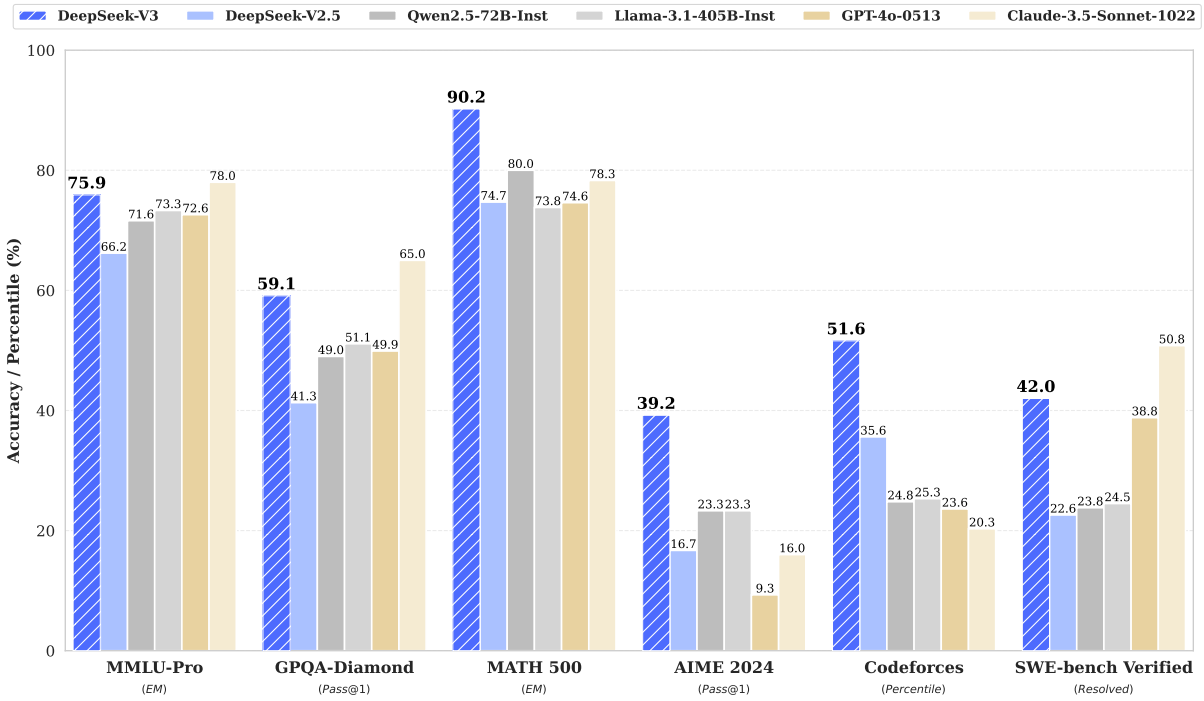

Figure 1 | Benchmark performance of DeepSeek-V3 and its counterparts.

Contents

1. Introduction

In recent years, Large Language Models (LLMs) have been undergoing rapid iteration and evolution (Anthropic, 2024; Google, 2024; OpenAI, 2024a), progressively diminishing the gap towards Artificial General Intelligence (AGI). Beyond closed-source models, open-source models, including DeepSeek series (DeepSeek-AI, 2024a,b,c; Guo et al., 2024), LLaMA series (AI@Meta, 2024a,b; Touvron et al., 2023a,b), Qwen series (Qwen, 2023, 2024a,b), and Mistral series (Jiang et al., 2023; Mistral, 2024), are also making significant strides, endeavoring to close the gap with their closed-source counterparts. To further push the boundaries of open-source model capabilities, we scale up our models and introduce DeepSeek-V3, a large Mixture-of-Experts (MoE) model with 671B parameters, of which 37B are activated for each token.

With a forward-looking perspective, we consistently strive for strong model performance and economical costs. Therefore, in terms of architecture, DeepSeek-V3 still adopts Multi-head Latent Attention (MLA) (DeepSeek-AI, 2024c) for efficient inference and DeepSeekMoE (Dai et al., 2024) for cost-effective training. These two architectures have been validated in DeepSeek-V2 (DeepSeek-AI, 2024c), demonstrating their capability to maintain robust model performance while achieving efficient training and inference. Beyond the basic architecture, we implement two additional strategies to further enhance the model capabilities. Firstly, DeepSeek-V3 pioneers an auxiliary-loss-free strategy (Wang et al., 2024a) for load balancing, with the aim of minimizing the adverse impact on model performance that arises from the effort to encourage load balancing. Secondly, DeepSeek-V3 employs a multi-token prediction training objective, which we have observed to enhance the overall performance on evaluation benchmarks.

In order to achieve efficient training, we support the FP8 mixed precision training and implement comprehensive optimizations for the training framework. Low-precision training has emerged as a promising solution for efficient training (Dettmers et al., 2022; Kalamkar et al., 2019; Narang et al., 2017; Peng et al., 2023b), its evolution being closely tied to advancements in hardware capabilities (Luo et al., 2024; Micikevicius et al., 2022; Rouhani et al., 2023a). In this work, we introduce an FP8 mixed precision training framework and, for the first time, validate its effectiveness on an extremely large-scale model. Through the support for FP8 computation and storage, we achieve both accelerated training and reduced GPU memory usage. As for the training framework, we design the DualPipe algorithm for efficient pipeline parallelism, which has fewer pipeline bubbles and hides most of the communication during training through computation-communication overlap. This overlap ensures that, as the model further scales up, as long as we maintain a constant computation-to-communication ratio, we can still employ fine-grained experts across nodes while achieving a near-zero all-to-all communication overhead. In addition, we also develop efficient cross-node all-to-all communication kernels to fully utilize InfiniBand (IB) and NVLink bandwidths. Furthermore, we meticulously optimize the memory footprint, making it possible to train DeepSeek-V3 without using costly tensor parallelism. Combining these efforts, we achieve high training efficiency.

During pre-training, we train DeepSeek-V3 on 14.8T high-quality and diverse tokens. The pre-training process is remarkably stable. Throughout the entire training process, we did not encounter any irrecoverable loss spikes or have to roll back. Next, we conduct a two-stage context length extension for DeepSeek-V3. In the first stage, the maximum context length is extended to 32K, and in the second stage, it is further extended to 128K. Following this, we conduct post-training, including Supervised Fine-Tuning (SFT) and Reinforcement Learning (RL) on the base model of DeepSeek-V3, to align it with human preferences and further unlock its potential. During the post-training stage, we distill the reasoning capability from the DeepSeek-R1 series of models, and meanwhile carefully maintain the balance between model accuracy

Training Costs	Pre-Training	Context Extension	Post-Training	Total
in H800 GPU Hours	2664K	119K	5K	2788K
in USD	$5.328M	$0.238M	$0.01M	$5.576M

Table 1 | Training costs of DeepSeek-V3, assuming the rental price of H800 is $2 per GPU hour.

and generation length.

We evaluate DeepSeek-V3 on a comprehensive array of benchmarks. Despite its economical training costs, comprehensive evaluations reveal that DeepSeek-V3-Base has emerged as the strongest open-source base model currently available, especially in code and math. Its chat version also outperforms other open-source models and achieves performance comparable to leading closed-source models, including GPT-4o and Claude-3.5-Sonnet, on a series of standard and open-ended benchmarks.

Lastly, we emphasize again the economical training costs of DeepSeek-V3, summarized in Table 1, achieved through our optimized co-design of algorithms, frameworks, and hardware. During the pre-training stage, training DeepSeek-V3 on each trillion tokens requires only 180K H800 GPU hours, i.e., 3.7 days on our cluster with 2048 H800 GPUs. Consequently, our pre-training stage is completed in less than two months and costs 2664K GPU hours. Combined with 119K GPU hours for the context length extension and 5K GPU hours for post-training, DeepSeek-V3 costs only 2.788M GPU hours for its full training. Assuming the rental price of the H800 GPU is $2 per GPU hour, our total training costs amount to only $5.576M. Note that the aforementioned costs include only the official training of DeepSeek-V3, excluding the costs associated with prior research and ablation experiments on architectures, algorithms, or data.

Our main contribution includes:

Architecture: Innovative Load Balancing Strategy and Training Objective

- On top of the efficient architecture of DeepSeek-V2, we pioneer an auxiliary-loss-free strategy for load balancing, which minimizes the performance degradation that arises from encouraging load balancing.
- We investigate a Multi-Token Prediction (MTP) objective and prove it beneficial to model performance. It can also be used for speculative decoding for inference acceleration.

Pre-Training: Towards Ultimate Training Efficiency

- We design an FP8 mixed precision training framework and, for the first time, validate the feasibility and effectiveness of FP8 training on an extremely large-scale model.
- Through the co-design of algorithms, frameworks, and hardware, we overcome the communication bottleneck in cross-node MoE training, achieving near-full computation-communication overlap. This significantly enhances our training efficiency and reduces the training costs, enabling us to further scale up the model size without additional overhead.
- At an economical cost of only 2.664M H800 GPU hours, we complete the pre-training of DeepSeek-V3 on 14.8T tokens, producing the currently strongest open-source base model. The subsequent training stages after pre-training require only 0.1M GPU hours.

Post-Training: Knowledge Distillation from DeepSeek-R1

- We introduce an innovative methodology to distill reasoning capabilities from the long-Chain-of-Thought (CoT) model, specifically from one of the DeepSeek R1 series models, into standard LLMs, particularly DeepSeek-V3. Our pipeline elegantly incorporates the

verification and reflection patterns of R1 into DeepSeek-V3 and notably improves its reasoning performance. Meanwhile, we also maintain control over the output style and length of DeepSeek-V3.

Summary of Core Evaluation Results

- **Knowledge**: (1) On educational benchmarks such as MMLU, MMLU-Pro, and GPQA, DeepSeek-V3 outperforms all other open-source models, achieving 88.5 on MMLU, 75.9 on MMLU-Pro, and 59.1 on GPQA. Its performance is comparable to leading closed-source models like GPT-4o and Claude-Sonnet-3.5, narrowing the gap between open-source and closed-source models in this domain. (2) For factuality benchmarks, DeepSeek-V3 demonstrates superior performance among open-source models on both SimpleQA and Chinese SimpleQA. While it trails behind GPT-4o and Claude-Sonnet-3.5 in English factual knowledge (SimpleQA), it surpasses these models in Chinese factual knowledge (Chinese SimpleQA), highlighting its strength in Chinese factual knowledge.
- **Code, Math, and Reasoning**: (1) DeepSeek-V3 achieves state-of-the-art performance on math-related benchmarks among all non-long-CoT open-source and closed-source models. Notably, it even outperforms o1-preview on specific benchmarks, such as MATH-500, demonstrating its robust mathematical reasoning capabilities. (2) On coding-related tasks, DeepSeek-V3 emerges as the top-performing model for coding competition benchmarks, such as LiveCodeBench, solidifying its position as the leading model in this domain. For engineering-related tasks, while DeepSeek-V3 performs slightly below Claude-Sonnet-3.5, it still outpaces all other models by a significant margin, demonstrating its competitiveness across diverse technical benchmarks.

In the remainder of this paper, we first present a detailed exposition of our DeepSeek-V3 model architecture (Section 2). Subsequently, we introduce our infrastructures, encompassing our compute clusters, the training framework, the support for FP8 training, the inference deployment strategy, and our suggestions on future hardware design. Next, we describe our pre-training process, including the construction of training data, hyper-parameter settings, long-context extension techniques, the associated evaluations, as well as some discussions (Section 4). Thereafter, we discuss our efforts on post-training, which include Supervised Fine-Tuning (SFT), Reinforcement Learning (RL), the corresponding evaluations, and discussions (Section 5). Lastly, we conclude this work, discuss existing limitations of DeepSeek-V3, and propose potential directions for future research (Section 6).

2. Architecture

We first introduce the basic architecture of DeepSeek-V3, featured by Multi-head Latent Attention (MLA) (DeepSeek-AI, 2024c) for efficient inference and DeepSeekMoE (Dai et al., 2024) for economical training. Then, we present a Multi-Token Prediction (MTP) training objective, which we have observed to enhance the overall performance on evaluation benchmarks. For other minor details not explicitly mentioned, DeepSeek-V3 adheres to the settings of DeepSeek-V2 (DeepSeek-AI, 2024c).

2.1. Basic Architecture

The basic architecture of DeepSeek-V3 is still within the Transformer (Vaswani et al., 2017) framework. For efficient inference and economical training, DeepSeek-V3 also adopts MLA and DeepSeekMoE, which have been thoroughly validated by DeepSeek-V2. Compared with DeepSeek-V2, an exception is that we additionally introduce an auxiliary-loss-free load balancing

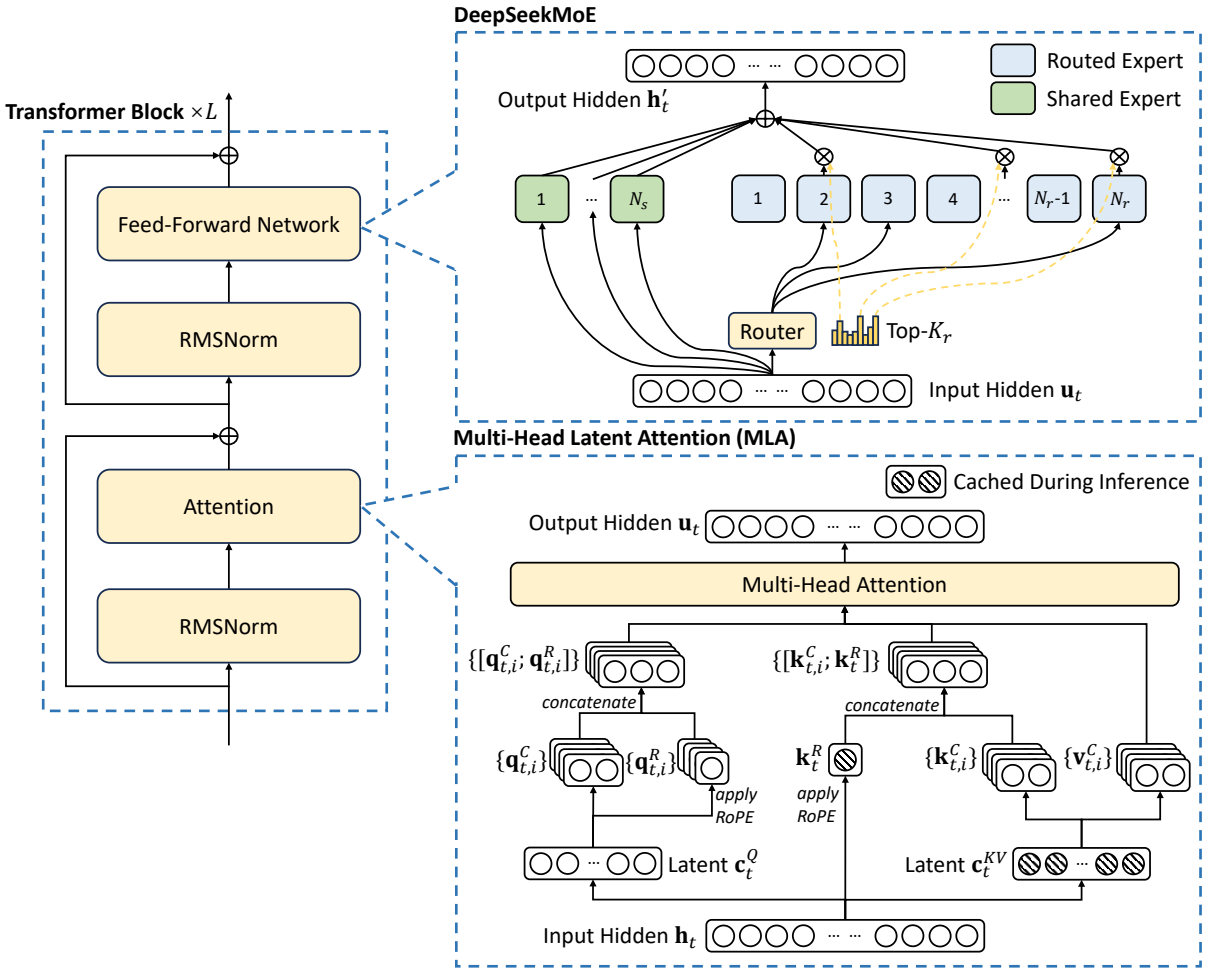

Figure 2 | Illustration of the basic architecture of DeepSeek-V3. Following DeepSeek-V2, we adopt MLA and DeepSeekMoE for efficient inference and economical training.

strategy (Wang et al., 2024a) for DeepSeekMoE to mitigate the performance degradation induced by the effort to ensure load balance. Figure 2 illustrates the basic architecture of DeepSeek-V3, and we will briefly review the details of MLA and DeepSeekMoE in this section.

2.1.1. *Multi-Head Latent Attention*

For attention, DeepSeek-V3 adopts the MLA architecture. Let d denote the embedding dimension, n_h denote the number of attention heads, d_h denote the dimension per head, and $\mathbf{h}_t \in \mathbb{R}^d$ denote the attention input for the t-th token at a given attention layer. The core of MLA is the low-rank joint compression for attention keys and values to reduce Key-Value (KV) cache during inference:

$$\boxed{\mathbf{c}_t^{KV}} = W^{DKV}\mathbf{h}_t, \tag{1}$$

$$[\mathbf{k}_{t,1}^C; \mathbf{k}_{t,2}^C; ...; \mathbf{k}_{t,n_h}^C] = \mathbf{k}_t^C = W^{UK}\mathbf{c}_t^{KV}, \tag{2}$$

$$\boxed{\mathbf{k}_t^R} = \mathrm{RoPE}(W^{KR}\mathbf{h}_t), \tag{3}$$

$$\mathbf{k}_{t,i} = [\mathbf{k}_{t,i}^C; \mathbf{k}_t^R], \tag{4}$$

$$[\mathbf{v}_{t,1}^C; \mathbf{v}_{t,2}^C; ...; \mathbf{v}_{t,n_h}^C] = \mathbf{v}_t^C = W^{UV}\mathbf{c}_t^{KV}, \tag{5}$$

where $\mathbf{c}_t^{KV} \in \mathbb{R}^{d_c}$ is the compressed latent vector for keys and values; $d_c (\ll d_h n_h)$ indicates the KV compression dimension; $W^{DKV} \in \mathbb{R}^{d_c \times d}$ denotes the down-projection matrix; $W^{UK}, W^{UV} \in \mathbb{R}^{d_h n_h \times d_c}$ are the up-projection matrices for keys and values, respectively; $W^{KR} \in \mathbb{R}^{d_h^R \times d}$ is the matrix used to produce the decoupled key that carries Rotary Positional Embedding (RoPE) (Su et al., 2024); $\mathrm{RoPE}(\cdot)$ denotes the operation that applies RoPE matrices; and $[\cdot;\cdot]$ denotes concatenation. Note that for MLA, only the blue-boxed vectors (i.e., $\mathbf{c}_t^{KV}$ and $\mathbf{k}_t^R$) need to be cached during generation, which results in significantly reduced KV cache while maintaining performance comparable to standard Multi-Head Attention (MHA) (Vaswani et al., 2017).

For the attention queries, we also perform a low-rank compression, which can reduce the activation memory during training:

$$\mathbf{c}_t^Q = W^{DQ}\mathbf{h}_t, \tag{6}$$

$$[\mathbf{q}_{t,1}^C; \mathbf{q}_{t,2}^C; ...; \mathbf{q}_{t,n_h}^C] = \mathbf{q}_t^C = W^{UQ}\mathbf{c}_t^Q, \tag{7}$$

$$[\mathbf{q}_{t,1}^R; \mathbf{q}_{t,2}^R; ...; \mathbf{q}_{t,n_h}^R] = \mathbf{q}_t^R = \mathrm{RoPE}(W^{QR}\mathbf{c}_t^Q), \tag{8}$$

$$\mathbf{q}_{t,i} = [\mathbf{q}_{t,i}^C; \mathbf{q}_{t,i}^R], \tag{9}$$

where $\mathbf{c}_t^Q \in \mathbb{R}^{d_c'}$ is the compressed latent vector for queries; $d_c' (\ll d_h n_h)$ denotes the query compression dimension; $W^{DQ} \in \mathbb{R}^{d_c' \times d}, W^{UQ} \in \mathbb{R}^{d_h n_h \times d_c'}$ are the down-projection and up-projection matrices for queries, respectively; and $W^{QR} \in \mathbb{R}^{d_h^R n_h \times d_c'}$ is the matrix to produce the decoupled queries that carry RoPE.

Ultimately, the attention queries ($\mathbf{q}_{t,i}$), keys ($\mathbf{k}_{j,i}$), and values ($\mathbf{v}_{j,i}^C$) are combined to yield the final attention output $\mathbf{u}_t$:

$$\mathbf{o}_{t,i} = \sum_{j=1}^{t} \mathrm{Softmax}_j\left(\frac{\mathbf{q}_{t,i}^T \mathbf{k}_{j,i}}{\sqrt{d_h + d_h^R}}\right)\mathbf{v}_{j,i}^C, \tag{10}$$

$$\mathbf{u}_t = W^O[\mathbf{o}_{t,1}; \mathbf{o}_{t,2}; ...; \mathbf{o}_{t,n_h}], \tag{11}$$

where $W^O \in \mathbb{R}^{d \times d_h n_h}$ denotes the output projection matrix.

2.1.2. *DeepSeekMoE with Auxiliary-Loss-Free Load Balancing*

Basic Architecture of DeepSeekMoE. For Feed-Forward Networks (FFNs), DeepSeek-V3 employs the DeepSeekMoE architecture (Dai et al., 2024). Compared with traditional MoE architectures like GShard (Lepikhin et al., 2021), DeepSeekMoE uses finer-grained experts and isolates some experts as shared ones. Let $\mathbf{u}_t$ denote the FFN input of the t-th token, we compute the FFN output $\mathbf{h}_t'$ as follows:

$$\mathbf{h}_t' = \mathbf{u}_t + \sum_{i=1}^{N_s} \mathrm{FFN}_i^{(s)}(\mathbf{u}_t) + \sum_{i=1}^{N_r} g_{i,t}\,\mathrm{FFN}_i^{(r)}(\mathbf{u}_t), \tag{12}$$

$$g_{i,t} = \frac{g_{i,t}'}{\sum_{j=1}^{N_r} g_{j,t}'}, \tag{13}$$

$$g_{i,t}' = \begin{cases} s_{i,t}, & s_{i,t} \in \mathrm{Topk}(\{s_{j,t} | 1 \leqslant j \leqslant N_r\}, K_r), \\ 0, & \text{otherwise}, \end{cases} \tag{14}$$

$$s_{i,t} = \mathrm{Sigmoid}\left(\mathbf{u}_t{}^T \mathbf{e}_i\right), \tag{15}$$

where N_s and N_r denote the numbers of shared experts and routed experts, respectively; $\mathrm{FFN}_i^{(s)}(\cdot)$ and $\mathrm{FFN}_i^{(r)}(\cdot)$ denote the i-th shared expert and the i-th routed expert, respectively; K_r denotes the number of activated routed experts; $g_{i,t}$ is the gating value for the i-th expert; $s_{i,t}$ is the token-to-expert affinity; $\mathbf{e}_i$ is the centroid vector of the i-th routed expert; and $\mathrm{Topk}(\cdot, K)$ denotes the set comprising K highest scores among the affinity scores calculated for the t-th token and all routed experts. Slightly different from DeepSeek-V2, DeepSeek-V3 uses the sigmoid function to compute the affinity scores, and applies a normalization among all selected affinity scores to produce the gating values.

Auxiliary-Loss-Free Load Balancing. For MoE models, an unbalanced expert load will lead to routing collapse (Shazeer et al., 2017) and diminish computational efficiency in scenarios with expert parallelism. Conventional solutions usually rely on the auxiliary loss (Fedus et al., 2021; Lepikhin et al., 2021) to avoid unbalanced load. However, too large an auxiliary loss will impair the model performance (Wang et al., 2024a). To achieve a better trade-off between load balance and model performance, we pioneer an auxiliary-loss-free load balancing strategy (Wang et al., 2024a) to ensure load balance. To be specific, we introduce a bias term b_i for each expert and add it to the corresponding affinity scores $s_{i,t}$ to determine the top-K routing:

$$g'_{i,t} = \begin{cases} s_{i,t}, & s_{i,t} + b_i \in \mathrm{Topk}(\{s_{j,t} + b_j | 1 \leqslant j \leqslant N_r\}, K_r), \\ 0, & \text{otherwise.} \end{cases} \tag{16}$$

Note that the bias term is only used for routing. The gating value, which will be multiplied with the FFN output, is still derived from the original affinity score $s_{i,t}$. During training, we keep monitoring the expert load on the whole batch of each training step. At the end of each step, we will decrease the bias term by γ if its corresponding expert is overloaded, and increase it by γ if its corresponding expert is underloaded, where γ is a hyper-parameter called bias update speed. Through the dynamic adjustment, DeepSeek-V3 keeps balanced expert load during training, and achieves better performance than models that encourage load balance through pure auxiliary losses.

Complementary Sequence-Wise Auxiliary Loss. Although DeepSeek-V3 mainly relies on the auxiliary-loss-free strategy for load balance, to prevent extreme imbalance within any single sequence, we also employ a complementary sequence-wise balance loss:

$$\mathcal{L}_{\mathrm{Bal}} = \alpha \sum_{i=1}^{N_r} f_i P_i, \tag{17}$$

$$f_i = \frac{N_r}{K_r T} \sum_{t=1}^{T} \mathbb{1}\left(s_{i,t} \in \mathrm{Topk}(\{s_{j,t} | 1 \leqslant j \leqslant N_r\}, K_r)\right), \tag{18}$$

$$s'_{i,t} = \frac{s_{i,t}}{\sum_{j=1}^{N_r} s_{j,t}}, \tag{19}$$

$$P_i = \frac{1}{T} \sum_{t=1}^{T} s'_{i,t}, \tag{20}$$

where the balance factor α is a hyper-parameter, which will be assigned an extremely small value for DeepSeek-V3; $\mathbb{1}(\cdot)$ denotes the indicator function; and T denotes the number of tokens in a sequence. The sequence-wise balance loss encourages the expert load on each sequence to be balanced.

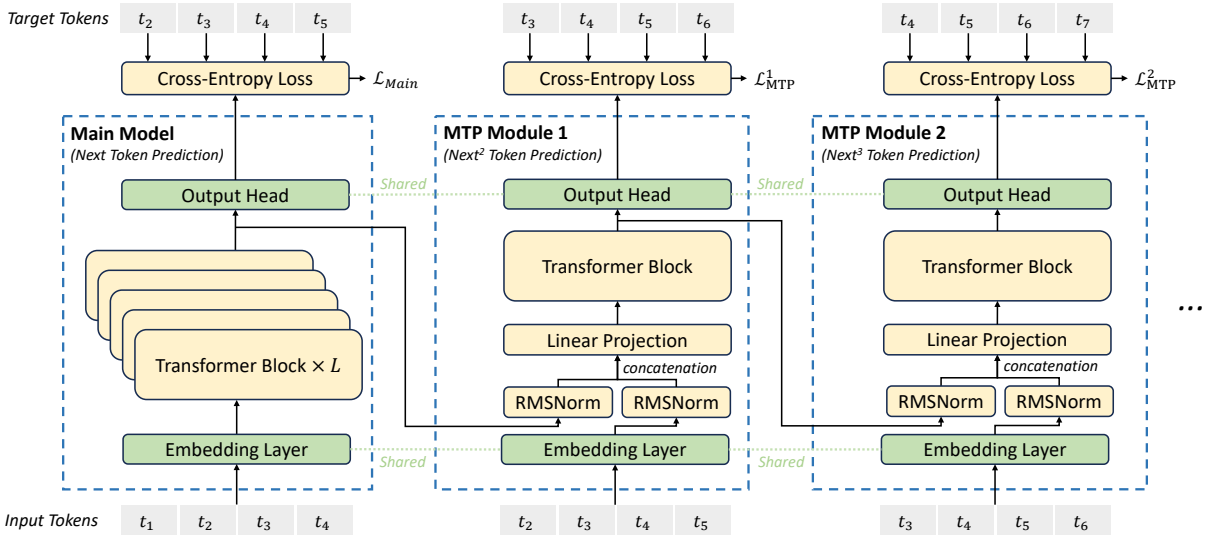

Figure 3 | Illustration of our Multi-Token Prediction (MTP) implementation. We keep the complete causal chain for the prediction of each token at each depth.

Node-Limited Routing. Like the device-limited routing used by DeepSeek-V2, DeepSeek-V3 also uses a restricted routing mechanism to limit communication costs during training. In short, we ensure that each token will be sent to at most M nodes, which are selected according to the sum of the highest $\frac{K_r}{M}$ affinity scores of the experts distributed on each node. Under this constraint, our MoE training framework can nearly achieve full computation-communication overlap.

No Token-Dropping. Due to the effective load balancing strategy, DeepSeek-V3 keeps a good load balance during its full training. Therefore, DeepSeek-V3 does not drop any tokens during training. In addition, we also implement specific deployment strategies to ensure inference load balance, so DeepSeek-V3 also does not drop tokens during inference.

2.2. Multi-Token Prediction

Inspired by Gloeckle et al. (2024), we investigate and set a Multi-Token Prediction (MTP) objective for DeepSeek-V3, which extends the prediction scope to multiple future tokens at each position. On the one hand, an MTP objective densifies the training signals and may improve data efficiency. On the other hand, MTP may enable the model to pre-plan its representations for better prediction of future tokens. Figure 3 illustrates our implementation of MTP. Different from Gloeckle et al. (2024), which parallelly predicts D additional tokens using independent output heads, we sequentially predict additional tokens and keep the complete causal chain at each prediction depth. We introduce the details of our MTP implementation in this section.

MTP Modules. To be specific, our MTP implementation uses D sequential modules to predict D additional tokens. The k-th MTP module consists of a shared embedding layer $\mathrm{Emb}(\cdot)$, a shared output head $\mathrm{OutHead}(\cdot)$, a Transformer block $\mathrm{TRM}_k(\cdot)$, and a projection matrix $M_k \in \mathbb{R}^{d \times 2d}$. For the i-th input token t_i, at the k-th prediction depth, we first combine the representation of the i-th token at the $(k-1)$-th depth $\mathbf{h}_i^{k-1} \in \mathbb{R}^d$ and the embedding of the $(i+k)$-th token $Emb(t_{i+k}) \in \mathbb{R}^d$

with the linear projection:

$$\mathbf{h}_i'^k = M_k[\text{RMSNorm}(\mathbf{h}_i^{k-1}); \text{RMSNorm}(\text{Emb}(t_{i+k}))], \tag{21}$$

where $[\cdot;\cdot]$ denotes concatenation. Especially, when $k = 1$, $\mathbf{h}_i^{k-1}$ refers to the representation given by the main model. Note that for each MTP module, its embedding layer is shared with the main model. The combined $\mathbf{h}_i'^k$ serves as the input of the Transformer block at the k-th depth to produce the output representation at the current depth $\mathbf{h}_i^k$:

$$\mathbf{h}_{1:T-k}^k = \text{TRM}_k(\mathbf{h}_{1:T-k}'^k), \tag{22}$$

where T represents the input sequence length and $_{i:j}$ denotes the slicing operation (inclusive of both the left and right boundaries). Finally, taking $\mathbf{h}_i^k$ as the input, the shared output head will compute the probability distribution for the k-th additional prediction token $P_{i+1+k}^k \in \mathbb{R}^V$, where V is the vocabulary size:

$$P_{i+k+1}^k = \text{OutHead}(\mathbf{h}_i^k). \tag{23}$$

The output head $\text{OutHead}(\cdot)$ linearly maps the representation to logits and subsequently applies the $\text{Softmax}(\cdot)$ function to compute the prediction probabilities of the k-th additional token. Also, for each MTP module, its output head is shared with the main model. Our principle of maintaining the causal chain of predictions is similar to that of EAGLE (Li et al., 2024b), but its primary objective is speculative decoding (Leviathan et al., 2023; Xia et al., 2023), whereas we utilize MTP to improve training.

MTP Training Objective. For each prediction depth, we compute a cross-entropy loss $\mathcal{L}_{\text{MTP}}^k$:

$$\mathcal{L}_{\text{MTP}}^k = \text{CrossEntropy}(P_{2+k:T+1}^k, t_{2+k:T+1}) = -\frac{1}{T}\sum_{i=2+k}^{T+1} \log P_i^k[t_i], \tag{24}$$

where T denotes the input sequence length, t_i denotes the ground-truth token at the i-th position, and $P_i^k[t_i]$ denotes the corresponding prediction probability of t_i, given by the k-th MTP module. Finally, we compute the average of the MTP losses across all depths and multiply it by a weighting factor λ to obtain the overall MTP loss $\mathcal{L}_{\text{MTP}}$, which serves as an additional training objective for DeepSeek-V3:

$$\mathcal{L}_{\text{MTP}} = \frac{\lambda}{D}\sum_{k=1}^{D} \mathcal{L}_{\text{MTP}}^k. \tag{25}$$

MTP in Inference. Our MTP strategy mainly aims to improve the performance of the main model, so during inference, we can directly discard the MTP modules and the main model can function independently and normally. Additionally, we can also repurpose these MTP modules for speculative decoding to further improve the generation latency.

3. Infrastructures

3.1. Compute Clusters

DeepSeek-V3 is trained on a cluster equipped with 2048 NVIDIA H800 GPUs. Each node in the H800 cluster contains 8 GPUs connected by NVLink and NVSwitch within nodes. Across different nodes, InfiniBand (IB) interconnects are utilized to facilitate communications.

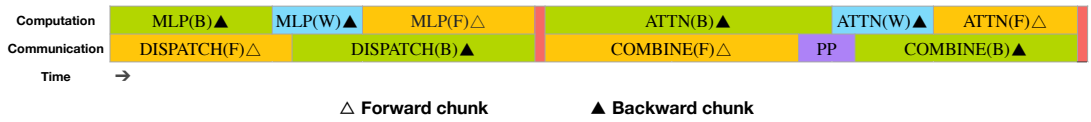

Figure 4 | Overlapping strategy for a pair of individual forward and backward chunks (the boundaries of the transformer blocks are not aligned). Orange denotes forward, green denotes "backward for input", blue denotes "backward for weights", purple denotes PP communication, and red denotes barriers. Both all-to-all and PP communication can be fully hidden.

3.2. Training Framework

The training of DeepSeek-V3 is supported by the HAI-LLM framework, an efficient and lightweight training framework crafted by our engineers from the ground up. On the whole, DeepSeek-V3 applies 16-way Pipeline Parallelism (PP) (Qi et al., 2023a), 64-way Expert Parallelism (EP) (Lepikhin et al., 2021) spanning 8 nodes, and ZeRO-1 Data Parallelism (DP) (Rajbhandari et al., 2020).

In order to facilitate efficient training of DeepSeek-V3, we implement meticulous engineering optimizations. Firstly, we design the DualPipe algorithm for efficient pipeline parallelism. Compared with existing PP methods, DualPipe has fewer pipeline bubbles. More importantly, it overlaps the computation and communication phases across forward and backward processes, thereby addressing the challenge of heavy communication overhead introduced by cross-node expert parallelism. Secondly, we develop efficient cross-node all-to-all communication kernels to fully utilize IB and NVLink bandwidths and conserve Streaming Multiprocessors (SMs) dedicated to communication. Finally, we meticulously optimize the memory footprint during training, thereby enabling us to train DeepSeek-V3 without using costly Tensor Parallelism (TP).

3.2.1. DualPipe and Computation-Communication Overlap

For DeepSeek-V3, the communication overhead introduced by cross-node expert parallelism results in an inefficient computation-to-communication ratio of approximately 1:1. To tackle this challenge, we design an innovative pipeline parallelism algorithm called DualPipe, which not only accelerates model training by effectively overlapping forward and backward computation-communication phases, but also reduces the pipeline bubbles.

The key idea of DualPipe is to overlap the computation and communication within a pair of individual forward and backward chunks. To be specific, we divide each chunk into four components: `attention`, `all-to-all dispatch`, `MLP`, and `all-to-all combine`. Specially, for a backward chunk, both `attention` and `MLP` are further split into two parts, `backward for input` and `backward for weights`, like in ZeroBubble (Qi et al., 2023b). In addition, we have a `PP communication` component. As illustrated in Figure 4, for a pair of forward and backward chunks, we rearrange these components and manually adjust the ratio of GPU SMs dedicated to communication versus computation. In this overlapping strategy, we can ensure that both all-to-all and PP communication can be fully hidden during execution. Given the efficient overlapping strategy, the full DualPipe scheduling is illustrated in Figure 5. It employs a bidirectional pipeline scheduling, which feeds micro-batches from both ends of the pipeline simultaneously and a significant portion of communications can be fully overlapped. This overlap also ensures that, as the model further scales up, as long as we maintain a constant computation-to-communication ratio, we can still employ fine-grained experts across nodes while achieving a near-zero all-to-all communication overhead.

Figure 5 | Example DualPipe scheduling for 8 PP ranks and 20 micro-batches in two directions. The micro-batches in the reverse direction are symmetric to those in the forward direction, so we omit their batch ID for illustration simplicity. Two cells enclosed by a shared black border have mutually overlapped computation and communication.

Method	Bubble	Parameter	Activation
1F1B	$(PP-1)(F+B)$	$1\times$	PP
ZB1P	$(PP-1)(F+B-2W)$	$1\times$	PP
DualPipe (Ours)	$(\frac{PP}{2}-1)(F\&B+B-3W)$	$2\times$	$PP+1$

Table 2 | Comparison of pipeline bubbles and memory usage across different pipeline parallel methods. F denotes the execution time of a forward chunk, B denotes the execution time of a full backward chunk, W denotes the execution time of a "backward for weights" chunk, and $F\&B$ denotes the execution time of two mutually overlapped forward and backward chunks.

In addition, even in more general scenarios without a heavy communication burden, DualPipe still exhibits efficiency advantages. In Table 2, we summarize the pipeline bubbles and memory usage across different PP methods. As shown in the table, compared with ZB1P (Qi et al., 2023b) and 1F1B (Harlap et al., 2018), DualPipe significantly reduces the pipeline bubbles while only increasing the peak activation memory by $\frac{1}{PP}$ times. Although DualPipe requires keeping two copies of the model parameters, this does not significantly increase the memory consumption since we use a large EP size during training. Compared with Chimera (Li and Hoefler, 2021), DualPipe only requires that the pipeline stages and micro-batches be divisible by 2, without requiring micro-batches to be divisible by pipeline stages. In addition, for DualPipe, neither the bubbles nor activation memory will increase as the number of micro-batches grows.

3.2.2. *Efficient Implementation of Cross-Node All-to-All Communication*

In order to ensure sufficient computational performance for DualPipe, we customize efficient cross-node all-to-all communication kernels (including dispatching and combining) to conserve the number of SMs dedicated to communication. The implementation of the kernels is co-designed with the MoE gating algorithm and the network topology of our cluster. To be specific, in our cluster, cross-node GPUs are fully interconnected with IB, and intra-node communications are handled via NVLink. NVLink offers a bandwidth of 160 GB/s, roughly 3.2 times that of IB (50 GB/s). To effectively leverage the different bandwidths of IB and NVLink, we limit each token to be dispatched to at most 4 nodes, thereby reducing IB traffic. For each token, when its routing decision is made, it will first be transmitted via IB to the GPUs with the same in-node index on its target nodes. Once it reaches the target nodes, we will endeavor to ensure that it is instantaneously forwarded via NVLink to specific GPUs that host their target experts, without being blocked by subsequently arriving tokens. In this way, communications via IB and NVLink are fully overlapped, and each token can efficiently select an average of 3.2 experts per node without incurring additional overhead from NVLink. This implies that, although DeepSeek-V3

selects only 8 routed experts in practice, it can scale up this number to a maximum of 13 experts (4 nodes × 3.2 experts/node) while preserving the same communication cost. Overall, under such a communication strategy, only 20 SMs are sufficient to fully utilize the bandwidths of IB and NVLink.

In detail, we employ the warp specialization technique (Bauer et al., 2014) and partition 20 SMs into 10 communication channels. During the dispatching process, (1) IB sending, (2) IB-to-NVLink forwarding, and (3) NVLink receiving are handled by respective warps. The number of warps allocated to each communication task is dynamically adjusted according to the actual workload across all SMs. Similarly, during the combining process, (1) NVLink sending, (2) NVLink-to-IB forwarding and accumulation, and (3) IB receiving and accumulation are also handled by dynamically adjusted warps. In addition, both dispatching and combining kernels overlap with the computation stream, so we also consider their impact on other SM computation kernels. Specifically, we employ customized PTX (Parallel Thread Execution) instructions and auto-tune the communication chunk size, which significantly reduces the use of the L2 cache and the interference to other SMs.

3.2.3. Extremely Memory Saving with Minimal Overhead

In order to reduce the memory footprint during training, we employ the following techniques.

Recomputation of RMSNorm and MLA Up-Projection. We recompute all RMSNorm operations and MLA up-projections during back-propagation, thereby eliminating the need to persistently store their output activations. With a minor overhead, this strategy significantly reduces memory requirements for storing activations.

Exponential Moving Average in CPU. During training, we preserve the Exponential Moving Average (EMA) of the model parameters for early estimation of the model performance after learning rate decay. The EMA parameters are stored in CPU memory and are updated asynchronously after each training step. This method allows us to maintain EMA parameters without incurring additional memory or time overhead.

Shared Embedding and Output Head for Multi-Token Prediction. With the DualPipe strategy, we deploy the shallowest layers (including the embedding layer) and deepest layers (including the output head) of the model on the same PP rank. This arrangement enables the physical sharing of parameters and gradients, of the shared embedding and output head, between the MTP module and the main model. This physical sharing mechanism further enhances our memory efficiency.

3.3. FP8 Training

Inspired by recent advances in low-precision training (Dettmers et al., 2022; Noune et al., 2022; Peng et al., 2023b), we propose a fine-grained mixed precision framework utilizing the FP8 data format for training DeepSeek-V3. While low-precision training holds great promise, it is often limited by the presence of outliers in activations, weights, and gradients (Fishman et al., 2024; He et al.; Sun et al., 2024). Although significant progress has been made in inference quantization (Frantar et al., 2022; Xiao et al., 2023), there are relatively few studies demonstrating successful application of low-precision techniques in large-scale language model

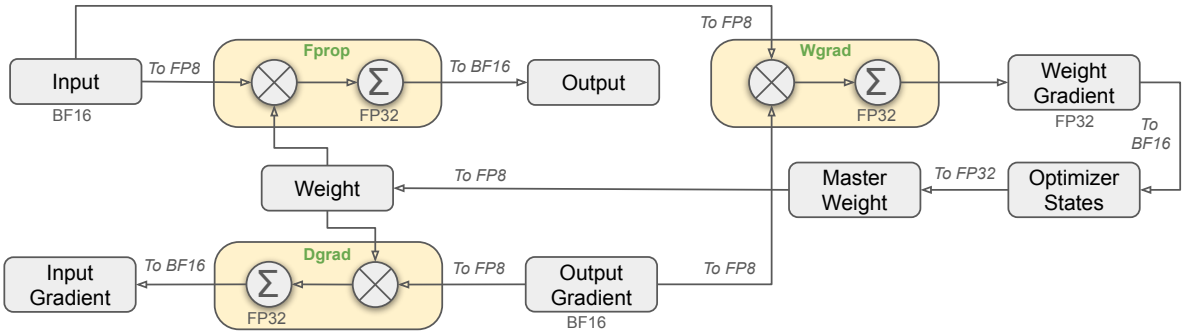

Figure 6 | The overall mixed precision framework with FP8 data format. For clarification, only the `Linear` operator is illustrated.

pre-training (Fishman et al., 2024). To address this challenge and effectively extend the dynamic range of the FP8 format, we introduce a fine-grained quantization strategy: tile-wise grouping with $1 \times N_c$ elements or block-wise grouping with $N_c \times N_c$ elements. The associated dequantization overhead is largely mitigated under our increased-precision accumulation process, a critical aspect for achieving accurate FP8 General Matrix Multiplication (GEMM). Moreover, to further reduce memory and communication overhead in MoE training, we cache and dispatch activations in FP8, while storing low-precision optimizer states in BF16. We validate the proposed FP8 mixed precision framework on two model scales similar to DeepSeek-V2-Lite and DeepSeek-V2, training for approximately 1 trillion tokens (see more details in Appendix B.1). Notably, compared with the BF16 baseline, the relative loss error of our FP8-training model remains consistently below 0.25%, a level well within the acceptable range of training randomness.

3.3.1. Mixed Precision Framework

Building upon widely adopted techniques in low-precision training (Kalamkar et al., 2019; Narang et al., 2017), we propose a mixed precision framework for FP8 training. In this framework, most compute-density operations are conducted in FP8, while a few key operations are strategically maintained in their original data formats to balance training efficiency and numerical stability. The overall framework is illustrated in Figure 6.

Firstly, in order to accelerate model training, the majority of core computation kernels, i.e., GEMM operations, are implemented in FP8 precision. These GEMM operations accept FP8 tensors as inputs and produce outputs in BF16 or FP32. As depicted in Figure 6, all three GEMMs associated with the `Linear` operator, namely `Fprop` (forward pass), `Dgrad` (activation backward pass), and `Wgrad` (weight backward pass), are executed in FP8. This design theoretically doubles the computational speed compared with the original BF16 method. Additionally, the FP8 `Wgrad` GEMM allows activations to be stored in FP8 for use in the backward pass. This significantly reduces memory consumption.

Despite the efficiency advantage of the FP8 format, certain operators still require a higher precision due to their sensitivity to low-precision computations. Besides, some low-cost operators can also utilize a higher precision with a negligible overhead to the overall training cost. For this reason, after careful investigations, we maintain the original precision (e.g., BF16 or FP32) for the following components: the embedding module, the output head, MoE gating modules, normalization operators, and attention operators. These targeted retentions of high precision ensure stable training dynamics for DeepSeek-V3. To further guarantee numerical stability, we store the master weights, weight gradients, and optimizer states in higher precision. While

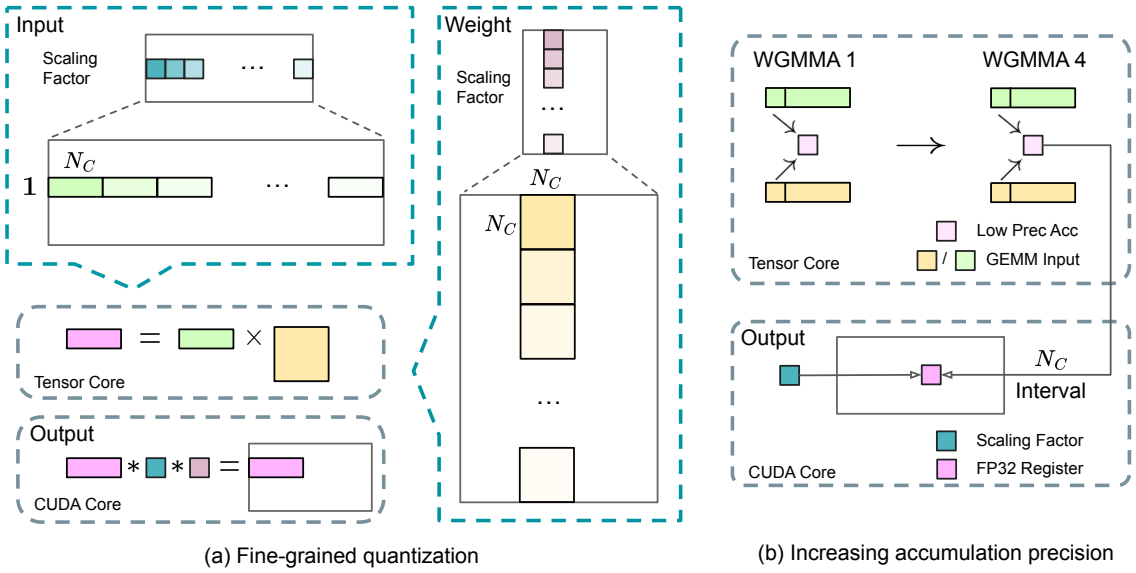

(a) Fine-grained quantization

(b) Increasing accumulation precision

Figure 7 | (a) We propose a fine-grained quantization method to mitigate quantization errors caused by feature outliers; for illustration simplicity, only `Fprop` is illustrated. (b) In conjunction with our quantization strategy, we improve the FP8 GEMM precision by promoting to CUDA Cores at an interval of $N_C = 128$ elements MMA for the high-precision accumulation.

these high-precision components incur some memory overheads, their impact can be minimized through efficient sharding across multiple DP ranks in our distributed training system.

3.3.2. *Improved Precision from Quantization and Multiplication*

Based on our mixed precision FP8 framework, we introduce several strategies to enhance low-precision training accuracy, focusing on both the quantization method and the multiplication process.

Fine-Grained Quantization. In low-precision training frameworks, overflows and underflows are common challenges due to the limited dynamic range of the FP8 format, which is constrained by its reduced exponent bits. As a standard practice, the input distribution is aligned to the representable range of the FP8 format by scaling the maximum absolute value of the input tensor to the maximum representable value of FP8 (Narang et al., 2017). This method makes low-precision training highly sensitive to activation outliers, which can heavily degrade quantization accuracy. To solve this, we propose a fine-grained quantization method that applies scaling at a more granular level. As illustrated in Figure 7 (a), (1) for activations, we group and scale elements on a `1x128` tile basis (i.e., per token per 128 channels); and (2) for weights, we group and scale elements on a `128x128` block basis (i.e., per 128 input channels per 128 output channels). This approach ensures that the quantization process can better accommodate outliers by adapting the scale according to smaller groups of elements. In Appendix B.2, we further discuss the training instability when we group and scale activations on a block basis in the same way as weights quantization.

One key modification in our method is the introduction of per-group scaling factors along the inner dimension of GEMM operations. This functionality is not directly supported in the standard FP8 GEMM. However, combined with our precise FP32 accumulation strategy, it can

be efficiently implemented.

Notably, our fine-grained quantization strategy is highly consistent with the idea of microscaling formats (Rouhani et al., 2023b), while the Tensor Cores of NVIDIA next-generation GPUs (Blackwell series) have announced the support for microscaling formats with smaller quantization granularity (NVIDIA, 2024a). We hope our design can serve as a reference for future work to keep pace with the latest GPU architectures.

Increasing Accumulation Precision. Low-precision GEMM operations often suffer from underflow issues, and their accuracy largely depends on high-precision accumulation, which is commonly performed in an FP32 precision (Kalamkar et al., 2019; Narang et al., 2017). However, we observe that the accumulation precision of FP8 GEMM on NVIDIA H800 GPUs is limited to retaining around 14 bits, which is significantly lower than FP32 accumulation precision. This problem will become more pronounced when the inner dimension `K` is large (Wortsman et al., 2023), a typical scenario in large-scale model training where the batch size and model width are increased. Taking GEMM operations of two random matrices with `K` = 4096 for example, in our preliminary test, the limited accumulation precision in Tensor Cores results in a maximum relative error of nearly 2%. Despite these problems, the limited accumulation precision is still the default option in a few FP8 frameworks (NVIDIA, 2024b), severely constraining the training accuracy.

In order to address this issue, we adopt the strategy of promotion to CUDA Cores for higher precision (Thakkar et al., 2023). The process is illustrated in Figure 7 (b). To be specific, during MMA (Matrix Multiply-Accumulate) execution on Tensor Cores, intermediate results are accumulated using the limited bit width. Once an interval of N_C is reached, these partial results will be copied to FP32 registers on CUDA Cores, where full-precision FP32 accumulation is performed. As mentioned before, our fine-grained quantization applies per-group scaling factors along the inner dimension `K`. These scaling factors can be efficiently multiplied on the CUDA Cores as the dequantization process with minimal additional computational cost.

It is worth noting that this modification reduces the WGMMA (Warpgroup-level Matrix Multiply-Accumulate) instruction issue rate for a single warpgroup. However, on the H800 architecture, it is typical for two WGMMA to persist concurrently: while one warpgroup performs the promotion operation, the other is able to execute the MMA operation. This design enables overlapping of the two operations, maintaining high utilization of Tensor Cores. Based on our experiments, setting $N_C = 128$ elements, equivalent to 4 WGMMAs, represents the minimal accumulation interval that can significantly improve precision without introducing substantial overhead.

Mantissa over Exponents. In contrast to the hybrid FP8 format adopted by prior work (NVIDIA, 2024b; Peng et al., 2023b; Sun et al., 2019b), which uses `E4M3` (4-bit exponent and 3-bit mantissa) in `Fprop` and `E5M2` (5-bit exponent and 2-bit mantissa) in `Dgrad` and `Wgrad`, we adopt the `E4M3` format on all tensors for higher precision. We attribute the feasibility of this approach to our fine-grained quantization strategy, i.e., tile and block-wise scaling. By operating on smaller element groups, our methodology effectively shares exponent bits among these grouped elements, mitigating the impact of the limited dynamic range.

Online Quantization. Delayed quantization is employed in tensor-wise quantization frameworks (NVIDIA, 2024b; Peng et al., 2023b), which maintains a history of the maximum absolute

values across prior iterations to infer the current value. In order to ensure accurate scales and simplify the framework, we calculate the maximum absolute value online for each `1x128` activation tile or `128x128` weight block. Based on it, we derive the scaling factor and then quantize the activation or weight online into the FP8 format.

3.3.3. Low-Precision Storage and Communication

In conjunction with our FP8 training framework, we further reduce the memory consumption and communication overhead by compressing cached activations and optimizer states into lower-precision formats.

Low-Precision Optimizer States. We adopt the BF16 data format instead of FP32 to track the first and second moments in the AdamW (Loshchilov and Hutter, 2017) optimizer, without incurring observable performance degradation. However, the master weights (stored by the optimizer) and gradients (used for batch size accumulation) are still retained in FP32 to ensure numerical stability throughout training.

Low-Precision Activation. As illustrated in Figure 6, the `Wgrad` operation is performed in FP8. To reduce the memory consumption, it is a natural choice to cache activations in FP8 format for the backward pass of the `Linear` operator. However, special considerations are taken on several operators for low-cost high-precision training:

> **(1) Inputs of the `Linear` after the attention operator.** These activations are also used in the backward pass of the attention operator, which makes it sensitive to precision. We adopt a customized `E5M6` data format exclusively for these activations. Additionally, these activations will be converted from an `1x128` quantization tile to an `128x1` tile in the backward pass. To avoid introducing extra quantization error, all the scaling factors are round scaled, i.e., integral power of 2.
>
> **(2) Inputs of the SwiGLU operator in MoE.** To further reduce the memory cost, we cache the inputs of the SwiGLU operator and recompute its output in the backward pass. These activations are also stored in FP8 with our fine-grained quantization method, striking a balance between memory efficiency and computational accuracy.

Low-Precision Communication. Communication bandwidth is a critical bottleneck in the training of MoE models. To alleviate this challenge, we quantize the activation before MoE up-projections into FP8 and then apply `dispatch` components, which is compatible with FP8 `Fprop` in MoE up-projections. Like the inputs of the `Linear` after the attention operator, scaling factors for this activation are integral power of 2. A similar strategy is applied to the activation gradient before MoE down-projections. For both the forward and backward `combine` components, we retain them in BF16 to preserve training precision in critical parts of the training pipeline.

3.4. Inference and Deployment

We deploy DeepSeek-V3 on the H800 cluster, where GPUs within each node are interconnected using NVLink, and all GPUs across the cluster are fully interconnected via IB. To simultaneously ensure both the Service-Level Objective (SLO) for online services and high throughput, we employ the following deployment strategy that separates the *prefilling* and *decoding* stages.

3.4.1. Prefilling

The minimum deployment unit of the prefilling stage consists of 4 nodes with 32 GPUs. The `attention` part employs 4-way Tensor Parallelism (TP4) with Sequence Parallelism (SP), combined with 8-way Data Parallelism (DP8). Its small TP size of 4 limits the overhead of TP communication. For the `MoE` part, we use 32-way Expert Parallelism (EP32), which ensures that each expert processes a sufficiently large batch size, thereby enhancing computational efficiency. For the `MoE` all-to-all communication, we use the same method as in training: first transferring tokens across nodes via IB, and then forwarding among the intra-node GPUs via NVLink. In particular, we use 1-way Tensor Parallelism for the dense MLPs in shallow layers to save TP communication.

To achieve load balancing among different experts in the `MoE` part, we need to ensure that each GPU processes approximately the same number of tokens. To this end, we introduce a deployment strategy of *redundant experts*, which duplicates high-load experts and deploys them redundantly. The high-load experts are detected based on statistics collected during the online deployment and are adjusted periodically (e.g., every 10 minutes). After determining the set of redundant experts, we carefully rearrange experts among GPUs within a node based on the observed loads, striving to balance the load across GPUs as much as possible without increasing the cross-node all-to-all communication overhead. For the deployment of DeepSeek-V3, we set 32 redundant experts for the prefilling stage. For each GPU, besides the original 8 experts it hosts, it will also host one additional redundant expert.

Furthermore, in the prefilling stage, to improve the throughput and hide the overhead of all-to-all and TP communication, we simultaneously process two micro-batches with similar computational workloads, overlapping the `attention` and `MoE` of one micro-batch with the `dispatch` and `combine` of another.

Finally, we are exploring a *dynamic redundancy* strategy for experts, where each GPU hosts more experts (e.g., 16 experts), but only 9 will be activated during each inference step. Before the all-to-all operation at each layer begins, we compute the globally optimal routing scheme on the fly. Given the substantial computation involved in the prefilling stage, the overhead of computing this routing scheme is almost negligible.

3.4.2. Decoding

During decoding, we treat the shared expert as a routed one. From this perspective, each token will select 9 experts during routing, where the shared expert is regarded as a heavy-load one that will always be selected. The minimum deployment unit of the decoding stage consists of 40 nodes with 320 GPUs. The `attention` part employs TP4 with SP, combined with DP80, while the `MoE` part uses EP320. For the `MoE` part, each GPU hosts only one expert, and 64 GPUs are responsible for hosting redundant experts and shared experts. All-to-all communication of the `dispatch` and `combine` parts is performed via direct point-to-point transfers over IB to achieve low latency. Additionally, we leverage the IBGDA (NVIDIA, 2022) technology to further minimize latency and enhance communication efficiency.

Similar to prefilling, we periodically determine the set of redundant experts in a certain interval, based on the statistical expert load from our online service. However, we do not need to rearrange experts since each GPU only hosts one expert. We are also exploring the *dynamic redundancy* strategy for decoding. However, this requires more careful optimization of the algorithm that computes the globally optimal routing scheme and the fusion with the `dispatch` kernel to reduce overhead.

Additionally, to enhance throughput and hide the overhead of all-to-all communication, we are also exploring processing two micro-batches with similar computational workloads simultaneously in the decoding stage. Unlike prefilling, `attention` consumes a larger portion of time in the decoding stage. Therefore, we overlap the `attention` of one micro-batch with the `dispatch+MoE+combine` of another. In the decoding stage, the batch size per expert is relatively small (usually within 256 tokens), and the bottleneck is memory access rather than computation. Since the `MoE` part only needs to load the parameters of one expert, the memory access overhead is minimal, so using fewer SMs will not significantly affect the overall performance. Therefore, to avoid impacting the computation speed of the `attention` part, we can allocate only a small portion of SMs to `dispatch+MoE+combine`.

3.5. Suggestions on Hardware Design

Based on our implementation of the all-to-all communication and FP8 training scheme, we propose the following suggestions on chip design to AI hardware vendors.

3.5.1. Communication Hardware

In DeepSeek-V3, we implement the overlap between computation and communication to hide the communication latency during computation. This significantly reduces the dependency on communication bandwidth compared to serial computation and communication. However, the current communication implementation relies on expensive SMs (e.g., we allocate 20 out of the 132 SMs available in the H800 GPU for this purpose), which will limit the computational throughput. Moreover, using SMs for communication results in significant inefficiencies, as tensor cores remain entirely -utilized.

Currently, the SMs primarily perform the following tasks for all-to-all communication:

- **Forwarding data** between the IB (InfiniBand) and NVLink domain while aggregating IB traffic destined for multiple GPUs within the same node from a single GPU.
- **Transporting data** between RDMA buffers (registered GPU memory regions) and input/output buffers.
- **Executing `reduce` operations** for `all-to-all combine`.
- **Managing fine-grained memory layout** during chunked data transferring to multiple experts across the IB and NVLink domain.

We aspire to see future vendors developing hardware that offloads these communication tasks from the valuable computation unit SM, serving as a GPU co-processor or a network co-processor like NVIDIA SHARP Graham et al. (2016). Furthermore, to reduce application programming complexity, we aim for this hardware to unify the IB (scale-out) and NVLink (scale-up) networks from the perspective of the computation units. With this unified interface, computation units can easily accomplish operations such as `read`, `write`, `multicast`, and `reduce` across the entire IB-NVLink-unified domain via submitting communication requests based on simple primitives.

3.5.2. Compute Hardware

Higher FP8 GEMM Accumulation Precision in Tensor Cores. In the current Tensor Core implementation of the NVIDIA Hopper architecture, FP8 GEMM (General Matrix Multiply) employs fixed-point accumulation, aligning the mantissa products by right-shifting based on the maximum exponent before addition. Our experiments reveal that it only uses the highest 14

bits of each mantissa product after sign-fill right shifting, and truncates bits exceeding this range. However, for example, to achieve precise FP32 results from the accumulation of 32 FP8×FP8 multiplications, at least 34-bit precision is required. Thus, we recommend that future chip designs increase accumulation precision in Tensor Cores to support full-precision accumulation, or select an appropriate accumulation bit-width according to the accuracy requirements of training and inference algorithms. This approach ensures that errors remain within acceptable bounds while maintaining computational efficiency.

Support for Tile- and Block-Wise Quantization. Current GPUs only support per-tensor quantization, lacking the native support for fine-grained quantization like our tile- and block-wise quantization. In the current implementation, when the N_C interval is reached, the partial results will be copied from Tensor Cores to CUDA cores, multiplied by the scaling factors, and added to FP32 registers on CUDA cores. Although the dequantization overhead is significantly mitigated combined with our precise FP32 accumulation strategy, the frequent data movements between Tensor Cores and CUDA cores still limit the computational efficiency. Therefore, we recommend future chips to support fine-grained quantization by enabling Tensor Cores to receive scaling factors and implement MMA with group scaling. In this way, the whole partial sum accumulation and dequantization can be completed directly inside Tensor Cores until the final result is produced, avoiding frequent data movements.

Support for Online Quantization. The current implementations struggle to effectively support online quantization, despite its effectiveness demonstrated in our research. In the existing process, we need to read 128 BF16 activation values (the output of the previous computation) from HBM (High Bandwidth Memory) for quantization, and the quantized FP8 values are then written back to HBM, only to be read again for MMA. To address this inefficiency, we recommend that future chips integrate FP8 cast and TMA (Tensor Memory Accelerator) access into a single fused operation, so quantization can be completed during the transfer of activations from global memory to shared memory, avoiding frequent memory reads and writes. We also recommend supporting a warp-level cast instruction for speedup, which further facilitates the better fusion of layer normalization and FP8 cast. Alternatively, a near-memory computing approach can be adopted, where compute logic is placed near the HBM. In this case, BF16 elements can be cast to FP8 directly as they are read from HBM into the GPU, reducing off-chip memory access by roughly 50%.

Support for Transposed GEMM Operations. The current architecture makes it cumbersome to fuse matrix transposition with GEMM operations. In our workflow, activations during the forward pass are quantized into `1x128` FP8 tiles and stored. During the backward pass, the matrix needs to be read out, dequantized, transposed, re-quantized into `128x1` tiles, and stored in HBM. To reduce memory operations, we recommend future chips to enable direct transposed reads of matrices from shared memory before MMA operation, for those precisions required in both training and inference. Combined with the fusion of FP8 format conversion and TMA access, this enhancement will significantly streamline the quantization workflow.

4. Pre-Training

4.1. Data Construction

Compared with DeepSeek-V2, we optimize the pre-training corpus by enhancing the ratio of mathematical and programming samples, while expanding multilingual coverage beyond English and Chinese. Also, our data processing pipeline is refined to minimize redundancy while maintaining corpus diversity. Inspired by Ding et al. (2024), we implement the document packing method for data integrity but do not incorporate cross-sample attention masking during training. Finally, the training corpus for DeepSeek-V3 consists of 14.8T high-quality and diverse tokens in our tokenizer.

In the training process of DeepSeekCoder-V2 (DeepSeek-AI, 2024a), we observe that the Fill-in-Middle (FIM) strategy does not compromise the next-token prediction capability while enabling the model to accurately predict middle text based on contextual cues. In alignment with DeepSeekCoder-V2, we also incorporate the FIM strategy in the pre-training of DeepSeek-V3. To be specific, we employ the Prefix-Suffix-Middle (PSM) framework to structure data as follows:

$$\texttt{<|fim\_begin|>}f_{\text{pre}}\texttt{<|fim\_hole|>}f_{\text{suf}}\texttt{<|fim\_end|>}f_{\text{middle}}\texttt{<|eos\_token|>}.$$

This structure is applied at the document level as a part of the pre-packing process. The FIM strategy is applied at a rate of 0.1, consistent with the PSM framework.

The tokenizer for DeepSeek-V3 employs Byte-level BPE (Shibata et al., 1999) with an extended vocabulary of 128K tokens. The pretokenizer and training data for our tokenizer are modified to optimize multilingual compression efficiency. In addition, compared with DeepSeek-V2, the new pretokenizer introduces tokens that combine punctuations and line breaks. However, this trick may introduce the token boundary bias (Lundberg, 2023) when the model processes multi-line prompts without terminal line breaks, particularly for few-shot evaluation prompts. To address this issue, we randomly split a certain proportion of such combined tokens during training, which exposes the model to a wider array of special cases and mitigates this bias.

4.2. Hyper-Parameters

Model Hyper-Parameters. We set the number of Transformer layers to 61 and the hidden dimension to 7168. All learnable parameters are randomly initialized with a standard deviation of 0.006. In MLA, we set the number of attention heads n_h to 128 and the per-head dimension d_h to 128. The KV compression dimension d_c is set to 512, and the query compression dimension d'_c is set to 1536. For the decoupled queries and key, we set the per-head dimension d^R_h to 64. We substitute all FFNs except for the first three layers with MoE layers. Each MoE layer consists of 1 shared expert and 256 routed experts, where the intermediate hidden dimension of each expert is 2048. Among the routed experts, 8 experts will be activated for each token, and each token will be ensured to be sent to at most 4 nodes. The multi-token prediction depth D is set to 1, i.e., besides the exact next token, each token will predict one additional token. As DeepSeek-V2, DeepSeek-V3 also employs additional RMSNorm layers after the compressed latent vectors, and multiplies additional scaling factors at the width bottlenecks. Under this configuration, DeepSeek-V3 comprises 671B total parameters, of which 37B are activated for each token.

Training Hyper-Parameters. We employ the AdamW optimizer (Loshchilov and Hutter, 2017) with hyper-parameters set to $\beta_1 = 0.9$, $\beta_2 = 0.95$, and weight_decay = 0.1. We set the maximum sequence length to 4K during pre-training, and pre-train DeepSeek-V3 on 14.8T tokens. As for

the learning rate scheduling, we first linearly increase it from 0 to 2.2×10^{-4} during the first 2K steps. Then, we keep a constant learning rate of 2.2×10^{-4} until the model consumes 10T training tokens. Subsequently, we gradually decay the learning rate to 2.2×10^{-5} in 4.3T tokens, following a cosine decay curve. During the training of the final 500B tokens, we keep a constant learning rate of 2.2×10^{-5} in the first 333B tokens, and switch to another constant learning rate of 7.3×10^{-6} in the remaining 167B tokens. The gradient clipping norm is set to 1.0. We employ a batch size scheduling strategy, where the batch size is gradually increased from 3072 to 15360 in the training of the first 469B tokens, and then keeps 15360 in the remaining training. We leverage pipeline parallelism to deploy different layers of a model on different GPUs, and for each layer, the routed experts will be uniformly deployed on 64 GPUs belonging to 8 nodes. As for the node-limited routing, each token will be sent to at most 4 nodes (i.e., $M = 4$). For auxiliary-loss-free load balancing, we set the bias update speed γ to 0.001 for the first 14.3T tokens, and to 0.0 for the remaining 500B tokens. For the balance loss, we set α to 0.0001, just to avoid extreme imbalance within any single sequence. The MTP loss weight λ is set to 0.3 for the first 10T tokens, and to 0.1 for the remaining 4.8T tokens.

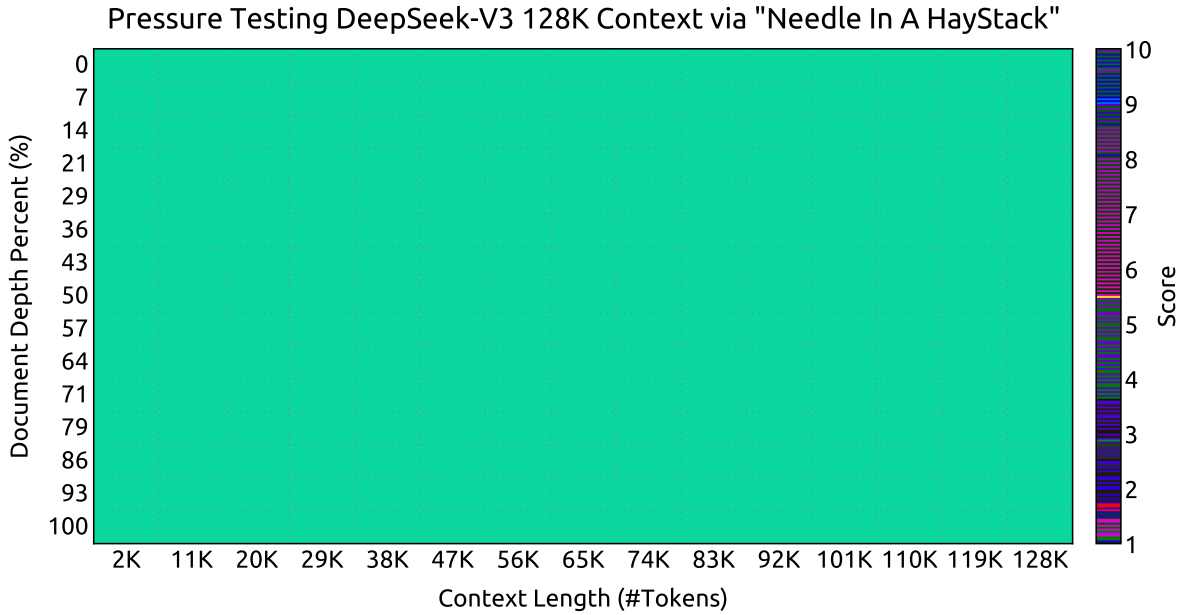

Figure 8 | Evaluation results on the "Needle In A Haystack" (NIAH) tests. DeepSeek-V3 performs well across all context window lengths up to 128K.

4.3. Long Context Extension

We adopt a similar approach to DeepSeek-V2 (DeepSeek-AI, 2024c) to enable long context capabilities in DeepSeek-V3. After the pre-training stage, we apply YaRN (Peng et al., 2023a) for context extension and perform two additional training phases, each comprising 1000 steps, to progressively expand the context window from 4K to 32K and then to 128K. The YaRN configuration is consistent with that used in DeepSeek-V2, being applied exclusively to the decoupled shared key $\mathbf{k}_t^R$. The hyper-parameters remain identical across both phases, with the scale $s = 40$, $\alpha = 1$, $\beta = 32$, and the scaling factor $\sqrt{t} = 0.1 \ln s + 1$. In the first phase, the sequence length is set to 32K, and the batch size is 1920. During the second phase, the sequence length is increased to 128K, and the batch size is reduced to 480. The learning rate for both phases is set to 7.3×10^{-6}, matching the final learning rate from the pre-training stage.

Through this two-phase extension training, DeepSeek-V3 is capable of handling inputs up to 128K in length while maintaining strong performance. Figure 8 illustrates that DeepSeek-V3, following supervised fine-tuning, achieves notable performance on the "Needle In A Haystack" (NIAH) test, demonstrating consistent robustness across context window lengths up to 128K.

4.4. Evaluations

4.4.1. Evaluation Benchmarks

The base model of DeepSeek-V3 is pretrained on a multilingual corpus with English and Chinese constituting the majority, so we evaluate its performance on a series of benchmarks primarily in English and Chinese, as well as on a multilingual benchmark. Our evaluation is based on our internal evaluation framework integrated in our HAI-LLM framework. Considered benchmarks are categorized and listed as follows, where underlined benchmarks are in Chinese and double-underlined benchmarks are multilingual ones:

Multi-subject multiple-choice datasets include MMLU (Hendrycks et al., 2020), MMLU-Redux (Gema et al., 2024), MMLU-Pro (Wang et al., 2024b), MMMLU (OpenAI, 2024b), C-Eval (Huang et al., 2023), and CMMLU (Li et al., 2023).

Language understanding and reasoning datasets include HellaSwag (Zellers et al., 2019), PIQA (Bisk et al., 2020), ARC (Clark et al., 2018), and BigBench Hard (BBH) (Suzgun et al., 2022).

Closed-book question answering datasets include TriviaQA (Joshi et al., 2017) and NaturalQuestions (Kwiatkowski et al., 2019).

Reading comprehension datasets include RACE Lai et al. (2017), DROP (Dua et al., 2019), C3 (Sun et al., 2019a), and CMRC (Cui et al., 2019).

Reference disambiguation datasets include CLUEWSC (Xu et al., 2020) and WinoGrande Sakaguchi et al. (2019).

Language modeling datasets include Pile (Gao et al., 2020).

Chinese understanding and culture datasets include CCPM (Li et al., 2021).

Math datasets include GSM8K (Cobbe et al., 2021), MATH (Hendrycks et al., 2021), MGSM (Shi et al., 2023), and CMath (Wei et al., 2023).

Code datasets include HumanEval (Chen et al., 2021), LiveCodeBench-Base (0801-1101) (Jain et al., 2024), MBPP (Austin et al., 2021), and CRUXEval (Gu et al., 2024).

Standardized exams include AGIEval (Zhong et al., 2023). Note that AGIEval includes both English and Chinese subsets.

Following our previous work (DeepSeek-AI, 2024b,c), we adopt perplexity-based evaluation for datasets including HellaSwag, PIQA, WinoGrande, RACE-Middle, RACE-High, MMLU, MMLU-Redux, MMLU-Pro, MMMLU, ARC-Easy, ARC-Challenge, C-Eval, CMMLU, C3, and CCPM, and adopt generation-based evaluation for TriviaQA, NaturalQuestions, DROP, MATH, GSM8K, MGSM, HumanEval, MBPP, LiveCodeBench-Base, CRUXEval, BBH, AGIEval, CLUEWSC, CMRC, and CMath. In addition, we perform language-modeling-based evaluation for Pile-test and use Bits-Per-Byte (BPB) as the metric to guarantee fair comparison among models using different tokenizers.

	Benchmark (Metric)	# Shots	DeepSeek-V2 Base	Qwen2.5 72B Base	LLaMA-3.1 405B Base	DeepSeek-V3 Base
	Architecture	-	MoE	Dense	Dense	MoE
	# Activated Params	-	21B	72B	405B	37B
	# Total Params	-	236B	72B	405B	671B
English	Pile-test (BPB)	-	0.606	0.638	**0.542**	0.548
	BBH (EM)	3-shot	78.8	79.8	82.9	**87.5**
	MMLU (EM)	5-shot	78.4	85.0	84.4	**87.1**
	MMLU-Redux (EM)	5-shot	75.6	83.2	81.3	**86.2**
	MMLU-Pro (EM)	5-shot	51.4	58.3	52.8	**64.4**
	DROP (F1)	3-shot	80.4	80.6	86.0	**89.0**
	ARC-Easy (EM)	25-shot	97.6	98.4	98.4	**98.9**
	ARC-Challenge (EM)	25-shot	92.2	94.5	**95.3**	**95.3**
	HellaSwag (EM)	10-shot	87.1	84.8	**89.2**	**88.9**
	PIQA (EM)	0-shot	83.9	82.6	**85.9**	84.7
	WinoGrande (EM)	5-shot	**86.3**	82.3	85.2	84.9
	RACE-Middle (EM)	5-shot	73.1	68.1	**74.2**	67.1
	RACE-High (EM)	5-shot	52.6	50.3	**56.8**	51.3
	TriviaQA (EM)	5-shot	80.0	71.9	**82.7**	**82.9**
	NaturalQuestions (EM)	5-shot	38.6	33.2	**41.5**	40.0
	AGIEval (EM)	0-shot	57.5	75.8	60.6	**79.6**
Code	HumanEval (Pass@1)	0-shot	43.3	53.0	54.9	**65.2**
	MBPP (Pass@1)	3-shot	65.0	72.6	68.4	**75.4**
	LiveCodeBench-Base (Pass@1)	3-shot	11.6	12.9	15.5	**19.4**
	CRUXEval-I (EM)	2-shot	52.5	59.1	58.5	**67.3**
	CRUXEval-O (EM)	2-shot	49.8	59.9	59.9	**69.8**
Math	GSM8K (EM)	8-shot	81.6	88.3	83.5	**89.3**
	MATH (EM)	4-shot	43.4	54.4	49.0	**61.6**
	MGSM (EM)	8-shot	63.6	76.2	69.9	**79.8**
	CMath (EM)	3-shot	78.7	84.5	77.3	**90.7**
Chinese	CLUEWSC (EM)	5-shot	82.0	82.5	**83.0**	**82.7**
	C-Eval (EM)	5-shot	81.4	89.2	72.5	**90.1**
	CMMLU (EM)	5-shot	84.0	**89.5**	73.7	88.8
	CMRC (EM)	1-shot	**77.4**	75.8	76.0	76.3
	C3 (EM)	0-shot	77.4	76.7	**79.7**	78.6
	CCPM (EM)	0-shot	**93.0**	88.5	78.6	92.0
Multilingual	MMMLU-non-English (EM)	5-shot	64.0	74.8	73.8	**79.4**

Table 3 | Comparison among DeepSeek-V3-Base and other representative open-source base models. All models are evaluated in our internal framework and share the same evaluation setting. Scores with a gap not exceeding 0.3 are considered to be at the same level. DeepSeek-V3-Base achieves the best performance on most benchmarks, especially on math and code tasks.

4.4.2. Evaluation Results

In Table 3, we compare the base model of DeepSeek-V3 with the state-of-the-art open-source base models, including DeepSeek-V2-Base (DeepSeek-AI, 2024c) (our previous release), Qwen2.5 72B Base (Qwen, 2024b), and LLaMA-3.1 405B Base (AI@Meta, 2024b). We evaluate all these models with our internal evaluation framework, and ensure that they share the same evaluation setting. Note that due to the changes in our evaluation framework over the past months, the performance of DeepSeek-V2-Base exhibits a slight difference from our previously reported results. Overall, DeepSeek-V3-Base comprehensively outperforms DeepSeek-V2-Base and Qwen2.5 72B Base, and surpasses LLaMA-3.1 405B Base in the majority of benchmarks, essentially becoming the strongest open-source model.

From a more detailed perspective, we compare DeepSeek-V3-Base with the other open-source base models individually. (1) Compared with DeepSeek-V2-Base, due to the improvements in our model architecture, the scale-up of the model size and training tokens, and the enhancement of data quality, DeepSeek-V3-Base achieves significantly better performance as expected. (2) Compared with Qwen2.5 72B Base, the state-of-the-art Chinese open-source model, with only half of the activated parameters, DeepSeek-V3-Base also demonstrates remarkable advantages, especially on English, multilingual, code, and math benchmarks. As for Chinese benchmarks, except for CMMLU, a Chinese multi-subject multiple-choice task, DeepSeek-V3-Base also shows better performance than Qwen2.5 72B. (3) Compared with LLaMA-3.1 405B Base, the largest open-source model with 11 times the activated parameters, DeepSeek-V3-Base also exhibits much better performance on multilingual, code, and math benchmarks. As for English and Chinese language benchmarks, DeepSeek-V3-Base shows competitive or better performance, and is especially good on BBH, MMLU-series, DROP, C-Eval, CMMLU, and CCPM.

Due to our efficient architectures and comprehensive engineering optimizations, DeepSeek-V3 achieves extremely high training efficiency. Under our training framework and infrastructures, training DeepSeek-V3 on each trillion tokens requires only 180K H800 GPU hours, which is much cheaper than training 72B or 405B dense models.

Benchmark (Metric)	# Shots	Small MoE Baseline	Small MoE w/ MTP	Large MoE Baseline	Large MoE w/ MTP
# Activated Params (Inference)	-	2.4B	2.4B	20.9B	20.9B
# Total Params (Inference)	-	15.7B	15.7B	228.7B	228.7B
# Training Tokens	-	1.33T	1.33T	540B	540B
Pile-test (BPB)	-	**0.729**	**0.729**	0.658	**0.657**
BBH (EM)	3-shot	39.0	**41.4**	70.0	**70.7**
MMLU (EM)	5-shot	50.0	**53.3**	**67.5**	66.6
DROP (F1)	1-shot	39.2	**41.3**	68.5	**70.6**
TriviaQA (EM)	5-shot	56.9	**57.7**	**67.0**	**67.3**
NaturalQuestions (EM)	5-shot	**22.7**	22.3	27.2	**28.5**
HumanEval (Pass@1)	0-shot	20.7	**26.8**	44.5	**53.7**
MBPP (Pass@1)	3-shot	35.8	**36.8**	61.6	**62.2**
GSM8K (EM)	8-shot	25.4	**31.4**	72.3	**74.0**
MATH (EM)	4-shot	10.7	**12.6**	38.6	**39.8**

Table 4 | Ablation results for the MTP strategy. The MTP strategy consistently enhances the model performance on most of the evaluation benchmarks.

4.5. Discussion

4.5.1. Ablation Studies for Multi-Token Prediction

In Table 4, we show the ablation results for the MTP strategy. To be specific, we validate the MTP strategy on top of two baseline models across different scales. At the small scale, we train a baseline MoE model comprising 15.7B total parameters on 1.33T tokens. At the large scale, we train a baseline MoE model comprising 228.7B total parameters on 540B tokens. On top of them, keeping the training data and the other architectures the same, we append a 1-depth MTP module onto them and train two models with the MTP strategy for comparison. Note that during inference, we directly discard the MTP module, so the inference costs of the compared models are exactly the same. From the table, we can observe that the MTP strategy consistently enhances the model performance on most of the evaluation benchmarks.

Benchmark (Metric)	# Shots	Small MoE Aux-Loss-Based	Small MoE Aux-Loss-Free	Large MoE Aux-Loss-Based	Large MoE Aux-Loss-Free
# Activated Params	-	2.4B	2.4B	20.9B	20.9B
# Total Params	-	15.7B	15.7B	228.7B	228.7B
# Training Tokens	-	1.33T	1.33T	578B	578B
Pile-test (BPB)	-	0.727	**0.724**	0.656	**0.652**
BBH (EM)	3-shot	37.3	**39.3**	66.7	**67.9**
MMLU (EM)	5-shot	51.0	**51.8**	**68.3**	67.2
DROP (F1)	1-shot	38.1	**39.0**	**67.1**	**67.1**
TriviaQA (EM)	5-shot	**58.3**	**58.5**	66.7	**67.7**
NaturalQuestions (EM)	5-shot	**23.2**	**23.4**	27.1	**28.1**
HumanEval (Pass@1)	0-shot	22.0	**22.6**	40.2	**46.3**
MBPP (Pass@1)	3-shot	**36.6**	35.8	59.2	**61.2**
GSM8K (EM)	8-shot	27.1	**29.6**	70.7	**74.5**
MATH (EM)	4-shot	**10.9**	**11.1**	37.2	**39.6**

Table 5 | Ablation results for the auxiliary-loss-free balancing strategy. Compared with the purely auxiliary-loss-based method, the auxiliary-loss-free strategy consistently achieves better model performance on most of the evaluation benchmarks.

4.5.2. Ablation Studies for the Auxiliary-Loss-Free Balancing Strategy

In Table 5, we show the ablation results for the auxiliary-loss-free balancing strategy. We validate this strategy on top of two baseline models across different scales. At the small scale, we train a baseline MoE model comprising 15.7B total parameters on 1.33T tokens. At the large scale, we train a baseline MoE model comprising 228.7B total parameters on 578B tokens. Both of the baseline models purely use auxiliary losses to encourage load balance, and use the sigmoid gating function with top-K affinity normalization. Their hyper-parameters to control the strength of auxiliary losses are the same as DeepSeek-V2-Lite and DeepSeek-V2, respectively. On top of these two baseline models, keeping the training data and the other architectures the same, we remove all auxiliary losses and introduce the auxiliary-loss-free balancing strategy for comparison. From the table, we can observe that the auxiliary-loss-free strategy consistently achieves better model performance on most of the evaluation benchmarks.

4.5.3. Batch-Wise Load Balance VS. Sequence-Wise Load Balance

The key distinction between auxiliary-loss-free balancing and sequence-wise auxiliary loss lies in their balancing scope: batch-wise versus sequence-wise. Compared with the sequence-wise auxiliary loss, batch-wise balancing imposes a more flexible constraint, as it does not enforce in-domain balance on each sequence. This flexibility allows experts to better specialize in different domains. To validate this, we record and analyze the expert load of a 16B auxiliary-loss-based baseline and a 16B auxiliary-loss-free model on different domains in the Pile test set. As illustrated in Figure 9, we observe that the auxiliary-loss-free model demonstrates greater expert specialization patterns as expected.

To further investigate the correlation between this flexibility and the advantage in model performance, we additionally design and validate a batch-wise auxiliary loss that encourages load balance on each training batch instead of on each sequence. The experimental results show that, when achieving a similar level of batch-wise load balance, the batch-wise auxiliary loss can also achieve similar model performance to the auxiliary-loss-free method. To be specific, in our experiments with 1B MoE models, the validation losses are: 2.258 (using a sequence-wise auxiliary loss), 2.253 (using the auxiliary-loss-free method), and 2.253 (using a batch-wise

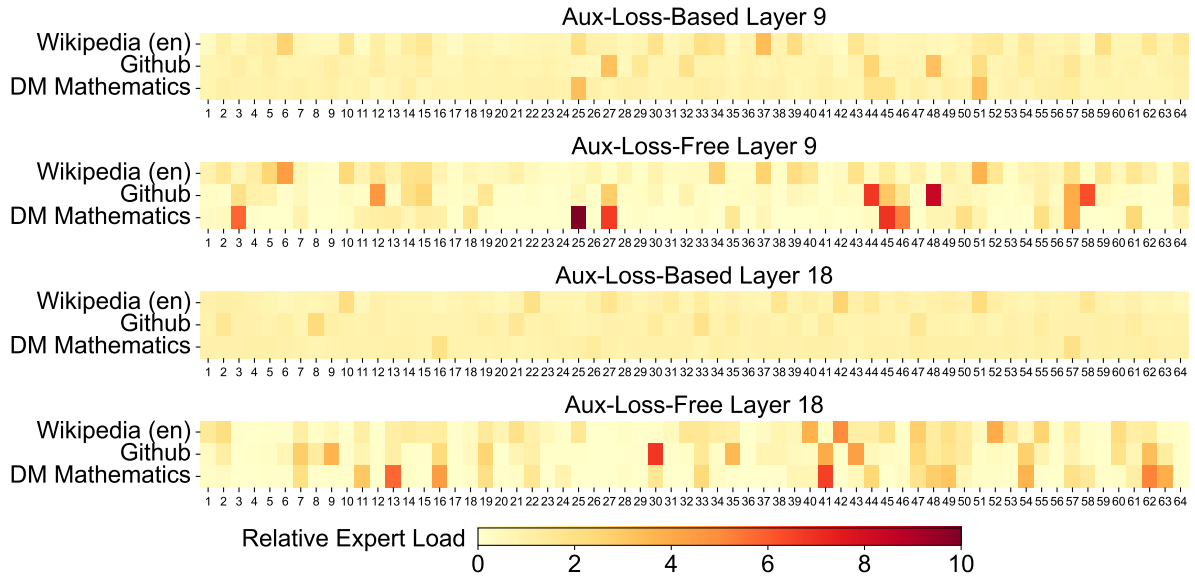

Figure 9 | Expert load of auxiliary-loss-free and auxiliary-loss-based models on three domains in the Pile test set. The auxiliary-loss-free model shows greater expert specialization patterns than the auxiliary-loss-based one. The relative expert load denotes the ratio between the actual expert load and the theoretically balanced expert load. Due to space constraints, we only present the results of two layers as an example, with the results of all layers provided in Appendix C.

auxiliary loss). We also observe similar results on 3B MoE models: the model using a sequence-wise auxiliary loss achieves a validation loss of 2.085, and the models using the auxiliary-loss-free method or a batch-wise auxiliary loss achieve the same validation loss of 2.080.

In addition, although the batch-wise load balancing methods show consistent performance advantages, they also face two potential challenges in efficiency: (1) load imbalance within certain sequences or small batches, and (2) domain-shift-induced load imbalance during inference. The first challenge is naturally addressed by our training framework that uses large-scale expert parallelism and data parallelism, which guarantees a large size of each micro-batch. For the second challenge, we also design and implement an efficient inference framework with redundant expert deployment, as described in Section 3.4, to overcome it.

5. Post-Training

5.1. Supervised Fine-Tuning

We curate our instruction-tuning datasets to include 1.5M instances spanning multiple domains, with each domain employing distinct data creation methods tailored to its specific requirements.

Reasoning Data. For reasoning-related datasets, including those focused on mathematics, code competition problems, and logic puzzles, we generate the data by leveraging an internal DeepSeek-R1 model. Specifically, while the R1-generated data demonstrates strong accuracy, it suffers from issues such as overthinking, poor formatting, and excessive length. Our objective is to balance the high accuracy of R1-generated reasoning data and the clarity and conciseness of regularly formatted reasoning data.

To establish our methodology, we begin by developing an expert model tailored to a specific domain, such as code, mathematics, or general reasoning, using a combined Supervised Fine-Tuning (SFT) and Reinforcement Learning (RL) training pipeline. This expert model serves as a data generator for the final model. The training process involves generating two distinct types of SFT samples for each instance: the first couples the problem with its original response in the format of <problem, original response>, while the second incorporates a system prompt alongside the problem and the R1 response in the format of <system prompt, problem, R1 response>.

The system prompt is meticulously designed to include instructions that guide the model toward producing responses enriched with mechanisms for reflection and verification. During the RL phase, the model leverages high-temperature sampling to generate responses that integrate patterns from both the R1-generated and original data, even in the absence of explicit system prompts. After hundreds of RL steps, the intermediate RL model learns to incorporate R1 patterns, thereby enhancing overall performance strategically.

Upon completing the RL training phase, we implement rejection sampling to curate high-quality SFT data for the final model, where the expert models are used as data generation sources. This method ensures that the final training data retains the strengths of DeepSeek-R1 while producing responses that are concise and effective.

Non-Reasoning Data. For non-reasoning data, such as creative writing, role-play, and simple question answering, we utilize DeepSeek-V2.5 to generate responses and enlist human annotators to verify the accuracy and correctness of the data.

SFT Settings. We fine-tune DeepSeek-V3-Base for two epochs using the SFT dataset, using the cosine decay learning rate scheduling that starts at 5×10^{-6} and gradually decreases to 1×10^{-6}. During training, each single sequence is packed from multiple samples. However, we adopt a sample masking strategy to ensure that these examples remain isolated and mutually invisible.

5.2. Reinforcement Learning

5.2.1. Reward Model

We employ a rule-based Reward Model (RM) and a model-based RM in our RL process.

Rule-Based RM. For questions that can be validated using specific rules, we adopt a rule-based reward system to determine the feedback. For instance, certain math problems have deterministic results, and we require the model to provide the final answer within a designated format (e.g., in a box), allowing us to apply rules to verify the correctness. Similarly, for LeetCode problems, we can utilize a compiler to generate feedback based on test cases. By leveraging rule-based validation wherever possible, we ensure a higher level of reliability, as this approach is resistant to manipulation or exploitation.

Model-Based RM. For questions with free-form ground-truth answers, we rely on the reward model to determine whether the response matches the expected ground-truth. Conversely, for questions without a definitive ground-truth, such as those involving creative writing, the reward model is tasked with providing feedback based on the question and the corresponding answer

as inputs. The reward model is trained from the DeepSeek-V3 SFT checkpoints. To enhance its reliability, we construct preference data that not only provides the final reward but also includes the chain-of-thought leading to the reward. This approach helps mitigate the risk of reward hacking in specific tasks.

5.2.2. Group Relative Policy Optimization

Similar to DeepSeek-V2 (DeepSeek-AI, 2024c), we adopt Group Relative Policy Optimization (GRPO) (Shao et al., 2024), which foregoes the critic model that is typically with the same size as the policy model, and estimates the baseline from group scores instead. Specifically, for each question q, GRPO samples a group of outputs $\{o_1, o_2, \cdots, o_G\}$ from the old policy model $\pi_{\theta_{old}}$ and then optimizes the policy model π_θ by maximizing the following objective:

$$\mathcal{J}_{GRPO}(\theta) = \mathbb{E}[q \sim P(Q), \{o_i\}_{i=1}^{G} \sim \pi_{\theta_{old}}(O|q)]$$
$$\frac{1}{G}\sum_{i=1}^{G}\left(\min\left(\frac{\pi_\theta(o_i|q)}{\pi_{\theta_{old}}(o_i|q)}A_i, \text{clip}\left(\frac{\pi_\theta(o_i|q)}{\pi_{\theta_{old}}(o_i|q)}, 1-\varepsilon, 1+\varepsilon\right)A_i\right) - \beta\mathbb{D}_{KL}\left(\pi_\theta||\pi_{ref}\right)\right), \tag{26}$$

$$\mathbb{D}_{KL}\left(\pi_\theta||\pi_{ref}\right) = \frac{\pi_{ref}(o_i|q)}{\pi_\theta(o_i|q)} - \log\frac{\pi_{ref}(o_i|q)}{\pi_\theta(o_i|q)} - 1, \tag{27}$$

where ε and β are hyper-parameters; π_{ref} is the reference model; and A_i is the advantage, derived from the rewards $\{r_1, r_2, \ldots, r_G\}$ corresponding to the outputs within each group:

$$A_i = \frac{r_i - \text{mean}(\{r_1, r_2, \cdots, r_G\})}{\text{std}(\{r_1, r_2, \cdots, r_G\})}. \tag{28}$$

We incorporate prompts from diverse domains, such as coding, math, writing, role-playing, and question answering, during the RL process. This approach not only aligns the model more closely with human preferences but also enhances performance on benchmarks, especially in scenarios where available SFT data are limited.

5.3. Evaluations

5.3.1. Evaluation Settings

Evaluation Benchmarks. Apart from the benchmark we used for base model testing, we further evaluate instructed models on IFEval (Zhou et al., 2023), FRAMES (Krishna et al., 2024), LongBench v2 (Bai et al., 2024), GPQA (Rein et al., 2023), SimpleQA (OpenAI, 2024c), C-SimpleQA (He et al., 2024), SWE-Bench Verified (OpenAI, 2024d), Aider [1], LiveCodeBench (Jain et al., 2024) (questions from August 2024 to November 2024), Codeforces [2], Chinese National High School Mathematics Olympiad (CNMO 2024)[3], and American Invitational Mathematics Examination 2024 (AIME 2024) (MAA, 2024).

Compared Baselines. We conduct comprehensive evaluations of our chat model against several strong baselines, including DeepSeek-V2-0506, DeepSeek-V2.5-0905, Qwen2.5 72B Instruct, LLaMA-3.1 405B Instruct, Claude-Sonnet-3.5-1022, and GPT-4o-0513. For the DeepSeek-V2 model series, we select the most representative variants for comparison. For closed-source models, evaluations are performed through their respective APIs.

[1] `https://aider.chat`
[2] `https://codeforces.com`
[3] `https://www.cms.org.cn/Home/comp/comp/cid/12.html`

Detailed Evaluation Configurations. For standard benchmarks including MMLU, DROP, GPQA, and SimpleQA, we adopt the evaluation prompts from the simple-evals framework[4]. We utilize the Zero-Eval prompt format (Lin, 2024) for MMLU-Redux in a zero-shot setting. For other datasets, we follow their original evaluation protocols with default prompts as provided by the dataset creators. For code and math benchmarks, the HumanEval-Mul dataset includes 8 mainstream programming languages (Python, Java, Cpp, C#, JavaScript, TypeScript, PHP, and Bash) in total. We use CoT and non-CoT methods to evaluate model performance on LiveCodeBench, where the data are collected from August 2024 to November 2024. The Codeforces dataset is measured using the percentage of competitors. SWE-Bench verified is evaluated using the agentless framework (Xia et al., 2024). We use the "diff" format to evaluate the Aider-related benchmarks. For mathematical assessments, AIME and CNMO 2024 are evaluated with a temperature of 0.7, and the results are averaged over 16 runs, while MATH-500 employs greedy decoding. We allow all models to output a maximum of 8192 tokens for each benchmark.

	Benchmark (Metric)	**DeepSeek V2-0506**	**DeepSeek V2.5-0905**	**Qwen2.5 72B-Inst.**	**LLaMA-3.1 405B-Inst.**	**Claude-3.5-Sonnet-1022**	**GPT-4o 0513**	**DeepSeek V3**
	Architecture	MoE	MoE	Dense	Dense	-	-	MoE
	# Activated Params	21B	21B	72B	405B	-	-	37B
	# Total Params	236B	236B	72B	405B	-	-	671B
English	MMLU (EM)	78.2	80.6	85.3	**88.6**	**88.3**	87.2	**88.5**
	MMLU-Redux (EM)	77.9	80.3	85.6	86.2	**88.9**	88.0	**89.1**
	MMLU-Pro (EM)	58.5	66.2	71.6	73.3	**78.0**	72.6	75.9
	DROP (3-shot F1)	83.0	87.8	76.7	88.7	88.3	83.7	**91.**
	IF-Eval (Prompt Strict)	57.7	80.6	84.1	86.0	**86.5**	84.3	86.1
	GPQA-Diamond (Pass@1)	35.3	41.3	49.0	51.1	**65.0**	49.9	59.1
	SimpleQA (Correct)	9.0	10.2	9.1	17.1	28.4	**38.2**	24.9
	FRAMES (Acc.)	66.9	65.4	69.8	70.0	72.5	**80.5**	73.3
	LongBench v2 (Acc.)	31.6	35.4	39.4	36.1	41.0	48.1	**48.7**
Code	HumanEval-Mul (Pass@1)	69.3	77.4	77.3	77.2	81.7	80.5	**82.6**
	LiveCodeBench (Pass@1-COT)	18.8	29.2	31.1	28.4	36.3	33.4	**40.5**
	LiveCodeBench (Pass@1)	20.3	28.4	28.7	30.1	32.8	34.2	**37.6**
	Codeforces (Percentile)	17.5	35.6	24.8	25.3	20.3	23.6	**51.6**
	SWE Verified (Resolved)	-	22.6	23.8	24.5	**50.8**	38.8	42.0
	Aider-Edit (Acc.)	60.3	71.6	65.4	63.9	**84.2**	72.9	79.7
	Aider-Polyglot (Acc.)	-	18.2	7.6	5.8	45.3	16.0	**49.6**
Math	AIME 2024 (Pass@1)	4.6	16.7	23.3	23.3	16.0	9.3	**39.2**
	MATH-500 (EM)	56.3	74.7	80.0	73.8	78.3	74.6	**90.2**
	CNMO 2024 (Pass@1)	2.8	10.8	15.9	6.8	13.1	10.8	**43.2**
Chinese	CLUEWSC (EM)	89.9	90.4	**91.4**	84.7	85.4	87.9	90.9
	C-Eval (EM)	78.6	79.5	86.1	61.5	76.7	76.0	**86.5**
	C-SimpleQA (Correct)	48.5	54.1	48.4	50.4	51.3	59.3	**64.8**

Table 6 | Comparison between DeepSeek-V3 and other representative chat models. All models are evaluated in a configuration that limits the output length to 8K. Benchmarks containing fewer than 1000 samples are tested multiple times using varying temperature settings to derive robust final results. DeepSeek-V3 stands as the best-performing open-source model, and also exhibits competitive performance against frontier closed-source models.

[4] `https://github.com/openai/simple-evals`

5.3.2. Standard Evaluation

Table 6 presents the evaluation results, showcasing that DeepSeek-V3 stands as the best-performing open-source model. Additionally, it is competitive against frontier closed-source models like GPT-4o and Claude-3.5-Sonnet.

English Benchmarks. MMLU is a widely recognized benchmark designed to assess the performance of large language models, across diverse knowledge domains and tasks. DeepSeek-V3 demonstrates competitive performance, standing on par with top-tier models such as LLaMA-3.1-405B, GPT-4o, and Claude-Sonnet 3.5, while significantly outperforming Qwen2.5 72B. Moreover, DeepSeek-V3 excels in MMLU-Pro, a more challenging educational knowledge benchmark, where it closely trails Claude-Sonnet 3.5. On MMLU-Redux, a refined version of MMLU with corrected labels, DeepSeek-V3 surpasses its peers. In addition, on GPQA-Diamond, a PhD-level evaluation testbed, DeepSeek-V3 achieves remarkable results, ranking just behind Claude 3.5 Sonnet and outperforming all other competitors by a substantial margin.

In long-context understanding benchmarks such as DROP, LongBench v2, and FRAMES, DeepSeek-V3 continues to demonstrate its position as a top-tier model. It achieves an impressive 91.6 F1 score in the 3-shot setting on DROP, outperforming all other models in this category. On FRAMES, a benchmark requiring question-answering over 100k token contexts, DeepSeek-V3 closely trails GPT-4o while outperforming all other models by a significant margin. This demonstrates the strong capability of DeepSeek-V3 in handling extremely long-context tasks. The long-context capability of DeepSeek-V3 is further validated by its best-in-class performance on LongBench v2, a dataset that was released just a few weeks before the launch of DeepSeek V3. On the factual knowledge benchmark, SimpleQA, DeepSeek-V3 falls behind GPT-4o and Claude-Sonnet, primarily due to its design focus and resource allocation. DeepSeek-V3 assigns more training tokens to learn Chinese knowledge, leading to exceptional performance on the C-SimpleQA. On the instruction-following benchmark, DeepSeek-V3 significantly outperforms its predecessor, DeepSeek-V2-series, highlighting its improved ability to understand and adhere to user-defined format constraints.

Code and Math Benchmarks. Coding is a challenging and practical task for LLMs, encompassing engineering-focused tasks like SWE-Bench-Verified and Aider, as well as algorithmic tasks such as HumanEval and LiveCodeBench. In engineering tasks, DeepSeek-V3 trails behind Claude-Sonnet-3.5-1022 but significantly outperforms open-source models. The open-source DeepSeek-V3 is expected to foster advancements in coding-related engineering tasks. By providing access to its robust capabilities, DeepSeek-V3 can drive innovation and improvement in areas such as software engineering and algorithm development, empowering developers and researchers to push the boundaries of what open-source models can achieve in coding tasks. In algorithmic tasks, DeepSeek-V3 demonstrates superior performance, outperforming all baselines on benchmarks like HumanEval-Mul and LiveCodeBench. This success can be attributed to its advanced knowledge distillation technique, which effectively enhances its code generation and problem-solving capabilities in algorithm-focused tasks.

On math benchmarks, DeepSeek-V3 demonstrates exceptional performance, significantly surpassing baselines and setting a new state-of-the-art for non-o1-like models. Specifically, on AIME, MATH-500, and CNMO 2024, DeepSeek-V3 outperforms the second-best model, Qwen2.5 72B, by approximately 10% in absolute scores, which is a substantial margin for such challenging benchmarks. This remarkable capability highlights the effectiveness of the distillation technique from DeepSeek-R1, which has been proven highly beneficial for non-o1-like models.

Model	Arena-Hard	AlpacaEval 2.0
DeepSeek-V2.5-0905	76.2	50.5
Qwen2.5-72B-Instruct	81.2	49.1
LLaMA-3.1 405B	69.3	40.5
GPT-4o-0513	80.4	51.1
Claude-Sonnet-3.5-1022	85.2	52.0
DeepSeek-V3	**85.5**	**70.0**

Table 7 | English open-ended conversation evaluations. For AlpacaEval 2.0, we use the length-controlled win rate as the metric.

Chinese Benchmarks. Qwen and DeepSeek are two representative model series with robust support for both Chinese and English. On the factual benchmark Chinese SimpleQA, DeepSeek-V3 surpasses Qwen2.5-72B by 16.4 points, despite Qwen2.5 being trained on a larger corpus compromising 18T tokens, which are 20% more than the 14.8T tokens that DeepSeek-V3 is pre-trained on.

On C-Eval, a representative benchmark for Chinese educational knowledge evaluation, and CLUEWSC (Chinese Winograd Schema Challenge), DeepSeek-V3 and Qwen2.5-72B exhibit similar performance levels, indicating that both models are well-optimized for challenging Chinese-language reasoning and educational tasks.

5.3.3. Open-Ended Evaluation

In addition to standard benchmarks, we also evaluate our models on open-ended generation tasks using LLMs as judges, with the results shown in Table 7. Specifically, we adhere to the original configurations of AlpacaEval 2.0 (Dubois et al., 2024) and Arena-Hard (Li et al., 2024a), which leverage GPT-4-Turbo-1106 as judges for pairwise comparisons. On Arena-Hard, DeepSeek-V3 achieves an impressive win rate of over 86% against the baseline GPT-4-0314, performing on par with top-tier models like Claude-Sonnet-3.5-1022. This underscores the robust capabilities of DeepSeek-V3, especially in dealing with complex prompts, including coding and debugging tasks. Furthermore, DeepSeek-V3 achieves a groundbreaking milestone as the first open-source model to surpass 85% on the Arena-Hard benchmark. This achievement significantly bridges the performance gap between open-source and closed-source models, setting a new standard for what open-source models can accomplish in challenging domains.

Similarly, DeepSeek-V3 showcases exceptional performance on AlpacaEval 2.0, outperforming both closed-source and open-source models. This demonstrates its outstanding proficiency in writing tasks and handling straightforward question-answering scenarios. Notably, it surpasses DeepSeek-V2.5-0905 by a significant margin of 20%, highlighting substantial improvements in tackling simple tasks and showcasing the effectiveness of its advancements.

5.3.4. DeepSeek-V3 as a Generative Reward Model

We compare the judgment ability of DeepSeek-V3 with state-of-the-art models, namely GPT-4o and Claude-3.5. Table 8 presents the performance of these models in RewardBench (Lambert et al., 2024). DeepSeek-V3 achieves performance on par with the best versions of GPT-4o-0806 and Claude-3.5-Sonnet-1022, while surpassing other versions. Additionally, the judgment ability of DeepSeek-V3 can also be enhanced by the voting technique. Therefore, we employ DeepSeek-V3 along with voting to offer self-feedback on open-ended questions, thereby improving the

Model	Chat	Chat-Hard	Safety	Reasoning	Average
GPT-4o-0513	96.6	70.4	86.7	84.9	84.7
GPT-4o-0806	96.1	76.1	88.1	86.6	86.7
GPT-4o-1120	95.8	71.3	86.2	85.2	84.6
Claude-3.5-sonnet-0620	96.4	74.0	81.6	84.7	84.2
Claude-3.5-sonnet-1022	96.4	79.7	91.1	87.6	88.7
DeepSeek-V3	96.9	79.8	87.0	84.3	87.0
DeepSeek-V3 (maj@6)	96.9	82.6	89.5	89.2	89.6

Table 8 | Performances of GPT-4o, Claude-3.5-sonnet and DeepSeek-V3 on RewardBench.

Model	LiveCodeBench-CoT		MATH-500	
	Pass@1	Length	Pass@1	Length
DeepSeek-V2.5 Baseline	31.1	718	74.6	769
DeepSeek-V2.5 +R1 Distill	37.4	783	83.2	1510

Table 9 | The contribution of distillation from DeepSeek-R1. The evaluation settings of LiveCodeBench and MATH-500 are the same as in Table 6.

effectiveness and robustness of the alignment process.

5.4. Discussion

5.4.1. Distillation from DeepSeek-R1

We ablate the contribution of distillation from DeepSeek-R1 based on DeepSeek-V2.5. The baseline is trained on short CoT data, whereas its competitor uses data generated by the expert checkpoints described above.

Table 9 demonstrates the effectiveness of the distillation data, showing significant improvements in both LiveCodeBench and MATH-500 benchmarks. Our experiments reveal an interesting trade-off: the distillation leads to better performance but also substantially increases the average response length. To maintain a balance between model accuracy and computational efficiency, we carefully selected optimal settings for DeepSeek-V3 in distillation.

Our research suggests that knowledge distillation from reasoning models presents a promising direction for post-training optimization. While our current work focuses on distilling data from mathematics and coding domains, this approach shows potential for broader applications across various task domains. The effectiveness demonstrated in these specific areas indicates that long-CoT distillation could be valuable for enhancing model performance in other cognitive tasks requiring complex reasoning. Further exploration of this approach across different domains remains an important direction for future research.

5.4.2. Self-Rewarding

Rewards play a pivotal role in RL, steering the optimization process. In domains where verification through external tools is straightforward, such as some coding or mathematics scenarios, RL demonstrates exceptional efficacy. However, in more general scenarios, constructing a feedback

mechanism through hard coding is impractical. During the development of DeepSeek-V3, for these broader contexts, we employ the constitutional AI approach (Bai et al., 2022), leveraging the voting evaluation results of DeepSeek-V3 itself as a feedback source. This method has produced notable alignment effects, significantly enhancing the performance of DeepSeek-V3 in subjective evaluations. By integrating additional constitutional inputs, DeepSeek-V3 can optimize towards the constitutional direction. We believe that this paradigm, which combines supplementary information with LLMs as a feedback source, is of paramount importance. The LLM serves as a versatile processor capable of transforming unstructured information from diverse scenarios into rewards, ultimately facilitating the self-improvement of LLMs. Beyond self-rewarding, we are also dedicated to uncovering other general and scalable rewarding methods to consistently advance the model capabilities in general scenarios.

5.4.3. Multi-Token Prediction Evaluation

Instead of predicting just the next single token, DeepSeek-V3 predicts the next 2 tokens through the MTP technique. Combined with the framework of speculative decoding (Leviathan et al., 2023; Xia et al., 2023), it can significantly accelerate the decoding speed of the model. A natural question arises concerning the acceptance rate of the additionally predicted token. Based on our evaluation, the acceptance rate of the second token prediction ranges between 85% and 90% across various generation topics, demonstrating consistent reliability. This high acceptance rate enables DeepSeek-V3 to achieve a significantly improved decoding speed, delivering 1.8 times TPS (Tokens Per Second).

6. Conclusion, Limitations, and Future Directions

In this paper, we introduce DeepSeek-V3, a large MoE language model with 671B total parameters and 37B activated parameters, trained on 14.8T tokens. In addition to the MLA and DeepSeekMoE architectures, it also pioneers an auxiliary-loss-free strategy for load balancing and sets a multi-token prediction training objective for stronger performance. The training of DeepSeek-V3 is cost-effective due to the support of FP8 training and meticulous engineering optimizations. The post-training also makes a success in distilling the reasoning capability from the DeepSeek-R1 series of models. Comprehensive evaluations demonstrate that DeepSeek-V3 has emerged as the strongest open-source model currently available, and achieves performance comparable to leading closed-source models like GPT-4o and Claude-3.5-Sonnet. Despite its strong performance, it also maintains economical training costs. It requires only 2.788M H800 GPU hours for its full training, including pre-training, context length extension, and post-training.

While acknowledging its strong performance and cost-effectiveness, we also recognize that DeepSeek-V3 has some limitations, especially on the deployment. Firstly, to ensure efficient inference, the recommended deployment unit for DeepSeek-V3 is relatively large, which might pose a burden for small-sized teams. Secondly, although our deployment strategy for DeepSeek-V3 has achieved an end-to-end generation speed of more than two times that of DeepSeek-V2, there still remains potential for further enhancement. Fortunately, these limitations are expected to be naturally addressed with the development of more advanced hardware.

DeepSeek consistently adheres to the route of open-source models with longtermism, aiming to steadily approach the ultimate goal of AGI (Artificial General Intelligence). In the future, we plan to strategically invest in research across the following directions.

- We will consistently study and refine our model architectures, aiming to further improve

both the training and inference efficiency, striving to approach efficient support for infinite context length. Additionally, we will try to break through the architectural limitations of Transformer, thereby pushing the boundaries of its modeling capabilities.
- We will continuously iterate on the quantity and quality of our training data, and explore the incorporation of additional training signal sources, aiming to drive data scaling across a more comprehensive range of dimensions.
- We will consistently explore and iterate on the deep thinking capabilities of our models, aiming to enhance their intelligence and problem-solving abilities by expanding their reasoning length and depth.
- We will explore more comprehensive and multi-dimensional model evaluation methods to prevent the tendency towards optimizing a fixed set of benchmarks during research, which may create a misleading impression of the model capabilities and affect our foundational assessment.

References

AI@Meta. Llama 3 model card, 2024a. URL https://github.com/meta-llama/llama3/blob/main/MODEL_CARD.md.

AI@Meta. Llama 3.1 model card, 2024b. URL https://github.com/meta-llama/llama-models/blob/main/models/llama3_1/MODEL_CARD.md.

Anthropic. Claude 3.5 sonnet, 2024. URL https://www.anthropic.com/news/claude-3-5-sonnet.

J. Austin, A. Odena, M. Nye, M. Bosma, H. Michalewski, D. Dohan, E. Jiang, C. Cai, M. Terry, Q. Le, et al. Program synthesis with large language models. arXiv preprint arXiv:2108.07732, 2021.

Y. Bai, S. Kadavath, S. Kundu, A. Askell, J. Kernion, A. Jones, A. Chen, A. Goldie, A. Mirhoseini, C. McKinnon, et al. Constitutional AI: Harmlessness from AI feedback. arXiv preprint arXiv:2212.08073, 2022.

Y. Bai, S. Tu, J. Zhang, H. Peng, X. Wang, X. Lv, S. Cao, J. Xu, L. Hou, Y. Dong, J. Tang, and J. Li. LongBench v2: Towards deeper understanding and reasoning on realistic long-context multitasks. arXiv preprint arXiv:2412.15204, 2024.

M. Bauer, S. Treichler, and A. Aiken. Singe: leveraging warp specialization for high performance on GPUs. In Proceedings of the 19th ACM SIGPLAN Symposium on Principles and Practice of Parallel Programming, PPoPP '14, page 119–130, New York, NY, USA, 2014. Association for Computing Machinery. ISBN 9781450326568. doi: 10.1145/2555243.2555258. URL https://doi.org/10.1145/2555243.2555258.

Y. Bisk, R. Zellers, R. L. Bras, J. Gao, and Y. Choi. PIQA: reasoning about physical commonsense in natural language. In The Thirty-Fourth AAAI Conference on Artificial Intelligence, AAAI 2020, The Thirty-Second Innovative Applications of Artificial Intelligence Conference, IAAI 2020, The Tenth AAAI Symposium on Educational Advances in Artificial Intelligence, EAAI 2020, New York, NY, USA, February 7-12, 2020, pages 7432–7439. AAAI Press, 2020. doi: 10.1609/aaai.v34i05.6239. URL https://doi.org/10.1609/aaai.v34i05.6239.

M. Chen, J. Tworek, H. Jun, Q. Yuan, H. P. de Oliveira Pinto, J. Kaplan, H. Edwards, Y. Burda, N. Joseph, G. Brockman, A. Ray, R. Puri, G. Krueger, M. Petrov, H. Khlaaf, G. Sastry, P. Mishkin,

B. Chan, S. Gray, N. Ryder, M. Pavlov, A. Power, L. Kaiser, M. Bavarian, C. Winter, P. Tillet, F. P. Such, D. Cummings, M. Plappert, F. Chantzis, E. Barnes, A. Herbert-Voss, W. H. Guss, A. Nichol, A. Paino, N. Tezak, J. Tang, I. Babuschkin, S. Balaji, S. Jain, W. Saunders, C. Hesse, A. N. Carr, J. Leike, J. Achiam, V. Misra, E. Morikawa, A. Radford, M. Knight, M. Brundage, M. Murati, K. Mayer, P. Welinder, B. McGrew, D. Amodei, S. McCandlish, I. Sutskever, and W. Zaremba. Evaluating large language models trained on code. CoRR, abs/2107.03374, 2021. URL https://arxiv.org/abs/2107.03374.

P. Clark, I. Cowhey, O. Etzioni, T. Khot, A. Sabharwal, C. Schoenick, and O. Tafjord. Think you have solved question answering? try arc, the AI2 reasoning challenge. CoRR, abs/1803.05457, 2018. URL http://arxiv.org/abs/1803.05457.

K. Cobbe, V. Kosaraju, M. Bavarian, M. Chen, H. Jun, L. Kaiser, M. Plappert, J. Tworek, J. Hilton, R. Nakano, et al. Training verifiers to solve math word problems. arXiv preprint arXiv:2110.14168, 2021.

Y. Cui, T. Liu, W. Che, L. Xiao, Z. Chen, W. Ma, S. Wang, and G. Hu. A span-extraction dataset for Chinese machine reading comprehension. In K. Inui, J. Jiang, V. Ng, and X. Wan, editors, Proceedings of the 2019 Conference on Empirical Methods in Natural Language Processing and the 9th International Joint Conference on Natural Language Processing (EMNLP-IJCNLP), pages 5883–5889, Hong Kong, China, Nov. 2019. Association for Computational Linguistics. doi: 10.18653/v1/D19-1600. URL https://aclanthology.org/D19-1600.

D. Dai, C. Deng, C. Zhao, R. X. Xu, H. Gao, D. Chen, J. Li, W. Zeng, X. Yu, Y. Wu, Z. Xie, Y. K. Li, P. Huang, F. Luo, C. Ruan, Z. Sui, and W. Liang. Deepseekmoe: Towards ultimate expert specialization in mixture-of-experts language models. CoRR, abs/2401.06066, 2024. URL https://doi.org/10.48550/arXiv.2401.06066.

DeepSeek-AI. Deepseek-coder-v2: Breaking the barrier of closed-source models in code intelligence. CoRR, abs/2406.11931, 2024a. URL https://doi.org/10.48550/arXiv.2406.11931.

DeepSeek-AI. Deepseek LLM: scaling open-source language models with longtermism. CoRR, abs/2401.02954, 2024b. URL https://doi.org/10.48550/arXiv.2401.02954.

DeepSeek-AI. Deepseek-v2: A strong, economical, and efficient mixture-of-experts language model. CoRR, abs/2405.04434, 2024c. URL https://doi.org/10.48550/arXiv.2405.04434.

T. Dettmers, M. Lewis, Y. Belkada, and L. Zettlemoyer. Gpt3. int8 (): 8-bit matrix multiplication for transformers at scale. Advances in Neural Information Processing Systems, 35:30318–30332, 2022.

H. Ding, Z. Wang, G. Paolini, V. Kumar, A. Deoras, D. Roth, and S. Soatto. Fewer truncations improve language modeling. arXiv preprint arXiv:2404.10830, 2024.

D. Dua, Y. Wang, P. Dasigi, G. Stanovsky, S. Singh, and M. Gardner. DROP: A reading comprehension benchmark requiring discrete reasoning over paragraphs. In J. Burstein, C. Doran, and T. Solorio, editors, Proceedings of the 2019 Conference of the North American Chapter of the Association for Computational Linguistics: Human Language Technologies, NAACL-HLT 2019, Minneapolis, MN, USA, June 2-7, 2019, Volume 1 (Long and Short Papers), pages 2368–2378. Association for Computational Linguistics, 2019. doi: 10.18653/V1/N19-1246. URL https://doi.org/10.18653/v1/n19-1246.

Y. Dubois, B. Galambosi, P. Liang, and T. B. Hashimoto. Length-controlled alpacaeval: A simple way to debias automatic evaluators. arXiv preprint arXiv:2404.04475, 2024.

W. Fedus, B. Zoph, and N. Shazeer. Switch transformers: Scaling to trillion parameter models with simple and efficient sparsity. CoRR, abs/2101.03961, 2021. URL https://arxiv.org/abs/2101.03961.

M. Fishman, B. Chmiel, R. Banner, and D. Soudry. Scaling FP8 training to trillion-token llms. arXiv preprint arXiv:2409.12517, 2024.

E. Frantar, S. Ashkboos, T. Hoefler, and D. Alistarh. Gptq: Accurate post-training quantization for generative pre-trained transformers. arXiv preprint arXiv:2210.17323, 2022.

L. Gao, S. Biderman, S. Black, L. Golding, T. Hoppe, C. Foster, J. Phang, H. He, A. Thite, N. Nabeshima, et al. The Pile: An 800GB dataset of diverse text for language modeling. arXiv preprint arXiv:2101.00027, 2020.

A. P. Gema, J. O. J. Leang, G. Hong, A. Devoto, A. C. M. Mancino, R. Saxena, X. He, Y. Zhao, X. Du, M. R. G. Madani, C. Barale, R. McHardy, J. Harris, J. Kaddour, E. van Krieken, and P. Minervini. Are we done with mmlu? CoRR, abs/2406.04127, 2024. URL https://doi.org/10.48550/arXiv.2406.04127.

F. Gloeckle, B. Y. Idrissi, B. Rozière, D. Lopez-Paz, and G. Synnaeve. Better & faster large language models via multi-token prediction. In Forty-first International Conference on Machine Learning, ICML 2024, Vienna, Austria, July 21-27, 2024. OpenReview.net, 2024. URL https://openreview.net/forum?id=pEWAcejiU2.

Google. Our next-generation model: Gemini 1.5, 2024. URL https://blog.google/technology/ai/google-gemini-next-generation-model-february-2024.

R. L. Graham, D. Bureddy, P. Lui, H. Rosenstock, G. Shainer, G. Bloch, D. Goldenerg, M. Dubman, S. Kotchubievsky, V. Koushnir, et al. Scalable hierarchical aggregation protocol (SHArP): A hardware architecture for efficient data reduction. In 2016 First International Workshop on Communication Optimizations in HPC (COMHPC), pages 1–10. IEEE, 2016.

A. Gu, B. Rozière, H. Leather, A. Solar-Lezama, G. Synnaeve, and S. I. Wang. Cruxeval: A benchmark for code reasoning, understanding and execution, 2024.

D. Guo, Q. Zhu, D. Yang, Z. Xie, K. Dong, W. Zhang, G. Chen, X. Bi, Y. Wu, Y. K. Li, F. Luo, Y. Xiong, and W. Liang. Deepseek-coder: When the large language model meets programming - the rise of code intelligence. CoRR, abs/2401.14196, 2024. URL https://doi.org/10.48550/arXiv.2401.14196.

A. Harlap, D. Narayanan, A. Phanishayee, V. Seshadri, N. Devanur, G. Ganger, and P. Gibbons. Pipedream: Fast and efficient pipeline parallel dnn training, 2018. URL https://arxiv.org/abs/1806.03377.

B. He, L. Noci, D. Paliotta, I. Schlag, and T. Hofmann. Understanding and minimising outlier features in transformer training. In The Thirty-eighth Annual Conference on Neural Information Processing Systems.

Y. He, S. Li, J. Liu, Y. Tan, W. Wang, H. Huang, X. Bu, H. Guo, C. Hu, B. Zheng, et al. Chinese simpleqa: A chinese factuality evaluation for large language models. arXiv preprint arXiv:2411.07140, 2024.

D. Hendrycks, C. Burns, S. Basart, A. Zou, M. Mazeika, D. Song, and J. Steinhardt. Measuring massive multitask language understanding. arXiv preprint arXiv:2009.03300, 2020.

D. Hendrycks, C. Burns, S. Kadavath, A. Arora, S. Basart, E. Tang, D. Song, and J. Steinhardt. Measuring mathematical problem solving with the math dataset. arXiv preprint arXiv:2103.03874, 2021.

Y. Huang, Y. Bai, Z. Zhu, J. Zhang, J. Zhang, T. Su, J. Liu, C. Lv, Y. Zhang, J. Lei, et al. C-Eval: A multi-level multi-discipline chinese evaluation suite for foundation models. arXiv preprint arXiv:2305.08322, 2023.

N. Jain, K. Han, A. Gu, W. Li, F. Yan, T. Zhang, S. Wang, A. Solar-Lezama, K. Sen, and I. Stoica. Livecodebench: Holistic and contamination free evaluation of large language models for code. CoRR, abs/2403.07974, 2024. URL https://doi.org/10.48550/arXiv.2403.07974.

A. Q. Jiang, A. Sablayrolles, A. Mensch, C. Bamford, D. S. Chaplot, D. d. l. Casas, F. Bressand, G. Lengyel, G. Lample, L. Saulnier, et al. Mistral 7b. arXiv preprint arXiv:2310.06825, 2023.

M. Joshi, E. Choi, D. Weld, and L. Zettlemoyer. TriviaQA: A large scale distantly supervised challenge dataset for reading comprehension. In R. Barzilay and M.-Y. Kan, editors, Proceedings of the 55th Annual Meeting of the Association for Computational Linguistics (Volume 1: Long Papers), pages 1601–1611, Vancouver, Canada, July 2017. Association for Computational Linguistics. doi: 10.18653/v1/P17-1147. URL https://aclanthology.org/P17-1147.

D. Kalamkar, D. Mudigere, N. Mellempudi, D. Das, K. Banerjee, S. Avancha, D. T. Vooturi, N. Jammalamadaka, J. Huang, H. Yuen, et al. A study of bfloat16 for deep learning training. arXiv preprint arXiv:1905.12322, 2019.

S. Krishna, K. Krishna, A. Mohananey, S. Schwarcz, A. Stambler, S. Upadhyay, and M. Faruqui. Fact, fetch, and reason: A unified evaluation of retrieval-augmented generation. CoRR, abs/2409.12941, 2024. doi: 10.48550/ARXIV.2409.12941. URL https://doi.org/10.48550/arXiv.2409.12941.

T. Kwiatkowski, J. Palomaki, O. Redfield, M. Collins, A. P. Parikh, C. Alberti, D. Epstein, I. Polosukhin, J. Devlin, K. Lee, K. Toutanova, L. Jones, M. Kelcey, M. Chang, A. M. Dai, J. Uszkoreit, Q. Le, and S. Petrov. Natural questions: a benchmark for question answering research. Trans. Assoc. Comput. Linguistics, 7:452–466, 2019. doi: 10.1162/tacl_a_00276. URL https://doi.org/10.1162/tacl_a_00276.

G. Lai, Q. Xie, H. Liu, Y. Yang, and E. H. Hovy. RACE: large-scale reading comprehension dataset from examinations. In M. Palmer, R. Hwa, and S. Riedel, editors, Proceedings of the 2017 Conference on Empirical Methods in Natural Language Processing, EMNLP 2017, Copenhagen, Denmark, September 9-11, 2017, pages 785–794. Association for Computational Linguistics, 2017. doi: 10.18653/V1/D17-1082. URL https://doi.org/10.18653/v1/d17-1082.

N. Lambert, V. Pyatkin, J. Morrison, L. Miranda, B. Y. Lin, K. Chandu, N. Dziri, S. Kumar, T. Zick, Y. Choi, et al. Rewardbench: Evaluating reward models for language modeling. arXiv preprint arXiv:2403.13787, 2024.

D. Lepikhin, H. Lee, Y. Xu, D. Chen, O. Firat, Y. Huang, M. Krikun, N. Shazeer, and Z. Chen. Gshard: Scaling giant models with conditional computation and automatic sharding. In 9th International Conference on Learning Representations, ICLR 2021. OpenReview.net, 2021. URL https://openreview.net/forum?id=qrwe7XHTmYb.

Y. Leviathan, M. Kalman, and Y. Matias. Fast inference from transformers via speculative decoding. In International Conference on Machine Learning, ICML 2023, 23-29 July 2023, Honolulu, Hawaii, USA, volume 202 of Proceedings of Machine Learning Research, pages 19274–19286. PMLR, 2023. URL https://proceedings.mlr.press/v202/leviathan23a.html.

H. Li, Y. Zhang, F. Koto, Y. Yang, H. Zhao, Y. Gong, N. Duan, and T. Baldwin. CMMLU: Measuring massive multitask language understanding in Chinese. arXiv preprint arXiv:2306.09212, 2023.

S. Li and T. Hoefler. Chimera: efficiently training large-scale neural networks with bidirectional pipelines. In Proceedings of the International Conference for High Performance Computing, Networking, Storage and Analysis, SC '21, page 1–14. ACM, Nov. 2021. doi: 10.1145/3458817.3476145. URL http://dx.doi.org/10.1145/3458817.3476145.

T. Li, W.-L. Chiang, E. Frick, L. Dunlap, T. Wu, B. Zhu, J. E. Gonzalez, and I. Stoica. From crowdsourced data to high-quality benchmarks: Arena-hard and benchbuilder pipeline. arXiv preprint arXiv:2406.11939, 2024a.

W. Li, F. Qi, M. Sun, X. Yi, and J. Zhang. Ccpm: A chinese classical poetry matching dataset, 2021.

Y. Li, F. Wei, C. Zhang, and H. Zhang. EAGLE: speculative sampling requires rethinking feature uncertainty. In Forty-first International Conference on Machine Learning, ICML 2024, Vienna, Austria, July 21-27, 2024. OpenReview.net, 2024b. URL https://openreview.net/forum?id=1NdN7eXyb4.

B. Y. Lin. ZeroEval: A Unified Framework for Evaluating Language Models, July 2024. URL https://github.com/WildEval/ZeroEval.

I. Loshchilov and F. Hutter. Decoupled weight decay regularization. arXiv preprint arXiv:1711.05101, 2017.

S. Lundberg. The art of prompt design: Prompt boundaries and token healing, 2023. URL https://towardsdatascience.com/the-art-of-prompt-design-prompt-boundaries-and-token-healing-3b2448b0be38.

Y. Luo, Z. Zhang, R. Wu, H. Liu, Y. Jin, K. Zheng, M. Wang, Z. He, G. Hu, L. Chen, et al. Ascend HiFloat8 format for deep learning. arXiv preprint arXiv:2409.16626, 2024.

MAA. American invitational mathematics examination - aime. In American Invitational Mathematics Examination - AIME 2024, February 2024. URL https://maa.org/math-competitions/american-invitational-mathematics-examination-aime.

P. Micikevicius, D. Stosic, N. Burgess, M. Cornea, P. Dubey, R. Grisenthwaite, S. Ha, A. Heinecke, P. Judd, J. Kamalu, et al. FP8 formats for deep learning. arXiv preprint arXiv:2209.05433, 2022.

Mistral. Cheaper, better, faster, stronger: Continuing to push the frontier of ai and making it accessible to all, 2024. URL https://mistral.ai/news/mixtral-8x22b.

S. Narang, G. Diamos, E. Elsen, P. Micikevicius, J. Alben, D. Garcia, B. Ginsburg, M. Houston, O. Kuchaiev, G. Venkatesh, et al. Mixed precision training. In Int. Conf. on Learning Representation, 2017.

B. Noune, P. Jones, D. Justus, D. Masters, and C. Luschi. 8-bit numerical formats for deep neural networks. arXiv preprint arXiv:2206.02915, 2022.

NVIDIA. Improving network performance of HPC systems using NVIDIA Magnum IO NVSHMEM and GPUDirect Async. https://developer.nvidia.com/blog/improving-network-performance-of-hpc-systems-using-nvidia-magnum-io-nvshmem-and-gpudirect-async, 2022.

NVIDIA. Blackwell architecture. https://www.nvidia.com/en-us/data-center/technologies/blackwell-architecture/, 2024a.

NVIDIA. TransformerEngine, 2024b. URL https://github.com/NVIDIA/TransformerEngine. Accessed: 2024-11-19.

OpenAI. Hello GPT-4o, 2024a. URL https://openai.com/index/hello-gpt-4o/.

OpenAI. Multilingual massive multitask language understanding (mmmlu), 2024b. URL https://huggingface.co/datasets/openai/MMMLU.

OpenAI. Introducing SimpleQA, 2024c. URL https://openai.com/index/introducing-simpleqa/.

OpenAI. Introducing SWE-bench verified we're releasing a human-validated subset of swe-bench that more, 2024d. URL https://openai.com/index/introducing-swe-bench-verified/.

B. Peng, J. Quesnelle, H. Fan, and E. Shippole. Yarn: Efficient context window extension of large language models. arXiv preprint arXiv:2309.00071, 2023a.

H. Peng, K. Wu, Y. Wei, G. Zhao, Y. Yang, Z. Liu, Y. Xiong, Z. Yang, B. Ni, J. Hu, et al. FP8-LM: Training FP8 large language models. arXiv preprint arXiv:2310.18313, 2023b.

P. Qi, X. Wan, G. Huang, and M. Lin. Zero bubble pipeline parallelism. arXiv preprint arXiv:2401.10241, 2023a.

P. Qi, X. Wan, G. Huang, and M. Lin. Zero bubble pipeline parallelism, 2023b. URL https://arxiv.org/abs/2401.10241.

Qwen. Qwen technical report. arXiv preprint arXiv:2309.16609, 2023.

Qwen. Introducing Qwen1.5, 2024a. URL https://qwenlm.github.io/blog/qwen1.5.

Qwen. Qwen2.5: A party of foundation models, 2024b. URL https://qwenlm.github.io/blog/qwen2.5.

S. Rajbhandari, J. Rasley, O. Ruwase, and Y. He. Zero: Memory optimizations toward training trillion parameter models. In SC20: International Conference for High Performance Computing, Networking, Storage and Analysis, pages 1–16. IEEE, 2020.

D. Rein, B. L. Hou, A. C. Stickland, J. Petty, R. Y. Pang, J. Dirani, J. Michael, and S. R. Bowman. GPQA: A graduate-level google-proof q&a benchmark. arXiv preprint arXiv:2311.12022, 2023.

B. D. Rouhani, R. Zhao, A. More, M. Hall, A. Khodamoradi, S. Deng, D. Choudhary, M. Cornea, E. Dellinger, K. Denolf, et al. Microscaling data formats for deep learning. arXiv preprint arXiv:2310.10537, 2023a.

B. D. Rouhani, R. Zhao, A. More, M. Hall, A. Khodamoradi, S. Deng, D. Choudhary, M. Cornea, E. Dellinger, K. Denolf, et al. Microscaling data formats for deep learning. arXiv preprint arXiv:2310.10537, 2023b.

K. Sakaguchi, R. L. Bras, C. Bhagavatula, and Y. Choi. Winogrande: An adversarial winograd schema challenge at scale, 2019.

Z. Shao, P. Wang, Q. Zhu, R. Xu, J. Song, M. Zhang, Y. Li, Y. Wu, and D. Guo. Deepseekmath: Pushing the limits of mathematical reasoning in open language models. arXiv preprint arXiv:2402.03300, 2024.

N. Shazeer, A. Mirhoseini, K. Maziarz, A. Davis, Q. V. Le, G. E. Hinton, and J. Dean. Outrageously large neural networks: The sparsely-gated mixture-of-experts layer. In 5th International Conference on Learning Representations, ICLR 2017. OpenReview.net, 2017. URL https://openreview.net/forum?id=B1ckMDqlg.

F. Shi, M. Suzgun, M. Freitag, X. Wang, S. Srivats, S. Vosoughi, H. W. Chung, Y. Tay, S. Ruder, D. Zhou, D. Das, and J. Wei. Language models are multilingual chain-of-thought reasoners. In The Eleventh International Conference on Learning Representations, ICLR 2023, Kigali, Rwanda, May 1-5, 2023. OpenReview.net, 2023. URL https://openreview.net/forum?id=fR3wGCk-IXp.

Y. Shibata, T. Kida, S. Fukamachi, M. Takeda, A. Shinohara, T. Shinohara, and S. Arikawa. Byte pair encoding: A text compression scheme that accelerates pattern matching. 1999.

J. Su, M. Ahmed, Y. Lu, S. Pan, W. Bo, and Y. Liu. Roformer: Enhanced transformer with rotary position embedding. Neurocomputing, 568:127063, 2024.

K. Sun, D. Yu, D. Yu, and C. Cardie. Investigating prior knowledge for challenging chinese machine reading comprehension, 2019a.

M. Sun, X. Chen, J. Z. Kolter, and Z. Liu. Massive activations in large language models. arXiv preprint arXiv:2402.17762, 2024.

X. Sun, J. Choi, C.-Y. Chen, N. Wang, S. Venkataramani, V. V. Srinivasan, X. Cui, W. Zhang, and K. Gopalakrishnan. Hybrid 8-bit floating point (HFP8) training and inference for deep neural networks. Advances in neural information processing systems, 32, 2019b.

M. Suzgun, N. Scales, N. Schärli, S. Gehrmann, Y. Tay, H. W. Chung, A. Chowdhery, Q. V. Le, E. H. Chi, D. Zhou, et al. Challenging big-bench tasks and whether chain-of-thought can solve them. arXiv preprint arXiv:2210.09261, 2022.

V. Thakkar, P. Ramani, C. Cecka, A. Shivam, H. Lu, E. Yan, J. Kosaian, M. Hoemmen, H. Wu, A. Kerr, M. Nicely, D. Merrill, D. Blasig, F. Qiao, P. Majcher, P. Springer, M. Hohnerbach, J. Wang, and M. Gupta. CUTLASS, Jan. 2023. URL https://github.com/NVIDIA/cutlass.

H. Touvron, T. Lavril, G. Izacard, X. Martinet, M.-A. Lachaux, T. Lacroix, B. Rozière, N. Goyal, E. Hambro, F. Azhar, et al. LLaMA: Open and efficient foundation language models. arXiv preprint arXiv:2302.13971, 2023a.

H. Touvron, L. Martin, K. Stone, P. Albert, A. Almahairi, Y. Babaei, N. Bashlykov, S. Batra, P. Bhargava, S. Bhosale, D. Bikel, L. Blecher, C. Canton-Ferrer, M. Chen, G. Cucurull, D. Esiobu, J. Fernandes, J. Fu, W. Fu, B. Fuller, C. Gao, V. Goswami, N. Goyal, A. Hartshorn, S. Hosseini,

R. Hou, H. Inan, M. Kardas, V. Kerkez, M. Khabsa, I. Kloumann, A. Korenev, P. S. Koura, M. Lachaux, T. Lavril, J. Lee, D. Liskovich, Y. Lu, Y. Mao, X. Martinet, T. Mihaylov, P. Mishra, I. Molybog, Y. Nie, A. Poulton, J. Reizenstein, R. Rungta, K. Saladi, A. Schelten, R. Silva, E. M. Smith, R. Subramanian, X. E. Tan, B. Tang, R. Taylor, A. Williams, J. X. Kuan, P. Xu, Z. Yan, I. Zarov, Y. Zhang, A. Fan, M. Kambadur, S. Narang, A. Rodriguez, R. Stojnic, S. Edunov, and T. Scialom. Llama 2: Open foundation and fine-tuned chat models. CoRR, abs/2307.09288, 2023b. doi: 10.48550/arXiv.2307.09288. URL https://doi.org/10.48550/arXiv.2307.09288.

A. Vaswani, N. Shazeer, N. Parmar, J. Uszkoreit, L. Jones, A. N. Gomez, Ł. Kaiser, and I. Polosukhin. Attention is all you need. Advances in neural information processing systems, 30, 2017.

L. Wang, H. Gao, C. Zhao, X. Sun, and D. Dai. Auxiliary-loss-free load balancing strategy for mixture-of-experts. CoRR, abs/2408.15664, 2024a. URL https://doi.org/10.48550/arXiv.2408.15664.

Y. Wang, X. Ma, G. Zhang, Y. Ni, A. Chandra, S. Guo, W. Ren, A. Arulraj, X. He, Z. Jiang, T. Li, M. Ku, K. Wang, A. Zhuang, R. Fan, X. Yue, and W. Chen. Mmlu-pro: A more robust and challenging multi-task language understanding benchmark. CoRR, abs/2406.01574, 2024b. URL https://doi.org/10.48550/arXiv.2406.01574.

T. Wei, J. Luan, W. Liu, S. Dong, and B. Wang. Cmath: Can your language model pass chinese elementary school math test?, 2023.

M. Wortsman, T. Dettmers, L. Zettlemoyer, A. Morcos, A. Farhadi, and L. Schmidt. Stable and low-precision training for large-scale vision-language models. Advances in Neural Information Processing Systems, 36:10271–10298, 2023.

H. Xi, C. Li, J. Chen, and J. Zhu. Training transformers with 4-bit integers. Advances in Neural Information Processing Systems, 36:49146–49168, 2023.

C. S. Xia, Y. Deng, S. Dunn, and L. Zhang. Agentless: Demystifying llm-based software engineering agents. arXiv preprint, 2024.

H. Xia, T. Ge, P. Wang, S. Chen, F. Wei, and Z. Sui. Speculative decoding: Exploiting speculative execution for accelerating seq2seq generation. In Findings of the Association for Computational Linguistics: EMNLP 2023, Singapore, December 6-10, 2023, pages 3909–3925. Association for Computational Linguistics, 2023. URL https://doi.org/10.18653/v1/2023.findings-emnlp.257.

G. Xiao, J. Lin, M. Seznec, H. Wu, J. Demouth, and S. Han. Smoothquant: Accurate and efficient post-training quantization for large language models. In International Conference on Machine Learning, pages 38087–38099. PMLR, 2023.

L. Xu, H. Hu, X. Zhang, L. Li, C. Cao, Y. Li, Y. Xu, K. Sun, D. Yu, C. Yu, Y. Tian, Q. Dong, W. Liu, B. Shi, Y. Cui, J. Li, J. Zeng, R. Wang, W. Xie, Y. Li, Y. Patterson, Z. Tian, Y. Zhang, H. Zhou, S. Liu, Z. Zhao, Q. Zhao, C. Yue, X. Zhang, Z. Yang, K. Richardson, and Z. Lan. CLUE: A chinese language understanding evaluation benchmark. In D. Scott, N. Bel, and C. Zong, editors, Proceedings of the 28th International Conference on Computational Linguistics, COLING 2020, Barcelona, Spain (Online), December 8-13, 2020, pages 4762–4772. International Committee on Computational Linguistics, 2020. doi: 10.18653/V1/2020.COLING-MAIN.419. URL https://doi.org/10.18653/v1/2020.coling-main.419.

R. Zellers, A. Holtzman, Y. Bisk, A. Farhadi, and Y. Choi. HellaSwag: Can a machine really finish your sentence? In A. Korhonen, D. R. Traum, and L. Màrquez, editors, Proceedings of the 57th Conference of the Association for Computational Linguistics, ACL 2019, Florence, Italy, July 28- August 2, 2019, Volume 1: Long Papers, pages 4791–4800. Association for Computational Linguistics, 2019. doi: 10.18653/v1/p19-1472. URL https://doi.org/10.18653/v1/p19-1472.

W. Zhong, R. Cui, Y. Guo, Y. Liang, S. Lu, Y. Wang, A. Saied, W. Chen, and N. Duan. AGIEval: A human-centric benchmark for evaluating foundation models. CoRR, abs/2304.06364, 2023. doi: 10.48550/arXiv.2304.06364. URL https://doi.org/10.48550/arXiv.2304.06364.

J. Zhou, T. Lu, S. Mishra, S. Brahma, S. Basu, Y. Luan, D. Zhou, and L. Hou. Instruction-following evaluation for large language models. arXiv preprint arXiv:2311.07911, 2023.

Appendix

A. Contributions and Acknowledgments

Research & Engineering
Aixin Liu
Bing Xue
Bingxuan Wang
Bochao Wu
Chengda Lu
Chenggang Zhao
Chengqi Deng
Chenyu Zhang*
Chong Ruan
Damai Dai
Daya Guo
Dejian Yang
Deli Chen
Erhang Li
Fangyun Lin
Fucong Dai
Fuli Luo*
Guangbo Hao
Guanting Chen
Guowei Li
H. Zhang
Han Bao*
Hanwei Xu
Haocheng Wang*
Haowei Zhang
Honghui Ding
Huajian Xin*
Huazuo Gao
Hui Qu
Jianzhong Guo
Jiashi Li
Jiawei Wang*
Jingchang Chen
Jingyang Yuan
Junjie Qiu
Junlong Li
Junxiao Song
Kai Dong
Kai Hu*
Kaige Gao
Kang Guan
Kexin Huang
Kuai Yu
Lean Wang
Lecong Zhang
Liang Zhao
Litong Wang
Liyue Zhang
Mingchuan Zhang
Minghua Zhang
Minghui Tang
Panpan Huang
Peiyi Wang
Qiancheng Wang
Qihao Zhu
Qinyu Chen
Qiushi Du
Ruiqi Ge
Ruisong Zhang
Ruizhe Pan
Runji Wang
Runxin Xu
Ruoyu Zhang
Shanghao Lu
Shangyan Zhou
Shanhuang Chen
Shengfeng Ye
Shirong Ma
Shiyu Wang
Shuiping Yu
Shunfeng Zhou
Shuting Pan
Tao Yun
Tian Pei
Wangding Zeng
Wanjia Zhao*
Wen Liu
Wenfeng Liang
Wenjun Gao
Wenqin Yu
Wentao Zhang
Xiao Bi
Xiaodong Liu
Xiaohan Wang
Xiaokang Chen
Xiaokang Zhang
Xiaotao Nie
Xin Cheng
Xin Liu

Xin Xie
Xingchao Liu
Xingkai Yu
Xinyu Yang
Xinyuan Li
Xuecheng Su
Xuheng Lin
Y.K. Li
Y.Q. Wang
Y.X. Wei
Yang Zhang
Yanhong Xu
Yao Li
Yao Zhao
Yaofeng Sun
Yaohui Wang
Yi Yu
Yichao Zhang
Yifan Shi
Yiliang Xiong
Ying He
Yishi Piao
Yisong Wang
Yixuan Tan
Yiyang Ma*
Yiyuan Liu
Yongqiang Guo
Yu Wu
Yuan Ou
Yuduan Wang
Yue Gong
Yuheng Zou
Yujia He
Yunfan Xiong
Yuxiang Luo
Yuxiang You
Yuxuan Liu
Yuyang Zhou
Z.F. Wu
Z.Z. Ren
Zehui Ren
Zhangli Sha
Zhe Fu
Zhean Xu
Zhenda Xie
Zhengyan Zhang
Zhewen Hao
Zhibin Gou
Zhicheng Ma
Zhigang Yan
Zhihong Shao
Zhiyu Wu
Zhuoshu Li
Zihui Gu
Zijia Zhu
Zijun Liu*
Zilin Li
Ziwei Xie
Ziyang Song
Ziyi Gao
Zizheng Pan

Data Annotation
Bei Feng
Hui Li
J.L. Cai
Jiaqi Ni
Lei Xu
Meng Li
Ning Tian
R.J. Chen
R.L. Jin
Ruyi Chen
S.S. Li
Shuang Zhou
Tianyu Sun
X.Q. Li
Xiangyue Jin
Xiaojin Shen
Xiaosha Chen
Xiaowen Sun
Xiaoxiang Wang
Xinnan Song
Xinyi Zhou
Y.X. Zhu
Yanhong Xu
Yanping Huang
Yaohui Li
Yi Zheng
Yuchen Zhu
Yunxian Ma
Zhen Huang
Zhipeng Xu
Zhongyu Zhang

Business & Compliance
Dongjie Ji

Jian Liang
Jin Chen
Leyi Xia
Miaojun Wang
Mingming Li
Peng Zhang
Shaoqing Wu
Shengfeng Ye
T. Wang
W.L. Xiao
Wei An
Xianzu Wang
Xinxia Shan
Ying Tang
Yukun Zha
Yuting Yan
Zhen Zhang

Within each role, authors are listed alphabetically by the first name. Names marked with * denote individuals who have departed from our team.

B. Ablation Studies for Low-Precision Training

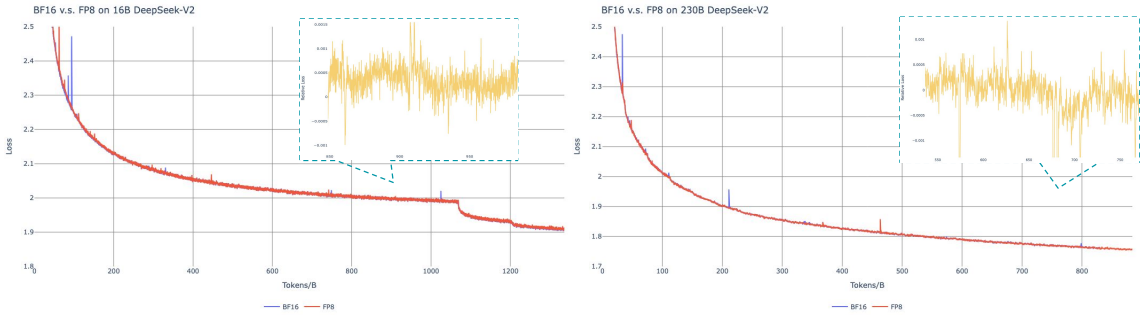

Figure 10 | Loss curves comparison between BF16 and FP8 training. Results are smoothed by Exponential Moving Average (EMA) with a coefficient of 0.9.

B.1. FP8 v.s. BF16 Training

We validate our FP8 mixed precision framework with a comparison to BF16 training on top of two baseline models across different scales. At the small scale, we train a baseline MoE model comprising approximately 16B total parameters on 1.33T tokens. At the large scale, we train a baseline MoE model comprising approximately 230B total parameters on around 0.9T tokens. We show the training curves in Figure 10 and demonstrate that the relative error remains below 0.25% with our high-precision accumulation and fine-grained quantization strategies.

B.2. Discussion About Block-Wise Quantization

Although our tile-wise fine-grained quantization effectively mitigates the error introduced by feature outliers, it requires different groupings for activation quantization, i.e., `1x128` in forward pass and `128x1` for backward pass. A similar process is also required for the activation gradient. A straightforward strategy is to apply block-wise quantization per `128x128` elements like the way we quantize the model weights. In this way, only transposition is required for backward. Therefore, we conduct an experiment where all tensors associated with `Dgrad` are quantized on a block-wise basis. The results reveal that the `Dgrad` operation which computes the activation gradients and back-propagates to shallow layers in a chain-like manner, is highly sensitive to precision. Specifically, block-wise quantization of activation gradients leads to

model divergence on an MoE model comprising approximately 16B total parameters, trained for around 300B tokens. We hypothesize that this sensitivity arises because activation gradients are highly imbalanced among tokens, resulting in token-correlated outliers (Xi et al., 2023). These outliers cannot be effectively managed by a block-wise quantization approach.

C. Expert Specialization Patterns of the 16B Aux-Loss-Based and Aux-Loss-Free Models

We record the expert load of the 16B auxiliary-loss-based baseline and the auxiliary-loss-free model on the Pile test set. The auxiliary-loss-free model tends to have greater expert specialization across all layers, as demonstrated in Figure 10.

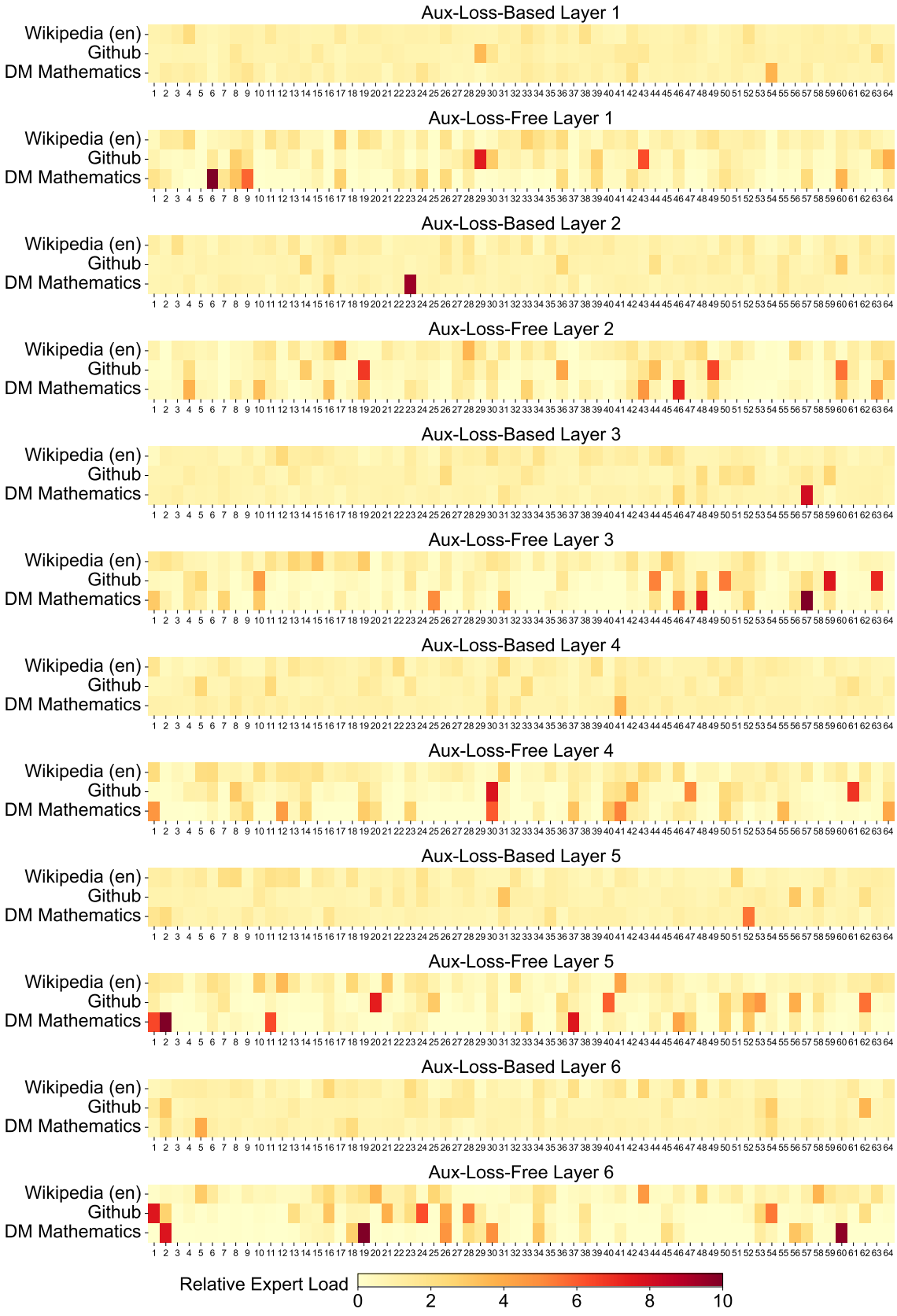
Aux-Loss-Based Layer 1
Aux-Loss-Free Layer 1
Aux-Loss-Based Layer 2
Aux-Loss-Free Layer 2
Aux-Loss-Based Layer 3
Aux-Loss-Free Layer 3
Aux-Loss-Based Layer 4
Aux-Loss-Free Layer 4
Aux-Loss-Based Layer 5
Aux-Loss-Free Layer 5
Aux-Loss-Based Layer 6
Aux-Loss-Free Layer 6
Wikipedia (en)
Github
DM Mathematics
1 2 3 4 5 6 7 8 9 10 11 12 13 14 15 16 17 18 19 20 21 22 23 24 25 26 27 28 29 30 31 32 33 34 35 36 37 38 39 40 41 42 43 44 45 46 47 48 49 50 51 52 53 54 55 56 57 58 59 60 61 62 63 64
Relative Expert Load
0
2
4
6
8
10

(a) Layers 1-7

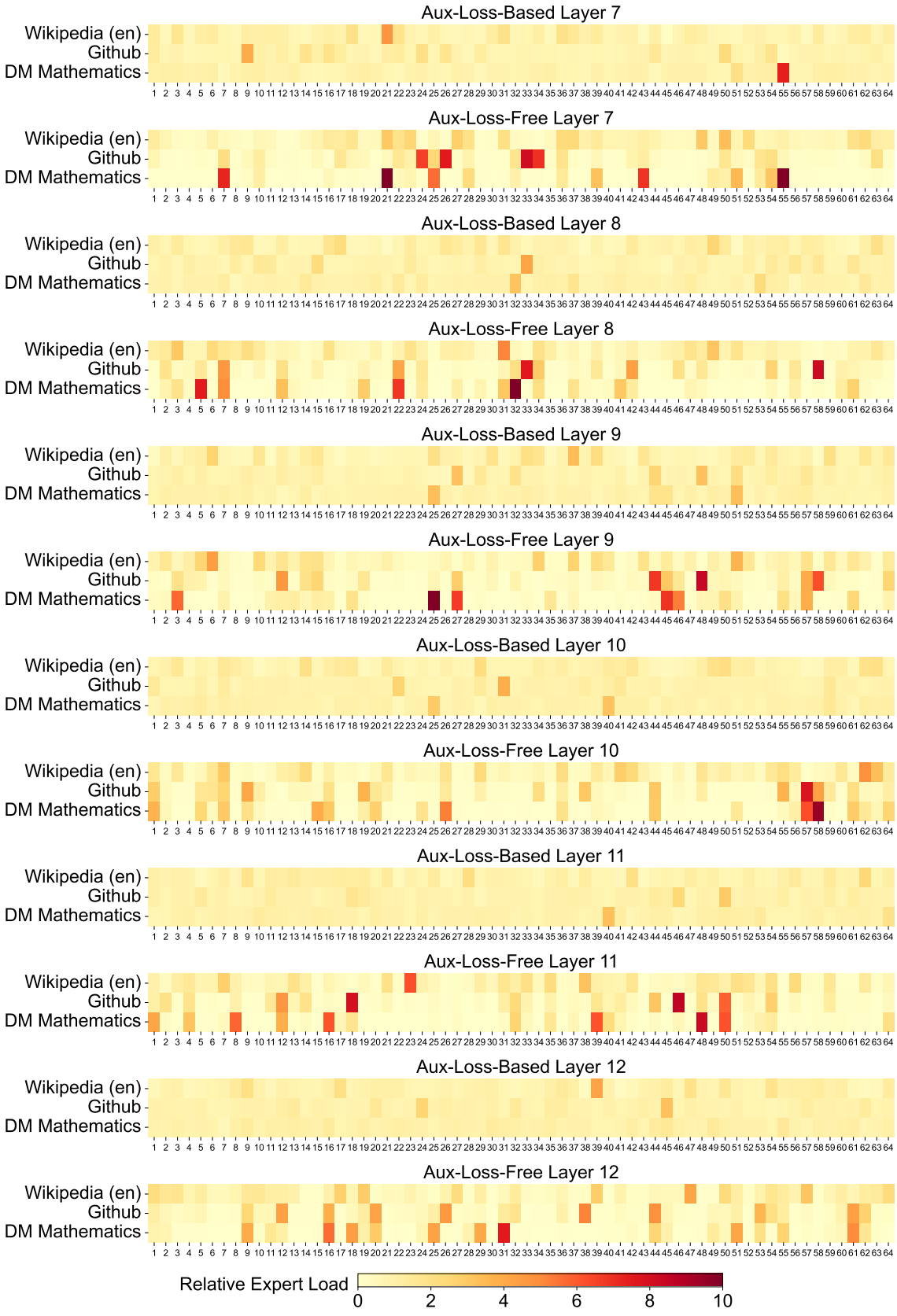
Aux-Loss-Based Layer 7
Aux-Loss-Free Layer 7
Aux-Loss-Based Layer 8
Aux-Loss-Free Layer 8
Aux-Loss-Based Layer 9
Aux-Loss-Free Layer 9
Aux-Loss-Based Layer 10
Aux-Loss-Free Layer 10
Aux-Loss-Based Layer 11
Aux-Loss-Free Layer 11
Aux-Loss-Based Layer 12
Aux-Loss-Free Layer 12
Wikipedia (en)
Github
DM Mathematics
1 2 3 4 5 6 7 8 9 10 11 12 13 14 15 16 17 18 19 20 21 22 23 24 25 26 27 28 29 30 31 32 33 34 35 36 37 38 39 40 41 42 43 44 45 46 47 48 49 50 51 52 53 54 55 56 57 58 59 60 61 62 63 64
Relative Expert Load
0
2
4
6
8
10

(b) Layers 7-13

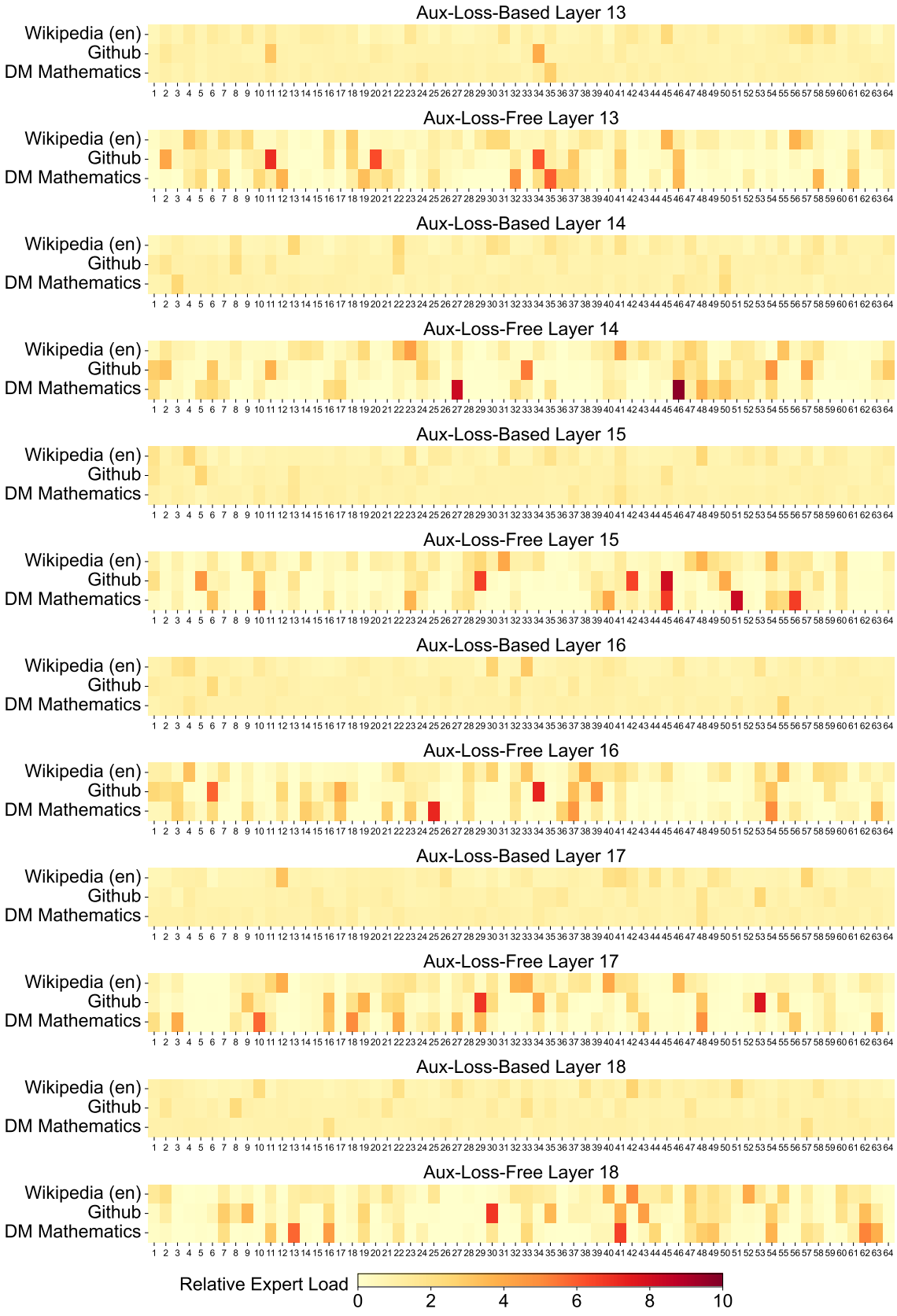

(c) Layers 13-19

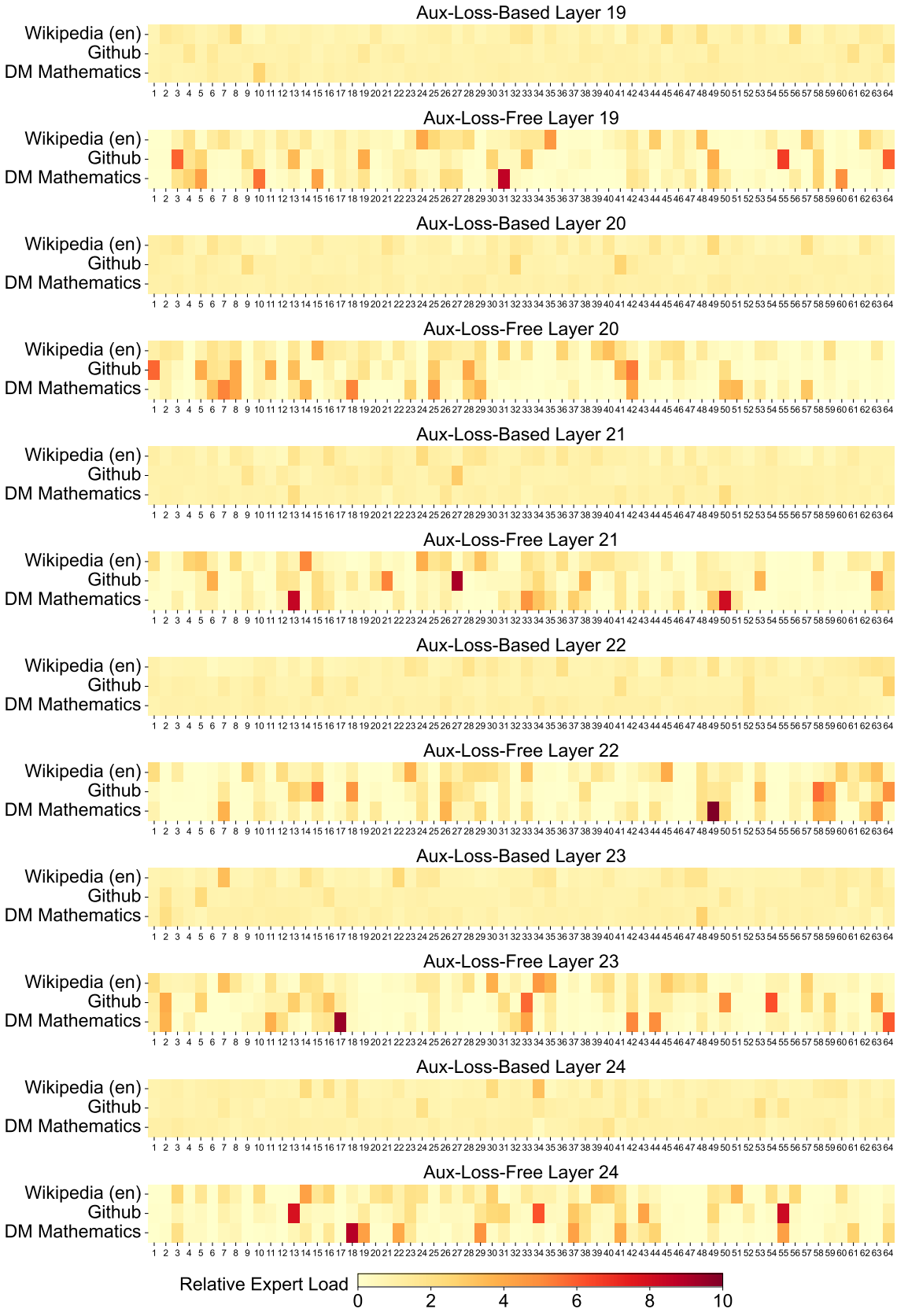

(d) Layers 19-25

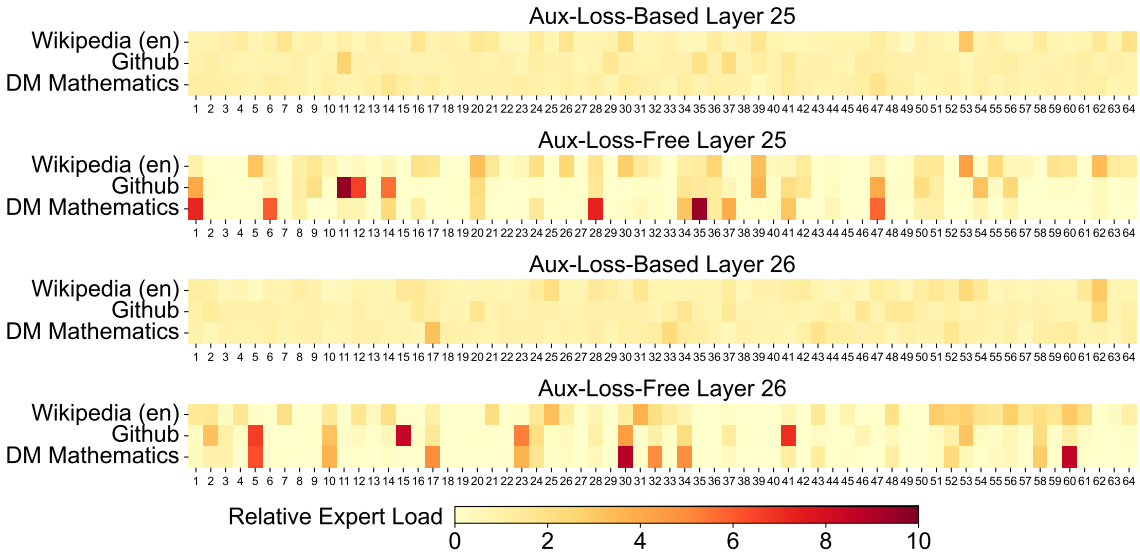

(e) Layers 25-27

Figure 10 | Expert load of auxiliary-loss-free and auxiliary-loss-based models on three domains in the Pile test set. The auxiliary-loss-free model shows greater expert specialization patterns than the auxiliary-loss-based one. The relative expert load denotes the ratio between the actual expert load and the theoretically balanced expert load.

Learning to Maximize Mutual Information for Chain-of-Thought Distillation

Xin Chen[1], **Hanxian Huang**[2], **Yanjun Gao**[3], **Yi Wang**[1], **Jishen Zhao**[2], **Ke Ding**[1]
[1]Applied ML Group, Intel Corp.
[2]University of California San Diego, [3]University of Wisconsin Madison
[1]{xin.chen, yi.a.wang, ke.ding}@intel.com,
[2]{hah008, jzhao}@ucsd.edu,
[3]ygao@medicine.wisc.edu

Abstract

Knowledge distillation, the technique of transferring knowledge from large, complex models to smaller ones, marks a pivotal step towards efficient AI deployment. Distilling Step-by-Step (DSS), a novel method utilizing chain-of-thought (CoT) distillation, has demonstrated promise by imbuing smaller models with the superior reasoning capabilities of their larger counterparts. In DSS, the distilled model acquires the ability to generate rationales and predict labels concurrently through a multi-task learning framework. However, DSS overlooks the intrinsic relationship between the two training tasks, leading to ineffective integration of CoT knowledge with the task of label prediction. To this end, we investigate the mutual relationship of the two tasks from Information Bottleneck perspective and formulate it as maximizing the mutual information of the representation features of the two tasks. We propose a variational approach to solve this optimization problem using a learning-based method. Our experimental results across four datasets demonstrate that our method outperforms the state-of-the-art DSS. Our findings offer insightful guidance for future research on language model distillation as well as applications involving CoT. Codes are available at https://github.com/xinchen9/cot_distillation_ACL2024.

1 Introduction

The capabilities of larger language models (LLMs) tend to scale with their model size, leading to a substantial demand for memory and compute resources (Chowdhery et al., 2023; Wei et al., 2022a). Distilling knowledge from larger LLMs to smaller LLMs has been crucial for the efficient deployment of AI (Hinton et al., 2015; Phuong and Lampert, 2019). Chain-of-Thought (CoT) (Wei et al., 2022b) distillation represents a pivotal advance in the quest to endow smaller language models with the sophisticated reasoning capabilities of their larger counterparts. By distilling complex thought processes into more compact models, this approach aims to democratize access to advanced natural language understanding and reasoning across a wider array of computational resources (Ma et al., 2023; Magister et al., 2023; Li et al., 2023).

Distilling Step-by-Step (DSS) (Hsieh et al., 2023) introduces a CoT distillation method that guides smaller models using rationales from LLMs within a multi-task learning (MTL) framework, training them for both label prediction and rationale generation tasks. While DSS brings out the benefits of reducing computational costs, it suffers from the same problem as the conventional MTL framework, that is the difficulty in effectively connecting the prediction and generation tasks. The intricacies inherent in training models within the MTL framework can undermine the effectiveness and reliability of the DSS process (Wang et al., 2023b). Despite the successful setup of an MTL framework in DSS, where the tasks of label prediction and rationale generation are intrinsically related, the current configuration may not optimally capture and maximize the mutual knowledge between these tasks. Furthermore, LLMs are prone to producing hallucinations and inconsistent rationales, which potentially mislead the student model toward incorrect answers and cause conflicts in MTL that destruct student model learning (Mueller et al., 2022).

To address this issue, we model the DSS using information bottleneck (IB) and investigate it from an information-theoretic viewpoint (Tishby and Zaslavsky, 2015). Subsequently, we formulate the DSS as an optimization problem to maximize mutual information (MI) of label prediction and rationale generation tasks. However, estimating MI from finite data is a known difficult problem (McAllester and Stratos, 2020; Belghazi et al., 2018). In this study, we introduce a variational

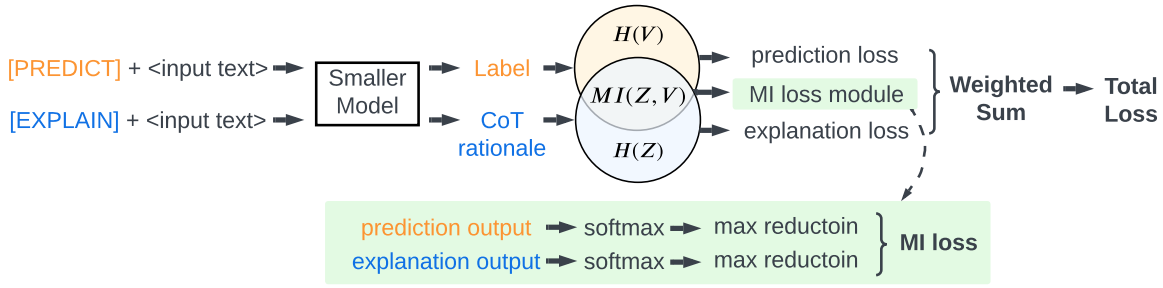

Figure 1: Overview of our approach: CoT distillation from an IB perspective and measurement of the intrinsic relationship between the two tasks by MI. The DSS is an MTL framework pipeline comprising label prediction and rationale generation tasks. H represents the entropy of representation features V and Z. Besides prediction loss and explanation losses used in conventional DSS, we design an auxiliary loss module to maximize MI between the two representation features. This process enhances CoT reasoning capacity through knowledge distillation.

method to estimate the MI. Recently, knowledge distillation has been used for solving the challenge of preserving task-specific training in MTL (Li and Bilen, 2020). Consequently, we propose a practical yet effective auxiliary loss to quantify the shared information between the prediction and the generation tasks, thereby enhancing the alignment between the two tasks and facilitating the knowledge transfer from CoT. We conduct comprehensive experiments with two smaller types of T5 models (Raffel et al., 2020), T5-base (220M) and T5-small (60M), on four popular datasets. Furthermore, we provide detailed analysis in Section 5. Our main contributions are summarized below:

- We reframe the MTL framework of DSS as a MI estimation challenge, aiming to maximize the MI between label prediction and rationale generation tasks. To achieve this, we introduce a variational approach grounded in the IB principle for effective MI estimation. To the best of our knowledge, we present the first work of improving CoT distillation from an IB perspective.
- Beyond establishing a theoretical foundation, we present a practical approach for MI estimation, incorporating a simple yet effective auxiliary loss to learning to maximize MI and enhance DSS.
- Our methodology demonstrably outperforms existing benchmarks across multiple datasets, evidencing the efficacy of our approach in enhancing the reasoning capabilities of distilled models.
- We conduct a systematic review of the relationship between predictive and explainable tasks under MTL training, presenting both qualitative and quantitative analysis results.

With the theoretical proofs and experiment results, we aim to provide stepping stones for future research on enhancing CoT distillation through an effective MTL framework, guided by principles from information theory.

2 Related Work

We present an overview of previous work across three areas related to our study: knowledge distillation, multi-task learning and information bottleneck.

Knowledge Distillation (KD) While originally designed for training small models by leveraging the extensive knowledge of larger models (Hinton et al., 2015), KL has been extended to a variety of applications due to its effective transfer of knowledge between models and tasks (Chen et al., 2021; Wang and Yoon, 2021; Sanh et al., 2019; Jiao et al., 2020). An crucial yet open challenge is how to effectively transfer the knowledge. To address the issue, previous studies (Zhang et al., 2022b; Allen-Zhu and Li, 2023; Zhang et al., 2021) extract different features and design auxiliary loss functions to enhance KL. Our work focus on improving the model by acquiring mutual knowledge in addressing both label prediction and rationale generation tasks.

Multi-Task Learning (MTL) Through exploiting commonalities and differences of relevant tasks, MTL can enhance improve learning efficiency and prediction accuracy by learning multiple objectives from a share representation (Caruana, 1997; Zhang and Yang, 2021). In recent years, MLT has been broadly applied to NLP tasks (Worsham and Kalita, 2020; Zhang et al., 2023; Liu et al., 2019). However, some works figure out that multiple tasks trained simultaneously could conflict with each other and it is challenging to optimize the perfor-

mance of all tasks simultaneously (Kendall et al., 2018; Lin et al., 2019). In recent years, KD has also been applied within MTL frameworks, achieving state-of-the-art results in various applications (Li and Bilen, 2020; Xu et al., 2023; Yang et al., 2022).

Information Bottleneck (IB) IB (Tishby and Zaslavsky, 2015; Slonim, 2002) provides a powerful statistical tool to learn representation to preserve complex intrinsic correlation structures over high dimensional data. As a general measure of the dependence between two random variables, MI is also widely used in deep learning to effectively represent the dependencies of features (Cover, 1999; Covert et al., 2023; Liu et al., 2009). MI estimation is known to be difficult, and recent progress has been made towards learning-based variational approaches (Tian et al., 2020; Covert et al., 2023; Bachman et al., 2019; Tschannen et al., 2019; Belghazi et al., 2018). Another challenge associated with the IB principle is the optimization process, which involves a trade-off between achieving a concise representation and maintaining strong predictive capabilities (Alemi et al., 2016; Wang et al., 2019). Consequently, optimizing IB becomes a complex task that heavily depends on the formulation of the problem and the provision of an effective optimization solution. Recent studies has applied IB to solve complex machine learning problems both in computer vision (Tian et al., 2021; Du et al., 2020; Wan et al., 2021) and NLP (Chen and Ji, 2020; Zhang et al., 2022a; Paranjape et al., 2020). In this paper, we formulate our CoT distillation problem with MTL training pipeline using IB and provide a learning-based solution to IB optimization for our CoT distillation problem, as detailed in Section 3.

3 Methodology

This section begins with an introduction to preliminaries of IB. Following this, we formulate our CoT distillation idea within the IB framework and propose a learning approach to optimize MI.

3.1 Preliminaries

Under the DSS framework, the prefixes [PREDICT] and [EXPLAIN] will be prepended to the input text, TEXT, for tasks corresponding to label prediction and rationale generation, respectively. In the label prediction task, given the input [PREDICT] + TEXT along with predictive labels $\mathbf{Y}$, a representation feature $\mathbf{V}$, where $\mathbf{V} \in \mathbb{R}^d$, is trained using $\mathbf{Y}$. Similarly, in the rationale generation task, the input [EXPLAIN] + TEXT and rationale label $\mathbf{R}$ guide the training of a representation feature $\mathbf{Z}$, where $\mathbf{Z} \in \mathbb{R}^d$, using $\mathbf{R}$.

Our goal is to distill CoT knowledge from larger LLMs to smaller LLMs models. To achieve this, based on the basis of IB (Tishby and Zaslavsky, 2015; Zhang et al., 2022a; Wang et al., 2019), we model the DSS as following:

$$I(Z;Y) = \int p(z,y) \log \frac{p(z,y)}{p(z)p(y)} dzdy. \quad (1)$$

where sampling observations $z \sim \mathbf{Z}$ and $v \sim \mathbf{V}$. Here $p(\cdot)$ represents the probability distribution.

To encourage CoT distillation to focus on the information represented in label $\mathbf{Y}$, we propose using IB to enforce an upper, bound I_c, on the information flow from the representation features V to the representation features Z. This is achieved by maximizing the following objective:

$$\max I(Z;Y) \;\; s.t. \;\; I(Z;V) \leq I_c. \quad (2)$$

By employing Lagrangian objective, IB allows Z to be maximally expressive about Y while being maximally compressive regarding the input data, as follows:

$$\mathcal{C}_{IB} = I(Z;V) - \beta I(Z;Y) \quad (3)$$

where β is the Lagrange multiplier. Clearly, Eq. 3 demonstrates the trade-off optimization between high mutual information and high compression (Zhang et al., 2022a; Alemi et al., 2016). In our scenario, given a predefined small student model, the compression ratio is fixed. Therefore, we formulate the CoT distillation as an optimization problem:

$$\max I(Z;V) \quad (4)$$

Due to symmetric property of MI, $I(Z;V) = I(V;Z)$. CoT distillation can also enhance rationale generation task with the label knowledge. This is validated in Section 5.

3.2 Variational Bounds of MI

We rewrite $I(Z;V)$ of Equation 4 as follows:

$$I(Z;V) = \mathbb{E}_{p(z,v)}\Big[\log \frac{p(v|z)}{p(v)}\Big] \quad (5)$$

According to (Poole et al., 2019; Covert et al., 2023), a tractable variational upper bound can be

established by introducing a variational approximation $q(v)$ to replace the intractable marginal $p(v)$, demonstrated by:

$$\begin{aligned} I(Z;V) &= \mathbb{E}_{p(z,v)}\Big[\log \frac{p(v|z)q(v)}{p(v)q(v)}\Big] \\ &= \mathbb{E}_{p(z,v)}\Big[\log \frac{p(v|z)}{q(v)}\Big] \\ &- KL(p(v)||q(v)) \end{aligned} \tag{6}$$

here $KL[\cdot||\cdot]$ denotes Kullback-Leibler divergence. The bound is tight when $q(v) = p(v)$. Consequently, $KL(p(v)||q(v))$ is equal to $KL(p(v)||p(v))$, which becomes zero. Therefore, we can derive at the following inequality:

$$I(Z;V) \leq \mathbb{E}_{p(z,v)}\Big[\log \frac{p(z|v)}{p(v)}\Big] \tag{7}$$

We can then express the MI from Eq. 5 as the follows:

$$\begin{aligned} \mathbb{E}_{p(z,v)}\Big[\log \frac{p(z|v)}{p(v)}\Big] &= \sum p(z,v)\log\frac{p(v|z)}{p(v)} \\ &= \sum p(z|v)p(v)\log p(v|z) \\ &- \sum p(v)p(z|v)\log p(v) \end{aligned} \tag{8}$$

Assuming that $p(v)$ is uniform distribution for maximal entropy (**?**), the term $\sum p(v)p(z|v)\log p(v)$ is considered as a constant. This also allows for the omission of $p(v)$ in $\sum p(z|v)p(v)\log p(v|z)$. By combining Eq. 5 and Eq. 8, then maximization of $I(Z;V)$ can be expressed as:

$$\begin{aligned} \max I(Z;V) &= \max \mathbb{E}_{p(z,v)}\Big[\log \frac{p(z|v)}{p(v)}\Big] \\ &\propto \max \sum p(z|v)\log p(v|z) \\ &= \max(-\sum p(z|v)\log\frac{1}{p(v|z)}) \\ &= \min(\sum p(z|v)\log\frac{1}{p(v|z)}) \\ &= \min(\sum CE(z|v, v|z)) \end{aligned} \tag{9}$$

here CE represents cross entropy. Accordingly, CoT distillation in Eq. 4 is transformed into the problem outlined in the above equation. This problem can be addressed with a learning-based method. To tackle this issue, we have developed a new MI loss that minimizes cross-entropy of representation features of the rationale generation ($p(z|v)$) and representation features of the label prediction ($p(v|z)$), effectively maximizing MI during CoT distillation process.

3.3 Training Loss

The training loss is given by

$$\mathcal{L}_{total} = \alpha_1\mathcal{L}_{\text{prediction}} + \alpha_2\mathcal{L}_{\text{generation}} + \alpha_3\mathcal{L}_{\text{CE}} \tag{10}$$

where α_1, α_2 and α_3 are regularization parameters, all of which are non-negative. $\mathcal{L}_{\text{prediction}}$ represents the loss of the label prediction task, and $\mathcal{L}_{\text{generation}}$ represents the loss of the rationale generation task. Both are general cross-entropy loss as defined in (Hsieh et al., 2023).

According to the last line of Equation 9, we define the our MI loss as

$$\mathcal{L}_{\text{CE}} = l(f(\mathbf{Z}), f(\mathbf{V})) \tag{11}$$

f represents our proposed mutual information (MI) loss module, and l denotes the cross-entropy loss. As shown in Figure 1, the MI loss module consists of softmax and max reduction layers. The softmax function separately calculates the distributions for the outputs of the vocabulary spaces in the label prediction and rationale generation tasks. Subsequently, a max reduction operation is employed to reduce the dimensionality of the predicted outputs from both tasks to a uniform dimension for the loss calculation. Specifically, in the label prediction task, dimensions are reduced from $\mathbb{R}^{m\times d}$ to $\mathbb{R}^{1\times d}$, and in the rationale generation task, from $\mathbb{R}^{n\times d}$ to $\mathbb{R}^{1\times d}$.

4 Experiments

4.1 Experimental Setting

Datasets. We conducted the experiments on four widely-used benchmark datasets across three different NLP tasks: e-SNLI (Camburu et al., 2018) and ANLI (Nie et al., 2020) for natural language inference; CQA (Talmor et al., 2018) for commonsense question answering; and SVAMP (Patel et al., 2021) for arithmetic math word problems. We used rationale generated by PaLM 540B (Chowdhery et al., 2023), which were collected and open-sourced by (Hsieh et al., 2023)[1].

[1]Data and DSS code are from https://github.com/google-research/distilling-step-by-step.

Setup. Based on CoT properties and the comparative experimental study in (Hsieh et al., 2023), our work adopted T5-base (220 million) and T5-small (60 million) to the student models. α_1 and α_2 were set as 0.5 and α_3 is set as 0.1. We trained our models on one A100 GPU with $80G$ memory. For T5 base model, the training time for the full-size four dataset was approximately 14.4 hours. For T5 small model, the training times was approximately 8.6 hours.

Baselines. We compare our work with the state-of-the-art DSS (Hsieh et al., 2023) by running their open-sourced code and include two other baseline reported in their work: (1) Standard Finetune, which involves using the prevailing pretrain-then-finetune paradigm to finetune a model with ground-truth labels through standard label supervision. (Howard and Ruder, 2018). (2) Single-task, which finetunes the model using both of the label and non-CoT rationale as supervision .

Evaluation Settings. Following the DSS work (Hsieh et al., 2023), we adopt the accuracy as the performance metrics across all four datasets. Higher accuracy indicates better results. Besides accuracy, we also adopt Expected Calibration Errors (ECE) and Average Confidence Scores to evaluate calibration of the T5-base model. A lower ECE and higher Average Confidence Scores indicate better performance. We adopt GPT-4 to evaluate Quality of CoT examples and subjective analysis. Please refer to our codes for more details.

4.2 Results

Experiments of T5-base Model. We present our experimental results of the T5-base model in Table 1. In single-task training, the rationale and label are concatenated into a single sequence, which is treated as the target in training models (Hsieh et al., 2023). Our proposed method consistently achieves better performance than standard fine-tuning and single-task methods on all datasets. Compared to DSS, our method outperforms DSS on ANLI, CQA, and SVAMP, and achieves nearly the same accuracy on e-SNLI

Experiments of T5-small Model. The experimental results of T5-small model are shown in Table 2. The patterns of the results are similar to those of T5-base. Our proposed method consistently achieves better performance than standard finetuning across all dataset. Compared to DSS, our method outperforms DSS on ANLI, CQA and SVAMP, and is just 0.2% less accuracy on e-SNLI.

	e-SNLI	ANLI	CQA	SVAMP
Finetuning	88.38	43.58	62.19	62.63
Single-task	88.88	43.50	61.37	63.00
DSS	**89.51**	49.58	63.29	65.50
Ours	89.50	**51.20**	**63.88**	**68.00**

Table 1: CoT distillation results on T5-base model.

	e-SNLI	ANLI	CQA	SVAMP
Finetuning	82.90	42.00	43.16	45.00
DSS	**83.43**	42.90	43.24	48.00
Ours	83.23	**43.70**	**43.90**	**52.50**

Table 2: CoT distillation results on T5-small model.

Model	e-SNLI	ANLI
DSS	82.65	42.80
Ours	82.81	45.50

Table 3: Results on two dataset on T5-base model with LLM generated labels.

Distillation with LLM Labels. We conducted an experiment on e-SNLI and ANLI dataset with T5-base model to evaluate the effect of label quality. We distilled the student models using labels generated by 540B PaLM instead of the ground truth. The results are shown in Table 3. Comparing Table 1 and Table 3, we observe the label quality affects the distillation results in both methods. Even With the noisy LLM labels, our model still outperforms DSS on both datasets.

Distillation with smaller datasets. To evaluate the performance of our models on smaller datasets, we distilled T5-base and T5-small models on various sizes of four datasets and compared to DSS method. The results are shown in Figure. 2 and 3 respectively.

4.3 Ablation Study

Effectiveness of Difference Dimension Reduction Method In our proposed MI loss module, we employ maximum reduction to align the dimension of different features. Additionally, mean reduction serves as an alternative method for dimension reduction. We hypothesize that important features can represent better than average features. In Table 4, we present the results of two different layer of MI module. The results indicate the supe-

	e-SNLI	ANLI	CQA	SVAMP
Mean	89.34	**51.40**	63.88	66.50
Max	**89.50**	51.20	**63.88**	**68.00**

Table 4: Results of Mean Reduction Vs Maximum Reduction on T5-based model.

riority of the MI module with maximum reduction.

Comparison with KL Divergence The KL divergence loss has been extensively utilized in KD tasks, serving as KL a metric for assessing the similarity between two data distributions (Hinton et al., 2015; Zhang et al., 2022b; Gou et al., 2021). While KL divergence has found widespread application in various KD scenarios, modeling DSS using IB framework proves to be more accurate than using similarity measures, as discussed in Section 3. To validate our hypothesis, we conduct experiments on T5-base model using all four datasets. As shown in Table 5, our proposed method consistently outperforms the KL divergence approach, demonstrating superior performance.

	e-SNLI	ANLI	CQA	SVAMP
KL Divergence	89.42	42.00	62.49	67.00
Ours	**89.50**	**51.2**	**63.88**	**68.00**

Table 5: Results of KD loss VS our proposed cross entropy loss, on T5-base model.

5 Discussion

5.1 Analysis on T5 Calibration

Calibration measures the alignment between a model's predicted accuracy and its confidence levels. Lee et al. (2022) introduced an innovative perspective on model distillation, positioning the teacher model not only as a source of knowledge but also as a tool for identifying mis-calibration during the training of the student model. This ability to maintain calibration and make reliable predictions is crucial for downstream applications and has been the focus of prior studies (Chen et al., 2023; Lee et al., 2022; Jiang et al., 2021). Here, we apply the Expected Calibration Errors (ECE) and Average Confidence Scores to reflect the alignment between the model's predicted probabilities and the actual outcomes, thereby gauging the reliability and certainty of its predictions. Despite the potential limitations inherent in these metrics, we still employ ECE in our experiments due to its simplicity and popularity, as in previous work on investigating the calibration quality of T5 (Chen et al., 2023; Lee et al., 2022).

We employ a 10-bin-based ECE metric and a softmax-based approach to compute average confidence scores from the test outputs across all four datasets. Given that e-SNLI and ANLI essentially represent the same task, we conduct an out-of-domain experiment by testing the model checkpoint trained on one dataset with the test set of the other. This analysis gives us insights into how well our model generalizes across similar tasks and the robustness of its predictions in out-of-domain scenarios and to assess the calibration quality of the model more comprehensively.

Table 6 presents the results of the distilled model calibration evaluation. Overall, both models report lower ECE and confidence scores on SVAMP and e-SNLI, indicating that these two tasks are more challenging and models are less certain about their prediction. Lower ECE values from our MI-based distillation approach are presented for e-SNLI and ANLI, and their respective out-of-domain tests. Notably, our method achieves an ECE of 4.35 in e-SNLI, significantly lower than DSS's 8.54. However, in SVAMP and CQA, our method records higher ECE, indicating potential areas for improvement in these domains. The trade-off in calibration accuracy in specific tasks like SVAMP and CQA compared to DSS suggests future directions for refining our approach.

Regarding average confidence scores (Conf.), our method generally maintains competitive confidence levels, with notable improvements in e-SNLI and ANLI. In e-SNLI, the confidence is lower (30.06) compared to DSS (34.33), which, combined with a lower ECE, suggests a more realistic confidence estimation. Conversely, in the out-of-domain scenarios for e-SNLI and ANLI, our method shows marginally higher confidence scores than DSS, which, coupled with the lower ECE, indicates robustness in out-of-domain generalization.

5.2 Analysis on CoT Output

5.2.1 Quality of CoT Examples by GPT-4 Evaluation

We evaluate the quality of CoT examples using GPT-4, as it achieves the state-of-the-art human alignment performance and is used for text generation evaluation in previous work (Liu et al., 2023;

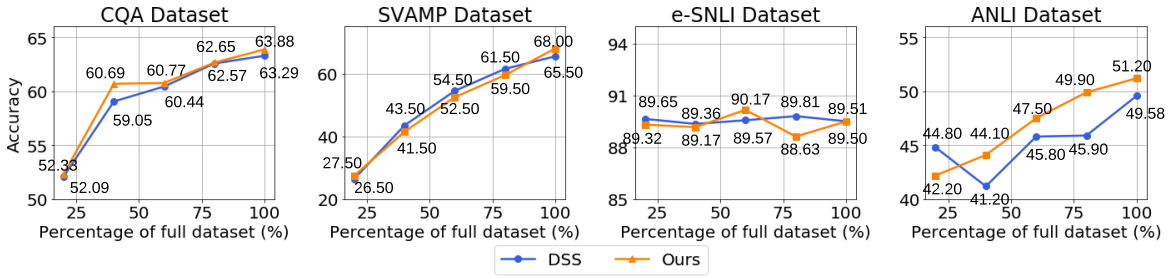

Figure 2: Comparison with DSS with varying sizes of training datasets on T5-base model.

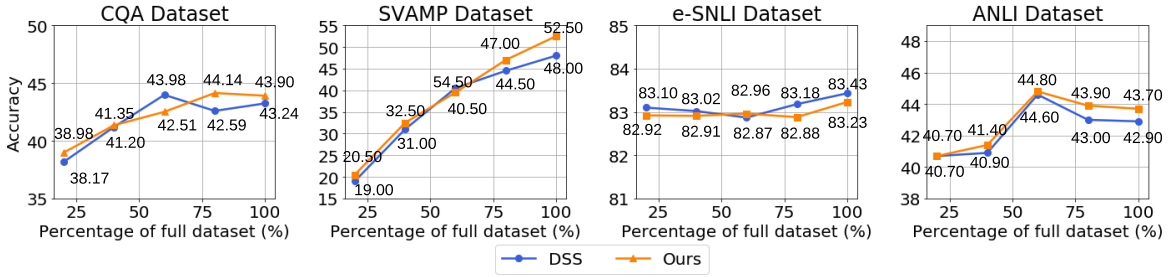

Figure 3: Comparison with DSS with varying sizes of training datasets on T5-small model.

Hsu et al., 2023; Wang et al., 2023a). Inspired by (Wang et al., 2023a), we ask GPT-4 to evaluate the quality of the provided CoT examples based on their coherency and relevancy to the input questions and answers. We randomly sample 50 CoT examples from the four datasets and ask GPT-4 to score based on a scale from 1 to 5, where 1 indicates completely incoherent and irrelevant responses, and 5 represents highly coherent, relevant, and helpful responses. For each sample, we run the same sample for four times to obtain self-consistency to measure the reliability of the responses. Table 7 presents the prompt we use for GPT-4 evaluation, average scores and standard deviation on the scores obtained over the four datasets. We report the scores on both provided CoT ("gold") rationales and distilled model predicted rationales.

The effectiveness of our MI-based distillation method is closely linked to the quality of CoT reasoning in the training data. When the CoT quality is high, as in SVAMP, a strong correlation is observed between the model's label prediction accuracy and the quality of its generated CoT. However, this correlation weakens significantly when the CoT quality is low (e-SNLI), suggesting that the model struggles to align label prediction with coherent rationale generation under poor training conditions. Interestingly, with average-quality CoT data (ANLI), the performance gap between our MI-based distillation and DSS is minimal, suggesting that the effectiveness of our approach is particularly reliant on the presence of high-quality reasoning in the training data.

5.2.2 Case Studies on the Output Rationale

We performed case studies on SVAMP and e-SNLI as illustrated in Figure 4 and 5. In the SVAMP example, the question asks the difference in the number of kids Julia played with from Monday to Tuesday, with specific numbers provided for Monday, Tuesday, and Wednesday. DSS generates an incorrect explanation, which contradicts the given question, resulting in to a wrong answer. Conversely, our method correctly identifies the comparison needed between the number of kids Julia played with on Monday and Tuesday, leading to the correct answer. Notably, our generated CoT reasoning is identical to the golden one, demonstrating that by precisely grasping the rationale, our approach effectively resolves the math problem. We also show the evaluation results (score and reasoning) from GPT-4, where our method gains a top score of 5 and DSS gains only a mere score of 1. This example showcases that the high-quality CoT generated by our method enhances problem-solving capabilities in math tasks like SVAMP.

Another example (Figure 5) is from e-SNLI,

Model	SVAMP		CQA		e-SNLI		ANLI		e-SNLI (Out)		ANLI (Out)	
	ECE	Conf.	ECE	Conf.	ECE	Conf.	ECE	Conf.	ECE	Conf.	ECE	Conf.
DSS	11.81	32.56	11.75	42.79	8.54	34.33	11.12	42.72	9.81	38.01	12.78	41.69
Ours	18.92	36.81	13.65	41.17	4.35	30.06	6.94	35.90	6.61	38.08	12.27	42.35

Table 6: Comparisons of our model and DSS on the expected calibration errors (ECE) and average confidence scores (Conf.).

Prompt for GPT 4 Evaluation
Given an input pair of a question and an answer of a *taskname* task, how good is the given Chain-of-thought example? From 1-5, where 1 is completely incoherent and irrelevant, 2 is somewhat incoherent and irrelevant, 3 is coherent, relevant but not helpful, 4 is somewhat helpful, and 5 is helpful and it explains the answer well.

Average Scores and Standard Deviation

Model	SVAMP	CQA	e-SNLI	ANLI
Gold	4.63±1.05	3.95±1.16	2.42±1.23	3.82±1.26
++	4.43±1.18	4.11±1.40	3.49±1.35	4.01±1.10
DSS	2.50±1.42	3.60±1.61	3.24±1.27	3.48±1.40
++	2.53±1.46	3.64±1.62	3.18±1.21	3.44±1.30
Ours	2.30±1.54	3.70±1.45	3.03±1.47	3.42±1.37
++	2.72±1.45	3.63±1.60	3.17±1.17	3.34±1.21

Table 7: Prompt used and results of 50 randomly sampled CoT examples from the four datasets evaluated by GPT-4. We use ++ to denote the setting with *self-consistency* evaluation.

Model	SVAMP	CQA	e-SNLI	ANLI
DSS	0.12	0.66	0.05	0.26
	$p > 0.05$	$p < 0.05$	$p > 0.05$	$p > 0.05$
Ours	0.42	0.53	0.03	0.26
	$p < 0.05$	$p < 0.05$	$p > 0.05$	$p > 0.05$

Table 8: Pearson correlation between CoT quality and accuracy of label prediction on the 50 random samples on the test set. We highlight the correlation with statistical significance ($p < 0.05$).

where the task is to identify whether the hypothesis is entailment, contradiction, or neutral, based on the given premise and hypothesis. Although both our method and DSS generate the correct label output, it is worth noting that, the CoT of our method points out the relationship between the premise and the hypothesis, while DSS only restates the hypothesis without providing any extra explanation or connecting the hypothesis to the premise. Our generated rationale also gains a higher score than DSS. A higher-quality rationale tends to facilitate more accurate label prediction, thereby enhancing overall task performance.

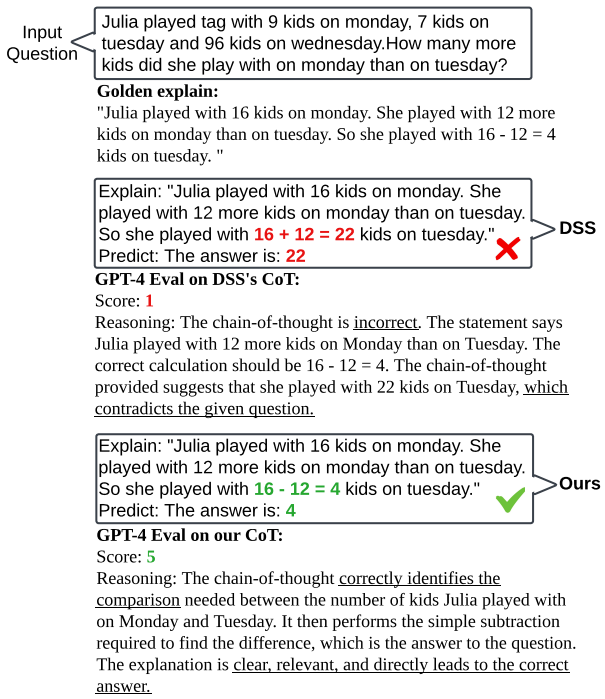

Figure 4: A case study of the output rationale on SVAMP.

6 Conclusion

In this paper, we re-investigate the DSS framework from a information-theoretic perspective. We model it using Information Bottleneck and propose to strengthen it by maximizing the mutual information between rationale generation and label prediction tasks. The proposed learning-based method can automatically optimize the CoT distillation and bolster the reasoning ability of the distilled small models. Our qualitative and quantitative analysis demonstrate the rationale behind our method and shed light on language model distillation and CoT applications.

7 Limitation

Our comparative analysis primarily focuses on the Distilling Step-by-Step (DSS) framework, which serves as our main benchmark. This concentrated comparison, while valuable for a deep understand-

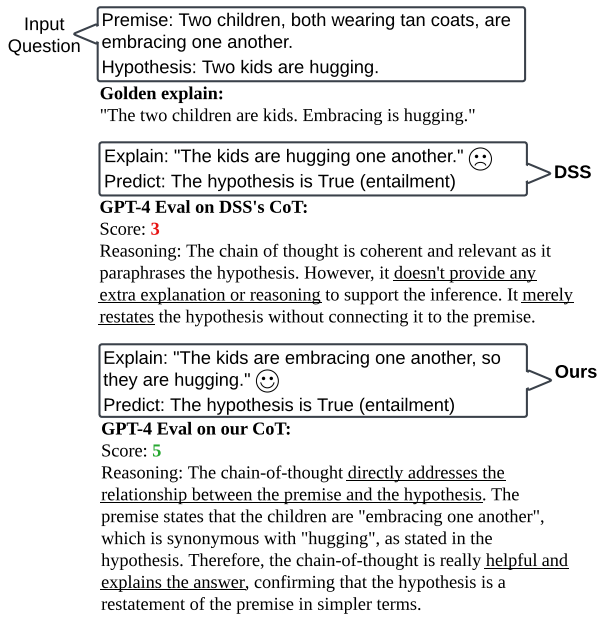

Figure 5: A case study of the output rationale on e-SNLI.

ing of DSS's nuances and our advancements over it, constitutes a limitation of our work. Specifically, our analysis does not extend to a broader range of knowledge distillation methods currently employed in the field. This focus may overlook the potential insights and contrasts that could emerge from evaluating our approach against a wider array of distillation techniques. Future research could benefit from a more expansive comparative study, incorporating diverse methodologies to fully contextualize our findings within the broader landscape of knowledge distillation practices. This broader comparison would not only validate the efficacy of our method in various settings but also illuminate areas for further refinement and innovation.

However, it is important to note that our contribution lies in providing an in-depth analysis from both theoretical and practical viewpoints to enhance the CoT distillation process. Our work delves into the intricacies of utilizing mutual information to improve distillation outcomes, offering significant advancements in understanding and applying CoT distillation techniques.

8 Ethical Issues

In this paper, we carefully considered the ethical implications in line with the ACL code of ethics. We evaluated the potential dual-use concerns, ensuring our research serves to benefit society and does not cause inadvertent harm. Our methodology and applications were thoroughly assessed for fairness, non-discrimination, and privacy, particularly in the context of data handling and model outputs. We also ensured our study did not expose any negative impact on individuals and groups. Moreover, we did not engage in academic dishonesty and adhered to high-quality processes and product standards in our professional work. We include this detailed discussion of these ethical considerations, affirming our commitment to responsible and beneficial computational linguistics research.

References

Alexander A Alemi, Ian Fischer, Joshua V Dillon, and Kevin Murphy. 2016. Deep variational information bottleneck. In *International Conference on Learning Representations*.

Zeyuan Allen-Zhu and Yuanzhi Li. 2023. Towards understanding ensemble, knowledge distillation and self-distillation in deep learning. In *The Eleventh International Conference on Learning Representations*.

Philip Bachman, R Devon Hjelm, and William Buchwalter. 2019. Learning representations by maximizing mutual information across views. *Advances in neural information processing systems*, 32.

Mohamed Ishmael Belghazi, Aristide Baratin, Sai Rajeshwar, Sherjil Ozair, Yoshua Bengio, Aaron Courville, and Devon Hjelm. 2018. Mutual information neural estimation. In *International conference on machine learning*, pages 531–540. PMLR.

Oana-Maria Camburu, Tim Rocktäschel, Thomas Lukasiewicz, and Phil Blunsom. 2018. e-snli: Natural language inference with natural language explanations. *Advances in Neural Information Processing Systems*, 31.

Rich Caruana. 1997. Multitask learning. *Machine learning*, 28:41–75.

Hanjie Chen and Yangfeng Ji. 2020. Learning variational word masks to improve the interpretability of neural text classifiers. In *Proceedings of the 2020 Conference on Empirical Methods in Natural Language Processing (EMNLP)*, pages 4236–4251.

Pengguang Chen, Shu Liu, Hengshuang Zhao, and Jiaya Jia. 2021. Distilling knowledge via knowledge review. In *Proceedings of the IEEE/CVF Conference on Computer Vision and Pattern Recognition*, pages 5008–5017.

Yangyi Chen, Lifan Yuan, Ganqu Cui, Zhiyuan Liu, and Heng Ji. 2023. A close look into the calibration of pre-trained language models. In *Proceedings of the 61st Annual Meeting of the Association for Computational Linguistics (Volume 1: Long Papers)*,

pages 1343–1367, Toronto, Canada. Association for Computational Linguistics.

Aakanksha Chowdhery, Sharan Narang, Jacob Devlin, Maarten Bosma, Gaurav Mishra, Adam Roberts, Paul Barham, Hyung Won Chung, Charles Sutton, Sebastian Gehrmann, et al. 2023. Palm: Scaling language modeling with pathways. *Journal of Machine Learning Research*, 24(240):1–113.

Thomas M Cover. 1999. *Elements of information theory*. John Wiley & Sons.

Ian Connick Covert, Wei Qiu, Mingyu Lu, Na Yoon Kim, Nathan J White, and Su-In Lee. 2023. Learning to maximize mutual information for dynamic feature selection. In *International Conference on Machine Learning*, pages 6424–6447. PMLR.

Yingjun Du, Jun Xu, Huan Xiong, Qiang Qiu, Xiantong Zhen, Cees GM Snoek, and Ling Shao. 2020. Learning to learn with variational information bottleneck for domain generalization. In *ECCV 2020*, pages 200–216. Springer.

Jianping Gou, Baosheng Yu, Stephen J Maybank, and Dacheng Tao. 2021. Knowledge distillation: A survey. *International Journal of Computer Vision*, 129:1789–1819.

Geoffrey Hinton, Oriol Vinyals, and Jeffrey Dean. 2015. Distilling the knowledge in a neural network. In *NIPS Deep Learning and Representation Learning Workshop*.

Jeremy Howard and Sebastian Ruder. 2018. Universal language model fine-tuning for text classification. *arXiv preprint arXiv:1801.06146*.

Cheng-Yu Hsieh, Chun-Liang Li, Chih-kuan Yeh, Hootan Nakhost, Yasuhisa Fujii, Alex Ratner, Ranjay Krishna, Chen-Yu Lee, and Tomas Pfister. 2023. Distilling step-by-step! outperforming larger language models with less training data and smaller model sizes. In *Findings of the Association for Computational Linguistics: ACL 2023*, pages 8003–8017, Toronto, Canada. Association for Computational Linguistics.

Ting-Yao Hsu, Chieh-Yang Huang, Ryan Rossi, Sungchul Kim, C Giles, and Ting-Hao Huang. 2023. Gpt-4 as an effective zero-shot evaluator for scientific figure captions. In *Findings of the Association for Computational Linguistics: EMNLP 2023*, pages 5464–5474.

Zhengbao Jiang, Jun Araki, Haibo Ding, and Graham Neubig. 2021. How can we know when language models know? on the calibration of language models for question answering. *Transactions of the Association for Computational Linguistics*, 9:962–977.

Xiaoqi Jiao, Yichun Yin, Lifeng Shang, Xin Jiang, Xiao Chen, Linlin Li, Fang Wang, and Qun Liu. 2020. Tinybert: Distilling bert for natural language understanding. In *Findings of the Association for Computational Linguistics: EMNLP 2020*, pages 4163–4174.

Alex Kendall, Yarin Gal, and Roberto Cipolla. 2018. Multi-task learning using uncertainty to weigh losses for scene geometry and semantics. In *Proceedings of the IEEE conference on computer vision and pattern recognition*, pages 7482–7491.

Dongkyu Lee, Zhiliang Tian, Yingxiu Zhao, Ka Chun Cheung, and Nevin Zhang. 2022. Hard gate knowledge distillation-leverage calibration for robust and reliable language model. In *Proceedings of the 2022 Conference on Empirical Methods in Natural Language Processing*, pages 9793–9803.

Liunian Harold Li, Jack Hessel, Youngjae Yu, Xiang Ren, Kai-Wei Chang, and Yejin Choi. 2023. Symbolic chain-of-thought distillation: Small models can also" think" step-by-step. *arXiv preprint arXiv:2306.14050*.

Wei-Hong Li and Hakan Bilen. 2020. Knowledge distillation for multi-task learning. In *Computer Vision–ECCV 2020 Workshops: Glasgow, UK, August 23–28, 2020, Proceedings, Part VI 16*, pages 163–176. Springer.

Xi Lin, Hui-Ling Zhen, Zhenhua Li, Qing-Fu Zhang, and Sam Kwong. 2019. Pareto multi-task learning. *Advances in neural information processing systems*, 32.

Huawen Liu, Jigui Sun, Lei Liu, and Huijie Zhang. 2009. Feature selection with dynamic mutual information. *Pattern Recognition*, 42(7):1330–1339.

Xiaodong Liu, Pengcheng He, Weizhu Chen, and Jianfeng Gao. 2019. Multi-task deep neural networks for natural language understanding. In *Proceedings of the 57th Annual Meeting of the Association for Computational Linguistics*, pages 4487–4496. Association for Computational Linguistics.

Yang Liu, Dan Iter, Yichong Xu, Shuohang Wang, Ruochen Xu, and Chenguang Zhu. 2023. Gpteval: Nlg evaluation using gpt-4 with better human alignment. *arXiv preprint arXiv:2303.16634*.

Yuhan Ma, Haiqi Jiang, and Chenyou Fan. 2023. Scicot: Leveraging large language models for enhanced knowledge distillation in small models for scientific qa. *arXiv preprint arXiv:2308.04679*.

Lucie Charlotte Magister, Jonathan Mallinson, Jakub Adamek, Eric Malmi, and Aliaksei Severyn. 2023. Teaching small language models to reason. In *Proceedings of the 61st Annual Meeting of the Association for Computational Linguistics (Volume 2: Short Papers)*, pages 1773–1781, Toronto, Canada.

David McAllester and Karl Stratos. 2020. Formal limitations on the measurement of mutual information. In *International Conference on Artificial Intelligence and Statistics*, pages 875–884. PMLR.

David Mueller, Nicholas Andrews, and Mark Dredze. 2022. Do text-to-text multi-task learners suffer from

task conflict? In *Findings of the Association for Computational Linguistics: EMNLP 2022*, pages 2843–2858.

Yixin Nie, Adina Williams, Emily Dinan, Mohit Bansal, Jason Weston, and Douwe Kiela. 2020. Adversarial nli: A new benchmark for natural language understanding. In *Proceedings of the 58th Annual Meeting of the Association for Computational Linguistics*. Association for Computational Linguistics.

Bhargavi Paranjape, Mandar Joshi, John Thickstun, Hannaneh Hajishirzi, and Luke Zettlemoyer. 2020. An information bottleneck approach for controlling conciseness in rationale extraction. In *Proceedings of the 2020 Conference on Empirical Methods in Natural Language Processing (EMNLP)*, pages 1938–1952.

Arkil Patel, Satwik Bhattamishra, and Navin Goyal. 2021. Are nlp models really able to solve simple math word problems? *arXiv preprint arXiv:2103.07191*.

Mary Phuong and Christoph Lampert. 2019. Towards understanding knowledge distillation. In *International conference on machine learning*, pages 5142–5151. PMLR.

Ben Poole, Sherjil Ozair, Aaron Van Den Oord, Alex Alemi, and George Tucker. 2019. On variational bounds of mutual information. In *International Conference on Machine Learning*, pages 5171–5180. PMLR.

Colin Raffel, Noam Shazeer, Adam Roberts, Katherine Lee, Sharan Narang, Michael Matena, Yanqi Zhou, Wei Li, and Peter J. Liu. 2020. Exploring the limits of transfer learning with a unified text-to-text transformer. *Journal of Machine Learning Research*, 21(140):1–67.

Victor Sanh, Lysandre Debut, Julien Chaumond, and Thomas Wolf. 2019. Distilbert, a distilled version of bert: smaller, faster, cheaper and lighter. *arXiv preprint arXiv:1910.01108*.

Noam Slonim. 2002. *The information bottleneck: Theory and applications*. Ph.D. thesis, Hebrew University of Jerusalem Jerusalem, Israel.

Alon Talmor, Jonathan Herzig, Nicholas Lourie, and Jonathan Berant. 2018. Commonsenseqa: A question answering challenge targeting commonsense knowledge. *arXiv preprint arXiv:1811.00937*.

Xudong Tian, Zhizhong Zhang, Shaohui Lin, Yanyun Qu, Yuan Xie, and Lizhuang Ma. 2021. Farewell to mutual information: Variational distillation for cross-modal person re-identification. In *Proceedings of the IEEE/CVF Conference on Computer Vision and Pattern Recognition*, pages 1522–1531.

Yonglong Tian, Dilip Krishnan, and Phillip Isola. 2020. Contrastive representation distillation. In *International Conference on Learning Representations*.

Naftali Tishby and Noga Zaslavsky. 2015. Deep learning and the information bottleneck principle. In *2015 ieee information theory workshop (itw)*, pages 1–5. IEEE.

Michael Tschannen, Josip Djolonga, Paul K Rubenstein, Sylvain Gelly, and Mario Lucic. 2019. On mutual information maximization for representation learning. In *International Conference on Learning Representations*.

Zhibin Wan, Changqing Zhang, Pengfei Zhu, and Qinghua Hu. 2021. Multi-view information-bottleneck representation learning. In *Proceedings of the AAAI conference on artificial intelligence*, volume 35, pages 10085–10092.

Boshi Wang, Sewon Min, Xiang Deng, Jiaming Shen, You Wu, Luke Zettlemoyer, and Huan Sun. 2023a. Towards understanding chain-of-thought prompting: An empirical study of what matters. In *Proceedings of the 61st Annual Meeting of the Association for Computational Linguistics (Volume 1: Long Papers)*, pages 2717–2739, Toronto, Canada. Association for Computational Linguistics.

Lin Wang and Kuk-Jin Yoon. 2021. Knowledge distillation and student-teacher learning for visual intelligence: A review and new outlooks. *IEEE transactions on pattern analysis and machine intelligence*, 44(6):3048–3068.

Peifeng Wang, Zhengyang Wang, Zheng Li, Yifan Gao, Bing Yin, and Xiang Ren. 2023b. SCOTT: Self-consistent chain-of-thought distillation. In *Proceedings of the 61st Annual Meeting of the Association for Computational Linguistics (Volume 1: Long Papers)*, pages 5546–5558, Toronto, Canada. Association for Computational Linguistics.

Qi Wang, Claire Boudreau, Qixing Luo, Pang-Ning Tan, and Jiayu Zhou. 2019. Deep multi-view information bottleneck. In *Proceedings of the 2019 SIAM International Conference on Data Mining*, pages 37–45. SIAM.

Jason Wei, Yi Tay, Rishi Bommasani, Colin Raffel, Barret Zoph, Sebastian Borgeaud, Dani Yogatama, Maarten Bosma, Denny Zhou, Donald Metzler, et al. 2022a. Emergent abilities of large language models. *arXiv preprint arXiv:2206.07682*.

Jason Wei, Xuezhi Wang, Dale Schuurmans, Maarten Bosma, Fei Xia, Ed Chi, Quoc V Le, Denny Zhou, et al. 2022b. Chain-of-thought prompting elicits reasoning in large language models. *Advances in Neural Information Processing Systems*, 35:24824–24837.

Joseph Worsham and Jugal Kalita. 2020. Multi-task learning for natural language processing in the 2020s: where are we going? *Pattern Recognition Letters*, 136:120–126.

Yangyang Xu, Yibo Yang, and Lefei Zhang. 2023. Multi-task learning with knowledge distillation for dense prediction. In *Proceedings of the IEEE/CVF*

International Conference on Computer Vision, pages 21550–21559.

Chenxiao Yang, Junwei Pan, Xiaofeng Gao, Tingyu Jiang, Dapeng Liu, and Guihai Chen. 2022. Cross-task knowledge distillation in multi-task recommendation. In *Proceedings of the AAAI Conference on Artificial Intelligence*, volume 36, pages 4318–4326.

Cenyuan Zhang, Xiang Zhou, Yixin Wan, Xiaoqing Zheng, Kai-Wei Chang, and Cho-Jui Hsieh. 2022a. Improving the adversarial robustness of nlp models by information bottleneck. In *Findings of the Association for Computational Linguistics: ACL 2022*, pages 3588–3598.

Linfeng Zhang, Chenglong Bao, and Kaisheng Ma. 2021. Self-distillation: Towards efficient and compact neural networks. *IEEE Transactions on Pattern Analysis and Machine Intelligence*, 44(8):4388–4403.

Linfeng Zhang, Xin Chen, Junbo Zhang, Runpei Dong, and Kaisheng Ma. 2022b. Contrastive deep supervision. In *European Conference on Computer Vision*, pages 1–19. Springer.

Yu Zhang and Qiang Yang. 2021. A survey on multi-task learning. *IEEE Transactions on Knowledge and Data Engineering*, 34(12):5586–5609.

Zhihan Zhang, Wenhao Yu, Mengxia Yu, Zhichun Guo, and Meng Jiang. 2023. A survey of multi-task learning in natural language processing: Regarding task relatedness and training methods. In *Proceedings of the 17th Conference of the European Chapter of the Association for Computational Linguistics*, pages 943–956.

On-Premise Artificial Intelligence as a Service for Small and Medium Size Setups

Carolina Fortuna[1⋆], *Din* Mušić[1,2⋆⋆], *Gregor* Cerar[1⋆⋆⋆], *Andrej* Čampa[3⋆⋆⋆⋆], *Panagiotis* Kapsalis[4†], and *Mihael* Mohorčič[1‡]

[1] *Jozef Stefan Institute, Jamova 39, Ljubljana, 1000, Slovenia.*
[2] *Jozef Stefan Institute Postgraduate School, Jamova 39, Ljubljana, 1000, Slovenia.*
[3] *Comsensus, Verovškova ulica 64, Ljubljana, 1000, Slovenia.*
[4] *National Technical University of Athens, Iroon Polytechneiou 9, Attiki, 15773, Greece.*

Abstract. Artificial Intelligence (AI) technologies are moving from customized deployments in specific domains towards generic solutions horizontally permeating vertical domains and industries. For instance, decisions on when to perform maintenance of roads or bridges or how to optimize public lighting in view of costs and safety in smart cities are increasingly informed by AI models. While various commercial solutions offer user friendly and easy to use AI as a Service (AIaaS), functionality-wise enabling the democratization of such ecosystems, open-source equivalent ecosystems are lagging behind. In this chapter, we discuss AIaaS functionality and corresponding technology stack and analyze possible realizations using open source user friendly technologies that are suitable for on-premise set-ups of small and medium sized users allowing full control over the data and technological platform without any third-party dependence or vendor lock-in.

1 Introduction

Artificial Intelligence (AI) technologies have been mostly used by experts to create new services and manage the extraction of value from large amount of data enabling the rise of some technology giants. However, recently they are moving from customized deployments in specific domains towards more generic solutions aiming for horizontally permeating various vertical domains and industries [1]. For instance, decisions on when to perform maintenance of roads or bridges [2] or how to optimize public lighting [3] in view of costs and safety in smart cities are increasingly informed by AI models. However, to be successful in increasing our overall productivity, the adoption by non-experts in their day-to-day use is further supported by efforts to lower the entry barrier by democratizing AI [4] through the development of intuitive, easy to set up, manage and use systems such as AI as a Service (AIaaS).

Figure 1 presents a three layer abstraction of the AIaaS technology stack consisting of physical resources, infrastructure automation and machine learning automation, while an alternative view of a three layer abstraction focused less on infrastructure automation and more on AIaaS for different target groups is presented in [5]. Existing cloud service providers initially developed computing and storage functionalities such as Storage-, Infrastructure-, Platform- as a Service that were able to abstract physical resources and thus enabled an ecosystem for accelerated application development and scale-up of various companies [6]. Subsequently, they added ad-

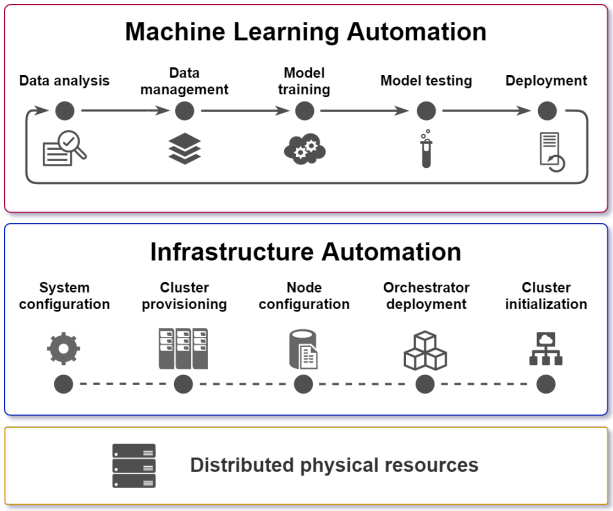

Figure 1: AIaaS technology stack.

⋆e-mail: carolina.fortuna@ijs.si
⋆⋆e-mail: din.music@ijs.si
⋆⋆⋆e-mail: gregor.cerar@ijs.si
⋆⋆⋆⋆e-mail: andrej.campa@comsensus.eu
†e-mail: pkapsalis@epu.ntua.gr
‡e-mail: miha.mohorcic@ijs.si

ditional layers of abstraction and functionality leading to the so-called XaaS that enable ever more advanced application development and value creation [7].

Various commercial solutions already offer user friendly and easy to use AIaaS solutions, functionality-wise enabling the democratization of such systems, but their business and technological models rely on controlling parts of the AIaaS technology stack. While cloud providers mostly own the physical resources and keep them off the users' premises [7], recent commercial offerings are also enabling on-premise infrastructure deployment of so-called edge cloud computing [8] where the physical resources may be on-premises while the infrastructure automation is managed by the provider. Fully controlled on-premises AIaaS stack is challenging and costly to deploy, and typically only available to large companies that have sufficient resources to realize it.

In this chapter we discuss the infrastructure and machine learning automation for AIaaS stacks such as the one depicted in Figure 1. We discuss the functionality and corresponding technology stack for these two layers and analyze possible realizations using open source user friendly technologies that are suitable for on-premise set-ups of small and medium sized users allowing full control over the data and technological platform without any third-party dependence or vendor lock-in.

Section 2 focuses on infrastructure automation, Section 3 focuses on machine learning automation while Section 4 concludes the chapter.

2 Infrastructure Automation

Cloud computing is already used in many businesses today [9] while many others are migrating to public clouds (i.e., AWS, GCP and MA) to reduce operational and management costs [10]. The advantage of such solutions is the simplicity involved in managing the underlying infrastructure where few clicks or few line changes in configuration files reflect in production as depicted on the left in Figure 2. Alternatively, when public cloud solutions are discouraged for strategic, political or financial reasons, operational costs can also be reduced by adopting open source tools such as OpenStack, Apache Mesos and Eucalyptus or using these to replace proprietary infrastructure management tools where already in place. The aforementioned open source solutions are well suited for large-scale environments such as data centres, but add unnecessary complexity and overhead for most smaller clusters [11].

For smaller, non-enterprise setups, such as hobby projects, home labs, or small and micro enterprises, it is hard to find a maintained solution that covers day to day needs. For such needs, one approach is to manually set up a cluster as depicted on the right side in Figure 2. Manual installation requires many steps to successfully set up a cluster. The first three steps that need to be performed only once are related to

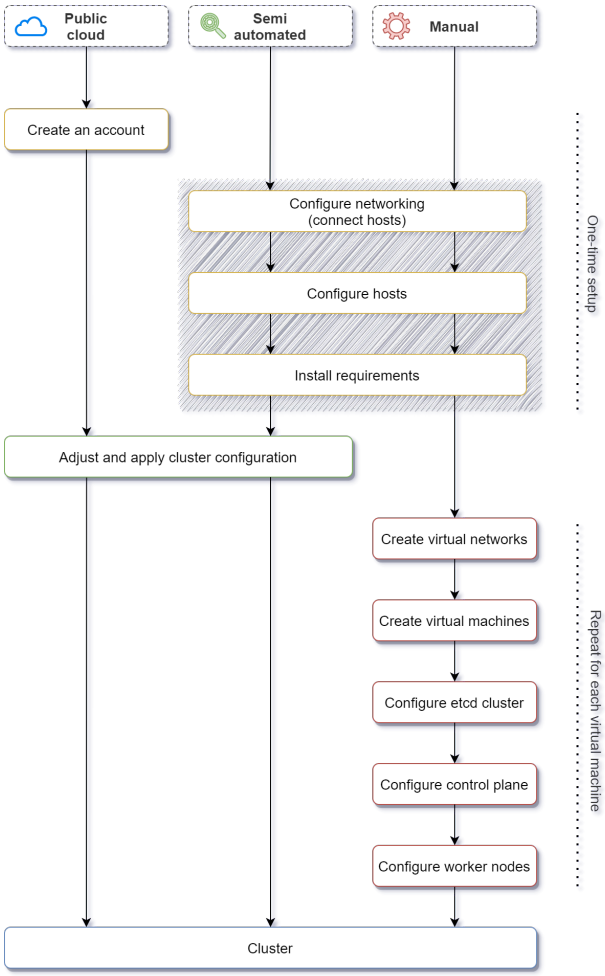

Figure 2: Comparison of infrastructure deployment steps on public cloud, semi-automated environments and manual installation.

preparing the hosts by installing and configuring the hypervisors and possibly some other required software as marked with the grey background in Figure 2. In public clouds, this step is not required, as the virtualized layer is prepared in advance by the operator and later all users share the same infrastructure. Next follows a series of steps, marked with red under the *Manual* process on the right in Figure 2, where each virtual machine must be manually created and configured. This process is prone to human errors and can take days or even weeks, depending on the size of the cluster. In case the cluster needs to be upgraded, each node must be manually reconfigured, which takes almost as much time as setting up a new cluster. These steps can be automated, resulting in a so-called *Semi-automated* process as illustrated in the middle in Figure 2.

Semi-automated solutions [12, 13] differ from public clouds in that the hosts still need to be preconfigured, while the other steps are automated. In fact, the host configuration process could also be automated by the end user, however, due to large differences be-

tween the environments, existing and emerging solutions assume manual configuration.

Infrastructure automation lifecycle in its most general form has four independent phases: cluster creation, scaling, upgrading and destruction.

Creation phase

As depicted in Figure 3, cluster creation can be realized through the following four steps: validation, preparation, provisioning and deployment.

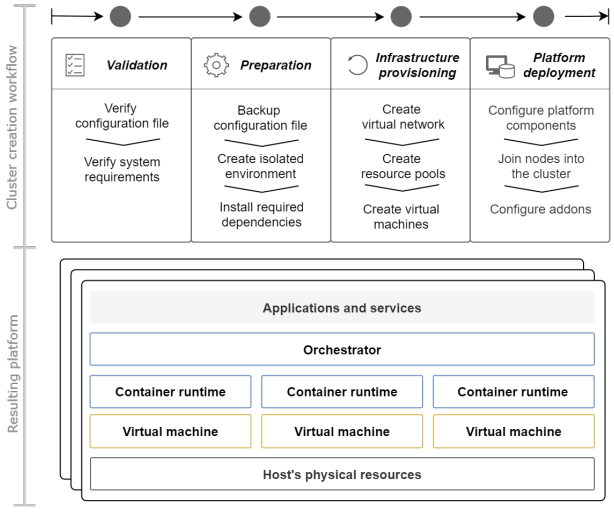

Figure 3: Infrastructure automation workflow and scheme of the resulting infrastructure.

Validation

The main objective of the validation step is to detect any potential errors as soon as possible. Depending on the user input, which can be either a terminal command or a set of configuration files, the actions triggered by the input must be predicted and checked whether they can cause potential inconveniences later in the cluster creation process. The validation process is critical to prevent unnecessary or potentially dangerous changes to the system and to save the user's time. Validation of input is followed by validation of system requirements. Based on user input, specific system requirements are verified.

Preparation

The preparation step ensures that missing packages, services, and dependencies are installed. However, conditions that cannot be met during the preparation step must abort the cluster deployment.

Infrastructure provisioning

After the successful validation and preparation step, the infrastructure deployment step begins. In this step, virtual components such as the virtual network, virtual machines and storage pools are provisioned according to the user's input. On each virtual machine an operating system is deployed and configured to make it accessible on the local network.

At the end of this step, the provisioned infrastructure consists of independent virtual components that are not yet configured to be used as a cluster. Therefore, an orchestrator needs to be deployed on top of the provisioned infrastructure. The orchestrator simplifies the management and coordination of applications and services running in the cluster by treating the entire cluster as a single entity.

Platform deployment

Platform deployment step is responsible for the installation of orchestrator and platform components, and connection of all nodes into the cluster. In this step, all orchestrator components, such as scheduler, server API, and other system controllers, are deployed on each provisioned virtual machine. In addition to traditional virtualization, containerization can also be used. Containerization is a popular, lightweight form of virtualization. It takes advantage of the host's operating system kernel to create isolated processes in different system namespaces. Compared to virtual machines, containers have low overhead because they do not require a dedicated operating system, making container creation, migration and deletion very efficient. By combining containerization with traditional virtualization, virtual machines provide a high level of isolation, while containers reduce workload overhead and facilitate cluster management. Containerization requires a container runtime, which can be installed and configured during this step. After successful cluster installation, the cluster, as depicted in Figure 4, is ready for the deployment of custom workload.

In addition to the four general steps, infrastructure automation may also include other optional steps. For instance, the installation of certain applications and services required on each deployed cluster, such as monitoring, logging, and authentication services, marked as *Platform Support Applications* in Figure 4, can be performed as part of infrastructure automation. However, the deployment of custom workloads, such as the machine learning operations pipeline, is typically separated from infrastructure automation to ensure loose coupling of the architecture.

Scaling, upgrading and destruction phases

In addition to the initial setup of the cluster, the infrastructure automation strategy must also include the subsequent management of the cluster, such as scaling and upgrading the cluster. As the workload increases or decreases, a running cluster may reach its capability limits or use its resources inefficiently. Therefore, scaling the cluster is an important part of the automation process. Cluster scaling consists of adding and removing cluster nodes. Scaling can be triggered either automatically based on collected

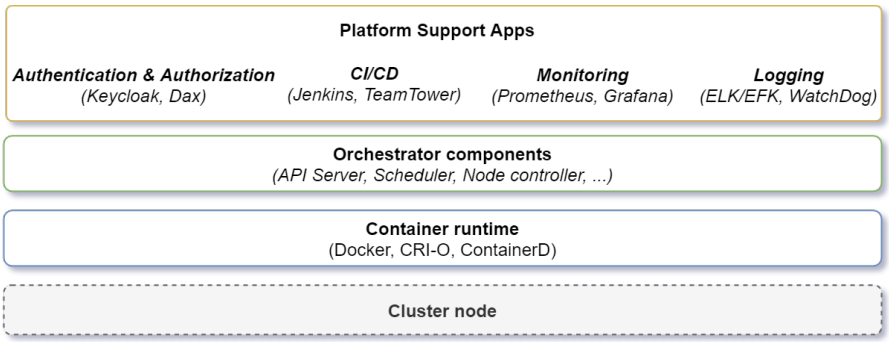

Figure 4: Example infrastructure resulting from the automation process.

cluster metrics or manually. In larger environments consisting of many clusters, automatic scaling enables better overall utilization of resources. Typically, resource usage of different clusters vary widely, and the ability to free up unused resources and make them available for other clusters to consume, reduces the required physical resources. However, auto-scaling requires additional components to manage the infrastructure, which increases the complexity of the environment. Therefore, for smaller environments that have more predictable resource consumption, manually triggered scaling may be sufficient.

The process of adding nodes to the cluster is similar to the initialization of the cluster. The additional virtual machines are created and configured first and then the platform components are installed on them. When the cluster nodes are ready, they are simply joined to the existing cluster. Removing nodes, on the other hand, is more difficult because these nodes are already in operation and contain an active workload. To gracefully remove a node, the node must first be drained, which means moving all of the workload to other running nodes. This ensures that services remain available after the node is removed.

In addition to cluster scaling, the cluster must be regularly maintained to ensure that all components are up to date. Compared to cluster scaling, upgrades still need to be automated, but are usually triggered manually. This is because the compatibility of newer components must be checked in advance, otherwise the upgrade could render the entire cluster unusable. There are many strategies for upgrading the cluster, but in-place upgrades are most common. With in-place strategy, every node in the cluster is upgraded sequentially one-by-one. This is done by draining the node, upgrading its components and rejoining the node back to cluster. No additional virtual components need to be created for this approach, which is why it is frequently used, especially in smaller environments.

Once the cluster reaches the end of its life, it can be removed. To remove the cluster completely, only the virtual components need to be stopped and deleted. However, if the cluster contains valuable data, the data must be safely migrated before the cluster is destroyed, because it will be lost during this process.

2.1 Technology stack

Figure 5 shows the most popular open source technologies commonly used for infrastructure automation. A sensible combination of such technologies can be employed to realize an on-premises infrastructure according to the example depicted in Figure 4.

Technologies are divided into 4 groups comprising of Virtualization, Containerization, Orchestration and Automation Tools. Virtualization technologies represent hypervisors that are essential for traditional virtualization on top of physical resources. They are capable of running multiple guest operating systems on a single physical host while isolating them from each other. KVM and Xen are open source projects, with KVM being the most widely used. Hyper-V and VMWare are good examples of proprietary alternatives.

The second group contains technologies for containerization. Just as traditional virtualization requires a hypervisor to manage virtual resources, container runtimes enable containerization. The most popular container runtimes are Docker, ContainerD, CRI-O, and RKT.

Container orchestrators can efficiently coordinate applications packaged as containers across multiple containerized environments. The most popular container orchestrator is Kubernetes, which also supports most of the container runtimes mentioned above. Nomad and OpenShift are seen as good alternatives for Kubernetes. Docker Swarm, on the other hand, offers native support for orchestrating Docker environments. However, it cannot be used with any other container runtime.

Finally, automation tools such as Ansible, Terraform, Pulumi, and Chef are used for provisioning a set of virtual machines, deploying container runtimes, and installing various dependencies. All these Infrastructure-as-a-Code (IaaC) tools belong to the declarative languages, in which the desired state of the infrastructure is described rather than precisely

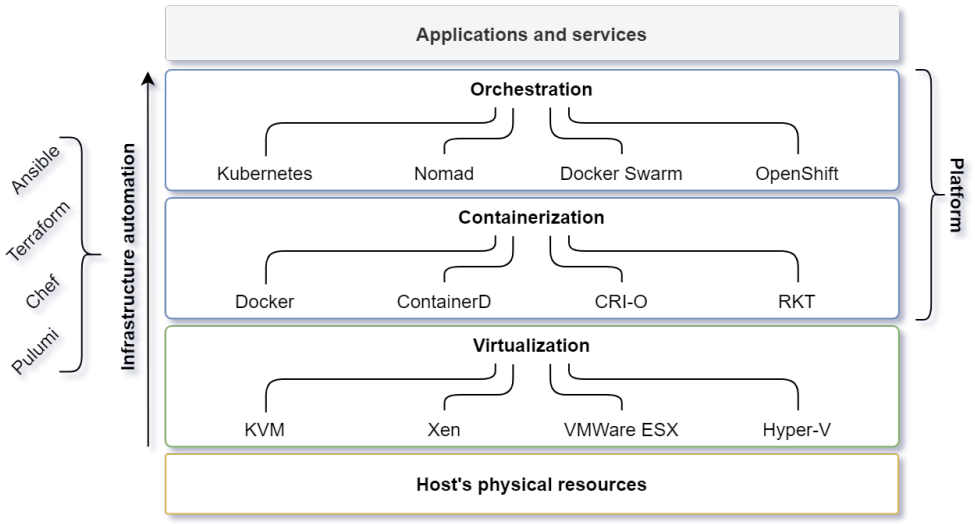

Figure 5: Infrastructure technology stack and popular automation tools.

defined with specific steps. However, typical imperative languages such as Go and Python can be used to achieve the same result. Imperative languages offer more freedom, but the automation process may take longer.

2.2 Semi-automated solutions for small and medium deployments

In Table 1 we have identified open source solutions that can be used to set up on-premise clusters. These solutions make use of the technologies discussed above and depicted in Figure 5.

All solutions analyzed in Table 1, Kubitect, Libvirt-k8s-provisioner (LKP), KubeNow, MicroK8s, and K3s, are classified as semi-automated because they have some unique requirements that must be met by the user. Kubitect and LKP are capable of creating virtualized resources as part of the automation process. MicroK8s and K3s can also be used on top of the traditional virtualization, however, they do not provide infrastructure automation as part of the solution. Thus, without additional automation, MicroK8s and K3s nodes must be manually configured on each host. KubeNow differs from other solutions as it can only be used with OpenStack, an open source private cloud solution, for on-premises deployments.

Kubitect, KubeNow and MicroK8s clusters are created and managed via custom command line interface (CLI) tools of the corresponding solutions. K3s and LKP clusters, on the other hand, are managed directly via scripts, which are less intuitive to use.

All solutions use Kubernetes as an application and service orchestrator and, with the exception of KubeNow, primarily use ContainerD as a container runtime environment. While KubeNow only supports Docker, LKP can be configured to use either Docker, CRI-O or ContainerD. However, Docker and ContainerD are de facto standard and should cover most users' needs.

In terms of implementation, each solution uses a different set of technologies to create Kubernetes clusters. The Kubitect CLI tool is written in Go and further takes advantage of Terraform and Ansible for infrastructure deployment and configuration. LKP uses only Terraform and Ansible. Consequently, different scripts must be run to create or destroy the cluster. MicroK8s and K3s, on the other hand, do not use Ansible or Terraform, but they also do not provide automation of the virtualized infrastructure. Instead, the entire solution is implemented using a single programming language. MikroK8s is written in Python and K3s in Go.

Besides the implementation details, the solutions differ mainly in the supported topologies and management features. LKP does not support cluster deployments across multiple physical hosts, which means that it is not possible to create truly high-availability (HA) clusters. Likewise, it does not provide any other management functions, such as scaling and upgrading existing clusters. Kubitect and KubeNow, on the other hand, support cluster deployment across multiple hosts. However, only Kubitect is capable of creating HA clusters, as KubeNow is limited to a single control plane node whose failure renders the entire cluster unusable. MicroK8s and K3s also support cluster deployments that span multiple hosts. However, since they do not have infrastructure automation out of the box, this must be done manually.

Every created cluster also requires a place to store the application's data. While most storage solutions are deployed on top of the Kubernetes orchestrator and are able to consume disks attached to the host, some solutions provide configuration of storage clusters out of the box. Kubitect and LKP both provide optional setup of distributed storage cluster that uses Rook as the storage orchestrator. Using Rook,

Table 1: Comparison of semi-automated infrastructure automation solutions for small and medium set-ups.

Projects \ Parameters	**Kubitect**	**LKP**	**KubeNow**	**MicroK8s**	**K3s**
On-premise traditional virtualization	Libvirt	Libvirt	OpenStack	/	/
Management tool	CLI tool (kubitect)	Ansible scripts	CLI tool (kn)	CLI tool (microk8s)	Shell scripts
Supported container runtimes	ContainerD	ContainerD, CRI-O, Docker	Docker	ContainerD	ContainerD
Container orchestrator	Kubernetes	Kubernetes	Kubernetes	Kubernetes	Kubernetes
Multi-host deployments	Y	N	Y	Y	Y
Cluster scaling	Y	N	Y	Y	Y
Cluster upgrades	Y	N	N	Y	Y
High availability (HA) cluster topology	Y	N	N	Y	Y
Out of the box storage solution	Rook	Rook	*Provider dependant*	/	Longhorn

different kinds of storage types can be used, such as filesystem, object store and block storage, which covers all requirements of Machine Learning Operations (MLOps). MicroK8s does not provide a distributed storage solution out of the box, neither as part of the cluster deployment nor as an optional add-on. In comparison, K3s offers the Longhorn deployment as an optional add-on module that is equivalent to Rook in terms of features. KubeNow is able to use the storage provided by the underlying cloud.

3 Machine Learning Automation

The development of machine-learning models follows a well defined knowledge discovery process (KDP) [14]. The main steps of the KDP consist of (1) data analysis, (2) data preparation (pre-processing), (3) model training and evaluation, and (4) model deployment [15], as also represented in Figure 6. In the past, such process and the enabling tools were familiar only to a limited number of domain experts and the process involved intense manual effort. However, in recent years, coordinated efforts have been taken by the private and public sectors to democratize AI and model development [16] to empower less specialized users.

The democratization process involves a division of labour and automation approach applied to the KDP, as elaborated more in details in [15], where rather than a domain expert executing step-by-step the process in Figure 6 from the start to the end, the process only needs to be controled at a few key steps. Furthermore, generic models can also be trained and made available through an Inference as a Service (IaaS) [5] model where the users only leverage an existing, pretrained model to make an inference used by their application or service. Such automation is enabled by MLOps [15].

As can be seen from MLOps automation process depicted in Figure 6, in the Data Ingestion and Purification phase, data from sensors or applications can be received in batch format such as hourly, daily or weekly batches or in a streaming format as it is being produced. The incoming data is then managed by feature stores rather than manually through generation scripts and file/database storage. Feature stores are data management services that harmonize data processing steps in producing features for different ML pipelines, making it more cost-effective and scalable compared to traditional approaches [17], and they can also be seen and made available as a service (i.e., STaaS).

During model training, various combinations of features available in the feature store are used to train ML models. The model training phase can be made available to ML developers as MLaaS, where they can tune and customize desired models on desired features [5], or they can be entirely abstracted and hidden from less advanced users. The resulting models are stored in a registry, evaluated and some of them eventually

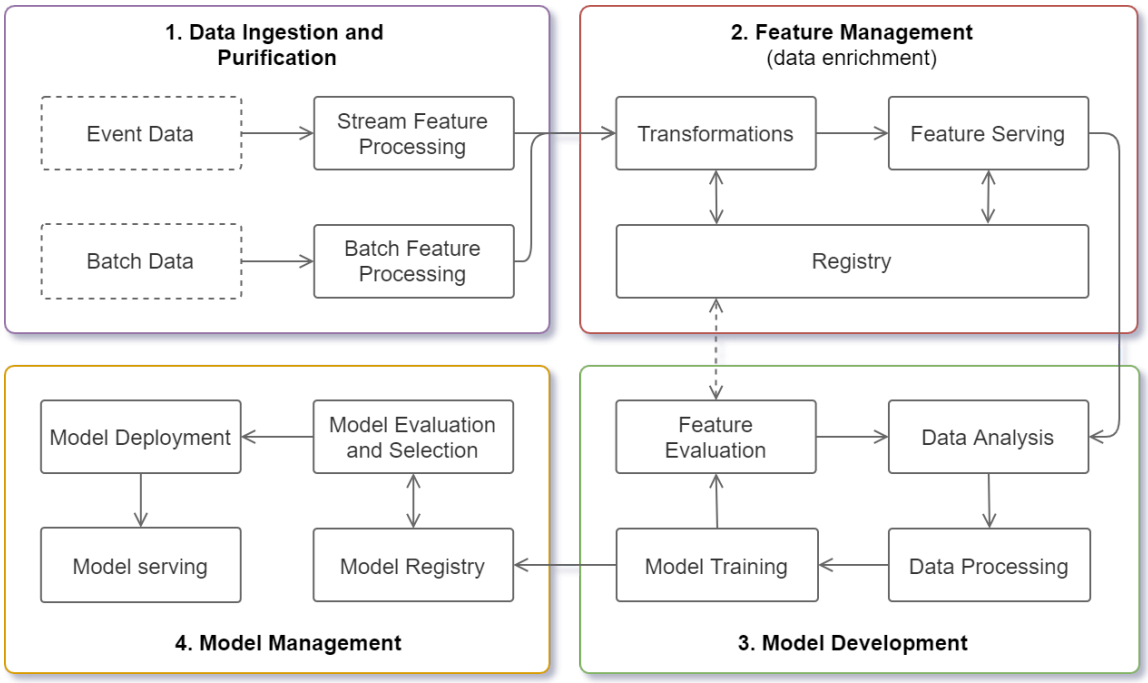

Figure 6: Machine learning automation workflow.

deployed as part of the Model Serving phase. The model evaluation and deployment enable the development of the IaaS model where less experienced users are able to select and use pre-trained models for their applications.

3.1 Technology stack

The choice of technologies available for realizing the ML automation workflow depicted in Figure 6 is becoming richer every year. In Figure 7, we provide an overview of possible candidates. During the data ingestion phase, a batch can for instance be retrieved from a database or STaaS service (e.g., BigQuery, Hive, Postgres) or a stream processing platform (e.g., Kafka, Spark, Flink).

For managing the features, fully automated solutions such as feature stores (e.g., Feast, Hopsworks) can be employed or it can also be realized using data versioning and data processing solutions such as DVC, Pandas, and Spark. Several closed source feature stores have been recently developed, while to the best of our knowledge, three feature management solutions are available as open source with their characteristics summarised in Table 2. It can be seen from the third column of the table that they include connectors to support fast interconnection with various storage solutions (e.g., BigQuery, S3, Postgres, ...) and streaming platforms (e.g., Kafka, Spark). As per columns three and four, it can be seen that all open source stores support offline and online storage such as public cloud provider's BigQuery, Azure, S3 and Snowflake or open source solutions such as PostgreSQL and Cassandra. As can be seen from the sixth column of the table, the open source feature stores can be deployed locally and also in the public cloud.

For the model development phase, the necessary tools include tools that enable code development and versioning (e.g., Kubeflow, Jupyter and Git), tools that are responsible to orchestrate model training such as Kubeflow Pipelines, Airflow and CML, as well as tools for speeding up training through parallelization such as Ray, Dask and Spark. Using the set of tools in this phase, MLaaS can be realized where developers are presented with a complete playground for custom model development.

The model serving comprises tools for model tracking, evaluation and serving such as Kubeflow and MLFlow. Especially these two tools are evolving rapidly with largely overlapping functionality in the model development and service phases of MLOps. BentoML, MLEM, TensorFlow Serving (TFX) and Kale can also be used for serving, *Neptune.ai* or *"Weights & Biases"* for versioning while Prometheus for model performance monitoring.

3.2 On-premise automation use case

Figure 8 shows an example of an on-premise ML automation platform. To build a model, we first require data. A feature store (e.g., Feast) can be set up to help dealing with live/streaming sensor data (i.e., events) from stream processor (e.g., Kafka) and historical data from a database(s)/file(s) (i.e., data warehouse/lake). A registry within a feature store contains instructions for obtaining or composing features. The example in Listing 1, for instance, defines mean hourly energy consumption as a feature. With

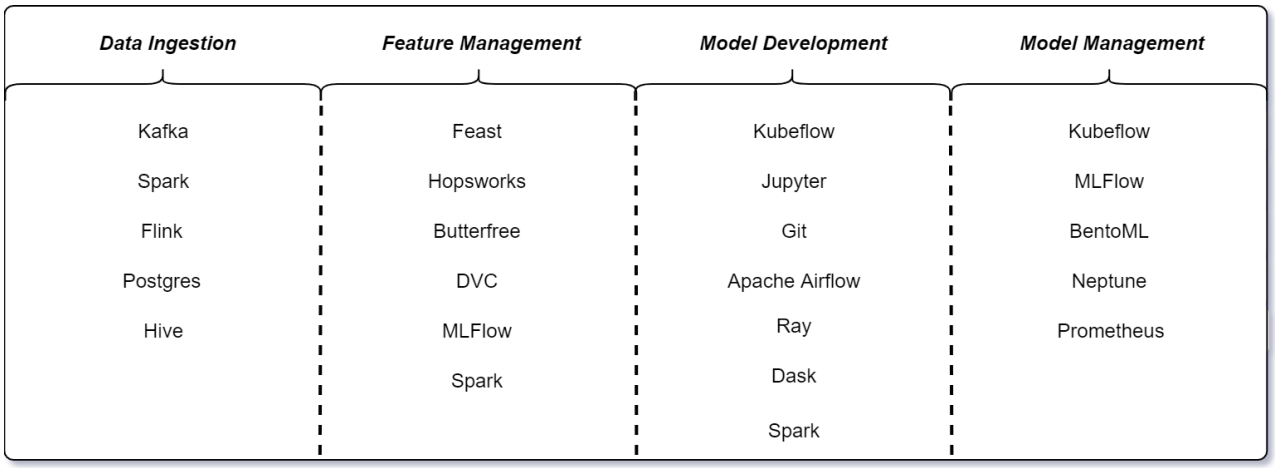

Figure 7: MLOps stack for on-premises deployment.

Table 2: List of open-source feature store solutions suitable for time series data.

Name	Open Source	Data Sources	Offline Storage	Online Storage	Deployment
Feast	Y	BigQuery, Hive, Kafka, Parquet, Postgres, Redshift, Snowflake, Spark, Synapse	BigQuery, Hive, Pandas, Postgres, Redshift, Snowflake, Spark, Synapse, Trino, custom	DynamoDB, Datastore, Redis, Azure Cache for Redis, Postgres, SQLite, custom	AWS Lambda, Kubernetes, local
Hopsworks	Y	Flink, Spark, custom Python, Java, or Scala connectors	Azure Data Lake Storage, HopsFS, any SQL with JDBC, Redshift, S3, Snowflake	any SQL with JDBC, Snowflake	AWS, Azure, Google Cloud, local
Butterfree	Y	Kafka, S3, Spark	S3, Spark Metastore	Cassandra	local

all the instructions set and all data sources available, the feature store manages access to the features for model training and models deployed in production. In addition, a feature store unifies access to features for a development and production environment. Once a new instruction is added to the feature store's registry, a new feature becomes immediately available.

The model training phase depicted in Figure 6 focuses on analyzing data and building ML models with ML pipelines. Data analysis can lead to a discovery of new features that can be valuable addition for future models. Therefore, they are contributed to the feature store (in previous phase) as instructions in the registry to benefit anyone using it. Machine learning pipelines, which define process from data to machine learning model, are specified in code (e.g., Python script, Jupyter Notebook) with help from ML frameworks. Data for pipelines are obtained preferably from a feature store or other external sources. Developed ML models are pushed automatically or manually to the MLFlow service (see Fig. 6).

The ML models can be developed using several open-source machine learning frameworks such as NumPy, SciPy, scikit-learn, XGBoost, PyTorch, TensorFlow, Keras, and JAX. In addition, these libraries can be extended with higher-order "AutoML" frameworks, such as AutoKeras or AutoSklearn. These frameworks automate search for optimal ML algorithms, architectures, and hyper-parameters for given data.

Tuning ML pipeline and therefore ML models is a complex process that usually requires multiple iterations. It should be noted that the feature importance in MLOps pipelines is assessed by the Model Training component depicted in Figure 6 subject to the availability of the features.

```
residential_hourly_stats = FileSource(
  path=str(residential_dataset_path),
  event_timestamp_column='timestamp',
)

consumption_hourly_stats_view = FeatureView(
  name='residential_hourly_stats',
  entities=['residential_id'],
  # Measurement validity period.
  # 1h in our case. Used when data is joined
  ttl=Duration(seconds=3600),
  # Describe features in the data
```

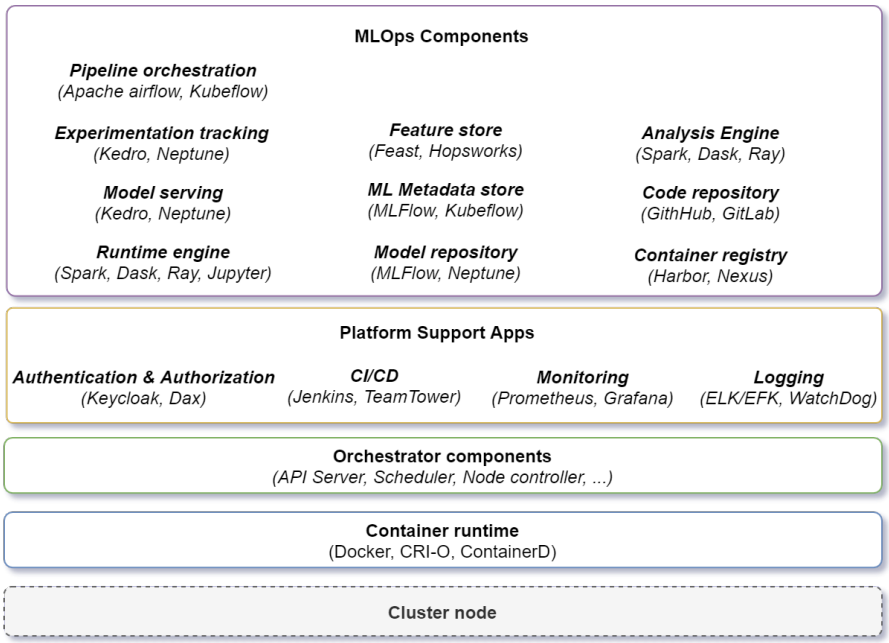

Figure 8: Example on-premise infrastructure for AIaaS.

```
  features=[
    Feature(name='ts', dtype=ValueType.FLOAT),
    Feature(name='energy', dtype=ValueType.FLOAT),
  ],
  online=True,
  # source of the data (parquet file in our case)
  batch_source=residential_hourly_stats,
  tags={},
)
```

Listing 1: Example recipe for generating the average household energy consumption over 1 hour feature (energy_mean).

To make the best out of an ML model development process, we consider good practice to keep track of ML pipeline source code with versioning tools (e.g., Git) and have it co-located on centralized services (e.g., GitHub, GitLab). This way, the MLOps system (especially the orchestrator) knows where to find and access the latest source code. With a source code branching feature of versioning tools, we can develop features or improvements in parallel and test them independently before they might get merged into the main branch.

ML pipeline steps (including the final ML algorithm) can be time-consuming in many cases. It would be inefficient to rebuild ML models with the same data and parameters more than once. To minimize this overhead, a developed model is pushed into model store (e.g., MLFlow, KubeFlow) service for later retrieval. The MLFlow service in our case keeps track of ML model artifacts. The artifacts are, for instance, model hyper-parameters, self-evaluation metrics, model's score/grade, and model's binary representation (i.e., inner state, model parameters, model weights) for later retrieval without (re)training. To keep the pipeline source code and artifacts connected for the record, MLFlow also preserves essential parts of source code, and source code commit hash. Code sample in Listing 2 shows required changes to pipeline code to utilize MLFlow service.

```
# Start recording the run
with mlflow.start_run():
    model.fit(X_train, y_train)

    # predict values for evaluation
    y_pred = model.predict(X_test)

    # MLFlow will store model into pickle for us.
    mlflow.sklearn.log_model(
        sk_model=model,
        artifact_path='model',
        registered_model_name=config.REGISTERED_MODEL_NAME, # model registration here or manually on web UI
        pip_requirements=['-r ./requirements.txt'],
    )

    # Log all relevant metrics for given task
    rmse = metrics.mean_squared_error(y_test, y_pred, squared=False)
    mlflow.log_metric('RMSE', rmse)
```

Listing 2: Example model development tracking with MLFlow.

Once models are preserved in model store (i.e., MLFlow), we can access and inspect them through the web or application programming interface (API). We can inspect individual models, their meta-data, input parameters and evaluation metrics, and compare them with other models. From a list of proposed/preserved models, we can manually (via web

interface) or automatically (with software) promote or demote models into *staging* (or testing) and *production* grade, which would happen after selected models undergo additional inspection and evaluation steps. The assigned labels help test deployment and production deployment infrastructure to pick the correct model.

Once the deployment process is triggered, the automated pipeline takes labeled models (*staging* or *production*), converts them into containers suitable for the model serving framework (e.g., BentoML), and pushes ready-made containers into blob storage (e.g., RedisDB, MinIO). From blob storage, models can be quickly (re)deployed by model serving framework service. Once deployed, MLOps pipeline exposes their interaction interfaces to the world.

For orchestration (including automation and synchronization) of the MLOps pipeline, we use Apache Airflow. To orchestrate, Apache Airflow requires instructions made out of small tasks. Tasks can depend on each other, but their inter-dependencies must form a directed acyclic graph (DAG). Airflow can be used to trigger model rebuilding, preparing staging and production containers and (re)deploying models.

Our on-premise use case consists of many complex interconnecting services. For instance, Apache Airflow orchestrator, Feast feature store, JupyterHub, MLFlow model storage and RedisDB blob storage. However, most of these services consist of many smaller hidden building blocks. For example, MLFlow model storage requires an MLFlow server, a PostgreSQL database for storing models' metadata, and MinIO for storing models' artifacts. To reduce the complexity, the usual practice is to containerize individual building blocks and present service as a single (unsplittable) entity such as pod (in Kubernetes context) or compose (in Docker context).

4 Conclusions

In this chapter, we discussed the importance of AIaaS along with recent developments in automation that enable on-premises AIaaS deployments, thus extending the benefits of such systems also to small and medium size setups requiring full control over the data and technological platform. We first focused on the general process required for on-premise infrastructure deployment and identified a number of existing open source tools and technologies for possible realizations. Then we discussed the general process required for machine learning pipeline automation in view of enabling AIaaS and also proceeded at identification of suitable technologies for its on-premise implementation. Overall, we argued that the available open source technologies are sufficiently mature and suitable for small to medium size on-premise setups of AIaaS functionality, and can be automatically configured and interconnected in such a way to support easy and intuitive setting up, use and management, hiding the complexity from the non-expert users. Such AIaaS setups can thus support gradual introduction of smart services also to various stakeholders and organizational entities in cities and towns of various sizes, and enable their extension and scaling with the increasing needs and introduction of new services and applications.

Acknowledgments

This work was funded in part by the Slovenian Research Agency under the grant P2-0016 and the European Commission under grant agreements 101000158 (MATRYCS) and 872525 (BD4OPEM).

References

[1] S. Makridakis, Futures **90**, 46 (2017)

[2] P. Martinez, E. Mohamed, O. Mohsen, Y. Mohamed, Journal of Performance of Constructed Facilities **34**, 04019108 (2020)

[3] J.F. De Paz, J. Bajo, S. Rodríguez, G. Villarrubia, J.M. Corchado, Information Sciences **372**, 241 (2016)

[4] A. Banifatemi, N. Miailhe, R. Buse Çetin, A. Cadain, Y. Lannquist, C. Hodes, in *Reflections on Artificial Intelligence for Humanity* (Springer, 2021), pp. 228–236

[5] M.H. Huang, R.T. Rust, Journal of Service Research **21**, 155 (2018)

[6] S. Goyal, International Journal of Computer Network and Information Security **6**, 20 (2014)

[7] W.K. Hon, C. Millard, J. Singh, Available at SSRN 4030064 (2022)

[8] W. Wang, M. Tornatore, Y. Zhao, H. Chen, Y. Li, A. Gupta, J. Zhang, B. Mukherjee, IEEE Transactions on Cloud Computing pp. 1–1 (2021)

[9] S. Marston, Z. Li, S. Bandyopadhyay, J. Zhang, A. Ghalsasi, Decision Support Systems **51**, 176 (2011)

[10] S. Bibi, D. Katsaros, P. Bozanis, IEEE software **29**, 86 (2012)

[11] A. Corradi, M. Fanelli, L. Foschini, Future Generation Computer Systems **32**, 118 (2014), special Section: The Management of Cloud Systems, Special Section: Cyber-Physical Society and Special Section: Special Issue on Exploiting Semantic Technologies with Particularization on Linked Data over Grid and Cloud Architectures

[12] M. Capuccini, A. Larsson, M. Carone, J.A. Novella, N. Sadawi, J. Gao, S. Toor, O. Spjuth, PeerJ Computer Science **5**, e232 (2019)

[13] libvirt-k8s-provider, *Automate your cluster provisioning from 0 to k8s!*, https://github.com/kubealex/libvirt-k8s-provisioner (2022), accessed: 26.04.2022

[14] U.M. Fayyad, G. Piatetsky-Shapiro, P. Smyth et al., *Knowledge Discovery and Data Mining: Towards a Unifying Framework.*, in *KDD* (1996), Vol. 96, pp. 82–88

[15] P. Ruf, M. Madan, C. Reich, D. Ould-Abdeslam, Applied Sciences **11**, 8861 (2021)

[16] B. Allen, S. Agarwal, J. Kalpathy-Cramer, K. Dreyer, Journal of the American College of Radiology **16**, 961 (2019)

[17] J. Patel, *Unification of Machine Learning Features*, in *2020 IEEE 44th Annual Computers, Software, and Applications Conference (COMPSAC)* (2020), pp. 1201–1205